Optical Fluorescence Imaging Techniques for the Early Detection of Cancer of the Gastrointestinal Tract and Skin

Thesis for the degree of Doctor of Philosophy

School of Physics and Astronomy
North Haugh
University of St. Andrews
St. Andrews
Fife KY16 9SS

Tracy Mckechnie

October 1999

Abstract

This thesis reports on the development of two systems, for the early detection of cancer. The first is an endoscopically-coupled cancer detection system for inspection of the gut and the second a multi-spectral imaging system for use in dermatology.

Throughout this research, I worked closely with the clinicians from the Department of Surgery and Dermatology at Ninewells Hospital in Dundee, to ensure the development of cancer detection systems suitable for use in the clinical environment. The optical imaging systems have been designed to target pre-cancerous tissue, before it advances and sets up secondary cancer sites. The imaging units exploit the principles of fluorescence detection, which involves administering a photosensitising drug that preferentially accumulates in cancerous tissue and subsequently imaging the emitted fluorescence. The photosensitising agent used is 5-aminolaevulinic acid, which metabolises within cancerous tissue to form protoporphyrin IX that absorbs strongly between 390-420nm and fluoresces near 635nm.

The first system was designed for detection of cancers in the gastrointestinal tract. The system comprises a modified light source, endoscope, camera and associated image processing system for

fluorescence detection. Both the ex-vivo and in-vivo results gathered during system evaluation are presented. The clinicians are now carrying out an intensive assessment programme, of the system, on patients in Ninewells Hospital.

The second system is a low-cost imaging unit for the illumination and real-time fluorescence imaging of skin lesions. This system allows the clinicians to identify the extent of the area of photosensitiser application, the tumour border and any surrounding satellite tumours. In addition to optimising the conditions for fluorescence detection and photodynamic therapy, the system can in principle be used to demarcate treatment zones.

Both systems are currently under clinical evaluation and have been responsible for initiating a substantial collaborative programme, between clinicians and physicists.

(i) I, hereby certify that this thesis, which is approximately 30,000 words in length, has been written by me, that it is the record of work carried out by me and that it has not been submitted in any previous application for a higher degree.

date 8 March 2000 signature of candidate

(ii) I was admitted as a research student in October 1996 [month, year] and as a candidate for the degree of Doctor of Philosophy in October, 1996 [month, year]; the higher study for which this is a record was carried out in the University of St. Andrews between 1996 [year] and 1999 [year].

date 8 March 2000 signature of candidate

(iii) I hereby certify that the candidate has fulfilled the conditions of the Resolution and Regulations appropriate for the degree of ..... in the University of St. Andrews and that the candidate is qualified to submit this thesis in application for that degree.

date..... signature of supervisor .....

Unrestricted

In submitting this thesis to the University of St. Andrews I understand that I am giving permission for it to be made available for use in accordance with the regulations of the University Library for the time being in force, subject to any copyright vested in the work not being affected thereby. I also understand that the title and abstract will be published, and that a copy of the work may be made and supplied to any bona fide library or research worker.

date 8 March 2000 signature of candidate

Acknowledgements

"Miles, is there any chance of getting me a job at shell?"

"No chance but let me talk to you about what I have to offer."

"Why don't the three of us go to Rufflets!".....

and my PhD was born..... ***July 1996.***

I would like to start by thanking Miles and Wilson for the lovely lunch at Rufflets, that changed my life!!

I want to take this opportunity to thank Miles for all the support, sarcasm and valuable experience that he has offered over the past three years. Thanks to Wilson for his expert advice and encouragement during the writing process. We made a great team and I learnt more than I ever expected.

Thank you, to Professor Cuschieri, Professor Ferguson and their respective teams for facilitating such a stimulating and successful collaboration and for helping us build bridges between the disciplines.

I would never have become such a well-rounded computer geek, without the expert help of Paul Lesso and Darren Steers. Thanks guys.

How will I ever forget the Padgett crowd, with all the many golfing games, computer car racing and ten pin bowling competitions. Thanks to you all for your help. Best of luck to Jacqueline in taking the project to the next dimension.

Most importantly I want to thank Andy, Mike, Mom and Dad for putting up with the constant highs and lows, of which I know there were many. These last three years would **never** have been possible without you all. Mom and Dad, I hope you like the product of your many years of investment, I am sure it will look great on the bookshelf!!!!!

CONTENTS

Chapter two

Chapter three

Chapter four

Chapter five

CHAPTER ONE

CANCER, DETECTION AND TREATMENT

The World Health Organisation estimates that cancer kills more than six million people annually. For decades, the number of deaths from cancer has been rising steadily, although the figures result from a larger and ageing population. In Britain, one in three people will be diagnosed as having cancer at some time during their life. One in four persons will eventually die of cancer.

The treatment of cancer has improved remarkably since 1920, when fewer than twenty percent of U.S. white patients with cancer survived. By 1996, the survival rate had doubled to forty percent. Cancer is a disease that has touched the lives of most individuals in one way or another. It affects people in all age groups and of every nationality and race.

The difficulties of fighting cancer lie not only in the many forms in which it presents itself but also in the many possible causes, such as inherited genetic abnormalities, chemicals and lifestyle habits such as smoking.

1.1 Introduction

In this chapter the development, detection and treatment of cancer is discussed. The theory behind the detection technique, used throughout this research project, is described in detail below.

1.2 Cancer

Cancer is responsible for about a quarter of all deaths in the industrialised world. It was in the second century that Greek Physician Galen first named this disease "karkinos" or "The Crab," after observing the claw like swollen veins surrounding a patient's tumour. Cancer has been found in 5000-year-old Egyptian mummies and the quest for its cause and cure is no less ancient.

In truth, the term cancer encompasses more than one hundred forms of disease. The human body contains hundreds of different types of cells, each of which can malfunction in its own distinctive way to cause cancer. Each cancer has its own unique features but the processes by which the tumours develop are similar.

In order to maintain specific tissue sizes appropriate to the requirements of the body, healthy cells regulate each other's reproduction. In a cancerous cell, the process of proliferation becomes unrestrained and excessive as shown in Figure 1.1.

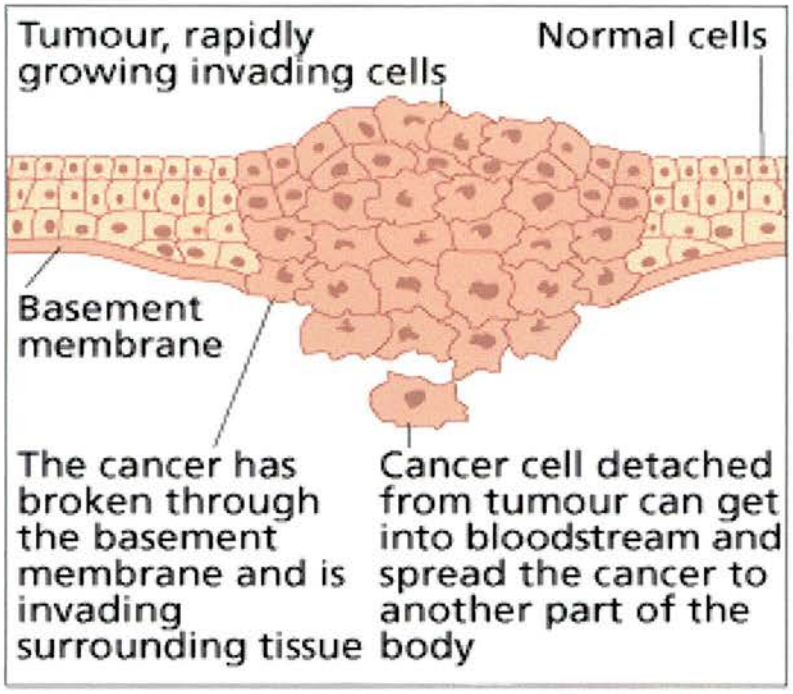

Figure 1.1: The growth and spreading of a tumour[1]

A tumour develops via a number of stages beginning with a single genetically altered cell and ending with a malignant growth. Each of these stages is detailed below.

Genetically altered cell

Tumour development begins when a cell within a normal population undergoes a genetic mutation that increases its rate of reproduction.

Hyperplasia

Cells and their offspring continue to appear normal but reproduce too frequently. After a period of time, which may be up to a number of years, one of these cells suffers another mutation that further multiplies the rate of reproduction.

Dysplasia

At this stage, the cells begin to appear abnormal in shape and orientation, while still suffering excessive proliferation. The tissue is now said to exhibit *dysplasia*. After a period, one of these cells will mutate again.

In-Situ Cancer

The affected cells show increased abnormality in shape and appearance. If the tumour has not yet broken through tissue boundaries, it is known as an *in-situ cancer* and may remain contained indefinitely.

Invasive Cancer

Once the genetic changes have taken place and the cells are able to enter the bloodstream and lymph glands; the tumour is said to have become malignant. The circulating malignant cells usually become trapped in the first vascular bed that they encounter, which is often the lung. Here they form a new tumour site known as a secondary tumour. Cancers of the digestive tract are most likely to spread (metastasise) to the liver because the blood flow circulates through the liver before going back to the heart. Thus, the lung and liver are the most common organs for the establishment of secondary cancer.

Not all tumours contain cancer cells, some are simply a result of overproducing cells; a growth of this kind is referred to as benign. Benign and malignant tumours do not respond to the body's mechanisms for limiting growth. Unlike benign growths, however, malignant tumours show an atypical cell structure, with cells that are not functional or specialised. The cells that make up a benign tumour obviously over proliferate but unlike malignant cancer cells, do not invade or metastasise to other parts of the body. Cancer becomes life threatening when the tissue forming a tumour disrupts the functioning of organs through competition for nutrients. The malignant tissue also becomes weaker than the healthy tissue and may rupture or haemorrhage.

1.2.1 Types of cancer

Epithelial tissue is skin tissue that covers and lines the body. As well as covering the outside of the body, epithelial cells cover much of the inside. They line the body's organs, for example, the digestive system and cavities

such as the inside of the chest and the abdomen. These cells are shown in figure 1.2.

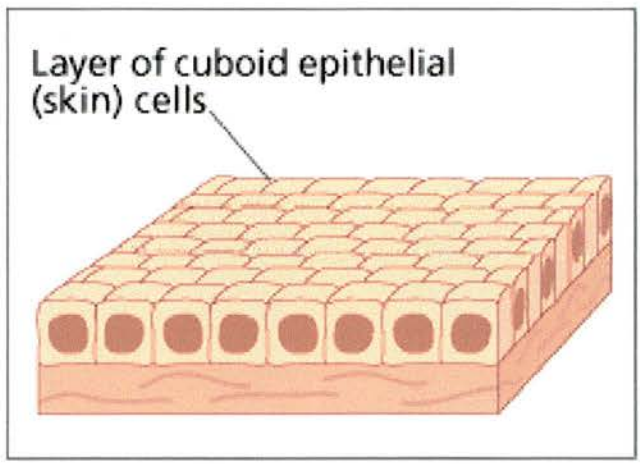

Figure 1.2: A layer of epithelial cells from which 85% of cancers originate[1]

Most malignancies are cancers originating from epithelial cells and are known as 'carcinomas'. Carcinomas make up about 85% of all cancers. There are various groups of epithelial cells and these develop into different types of cancer. For example, epithelial cells can be:

i) Cells that cover flat surfaces: Squamous cells.

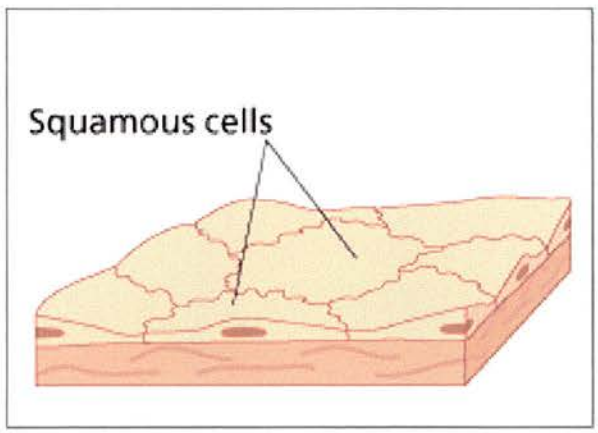

Figure 1.3: Squamous cells[1]

ii) glandular cells called adenomatous cells

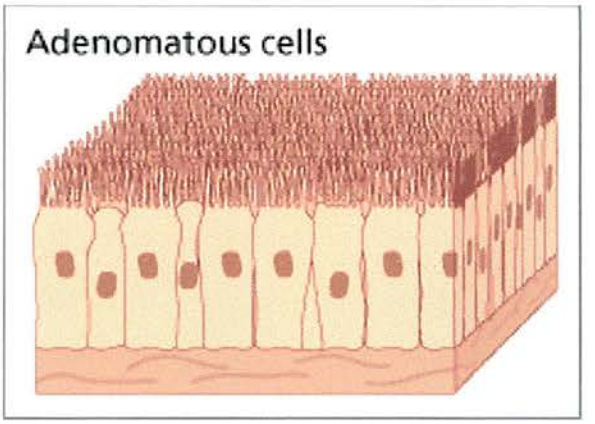

Figure 1.4: Adenomatous cells[1]

Cancers derive their names from the cell and part of the body from which they originate. For example, a patient would be diagnosed with "adenocarcinoma of the oesophagus" or "squamous cell carcinoma of the colon."

1.2.2 Cancer Statistics

One in three people in Britain will be diagnosed with cancer in their lifetime, but some cancers are more life threatening than others. Below is a list of the ten most life threatening cancers in men and woman in the UK.

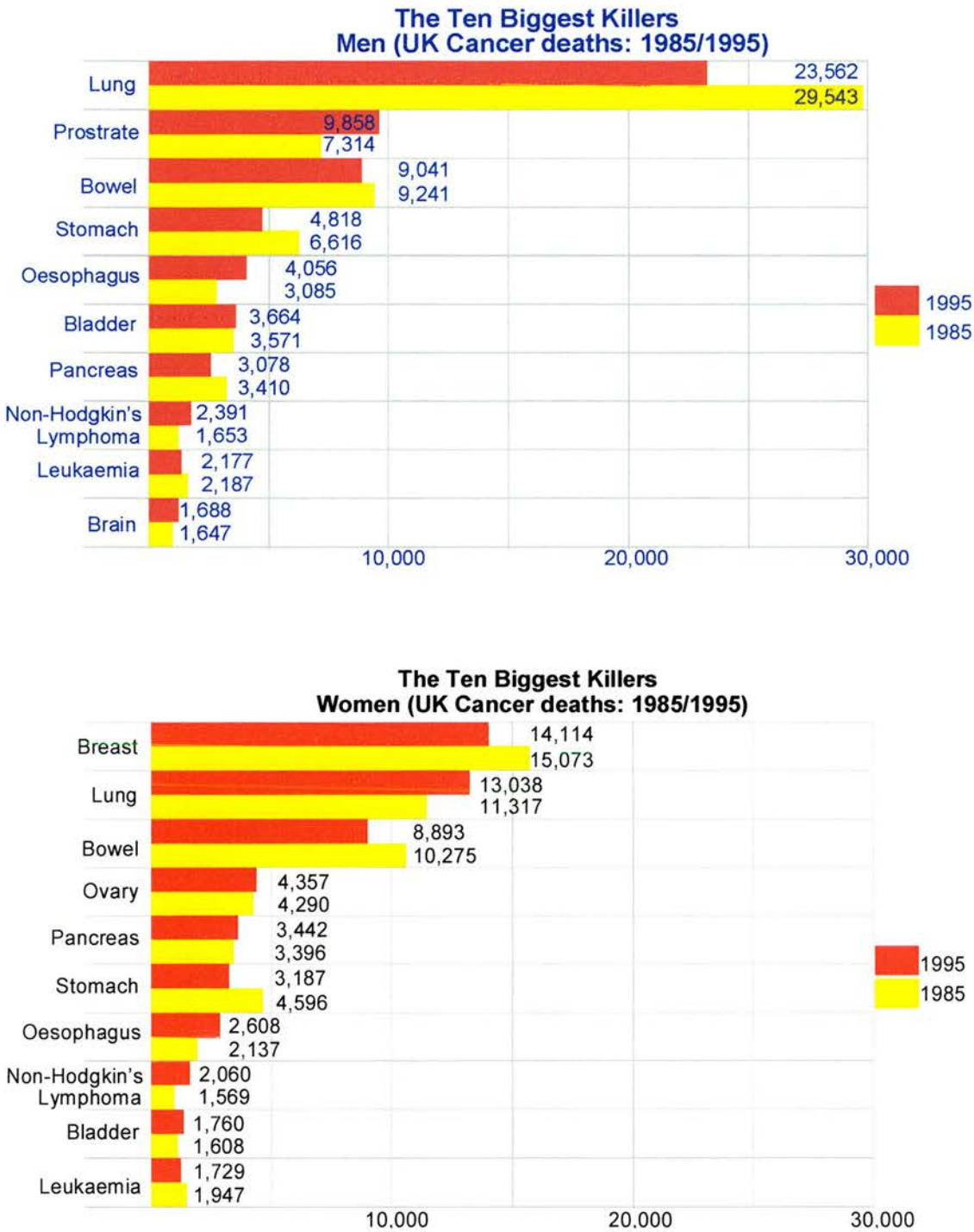

Figure 1.5: Cancer death statistics for men and women in the United Kingdom in 1985 and 1995. (Data from Imperial cancer research fund)

In both men and women, oesophageal, bowel and stomach cancers are among the top seven cancer killers in the United Kingdom. These statistics indicate the necessity for techniques that will enable clinicians to specifically

detect and treat these cancers appropriately.

Although the ranking of these cancers differs between continents, oesophageal, stomach and colon remain potential killers. For example, gastric carcinoma is a leading health problem in Japan [2], whereas oesophageal cancer is common in several developing countries [3].

1.3 Gastrointestinal Tract

Organs comprising the gastrointestinal tract (GI tract) are the mouth, oesophagus, stomach, small intestine, large intestine and rectum. The GI tract contains the food from the time it is eaten until it is digested and eliminated from the body.

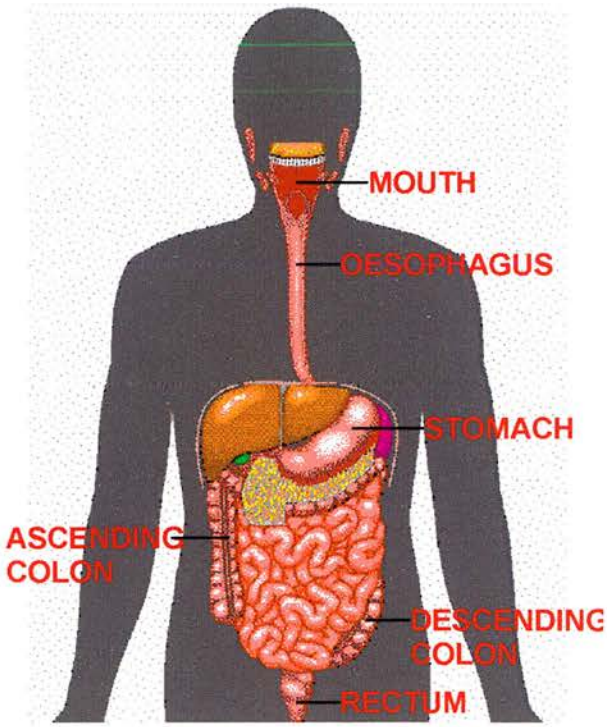

Figure 1.6: Gastrointestinal Tract[1]

The oesophagus is the muscular tube that connects the throat to the stomach. It is located between the trachea (windpipe) and the spine. In an adult, the oesophagus is about 25 centimetres in length.

The stomach is the most dilated portion of the digestive system and is situated between the oesophagus and the beginning of the small intestine (duodenum). The stomach completes the initial digestive process by producing gastric juice (acidic) to breakdown proteins.

The colon has six major divisions, which are the caecum, ascending colon; transverse colon; descending colon; sigmoid colon and rectum. The total length is approximately one and a half metres in an adult and is responsible for forming, storing and expelling waste matter.

1.4 High Risk Conditions

From the considerable time and money invested in cancer research, the overriding lesson learnt is that the earlier that cancer can be detected, the more effective any form of treatment will be. It is for this reason that sections of the population with an increased risk of developing cancer must be identified and screened regularly. An effective screening programme identifies any early signs of cancerous tissue that are subsequently treated and prevented from becoming malignant.

Two such pre-cancerous conditions are Barrett's Oesophagus [4] and Chronic Ulcerative Colitis [5], both of which have significant risks for developing adenocarcinoma [6].

1.4.1 Barrett's Oesophagus

Barrett's Oesophagus or "columnar metaplasia of the oesophagus" is believed to develop as a response to mucosal injury, induced by gastro-oesophageal reflux (indigestion). The consequence of this action, is that the normal white tissue (squamous epithelium), lining the oesophagus, is replaced by a red mucus secreting tissue (columnar metaplastic epithelium)

that is resistant to acid. Figure 1.7 shows two examples of Barrett's Oesophagus.

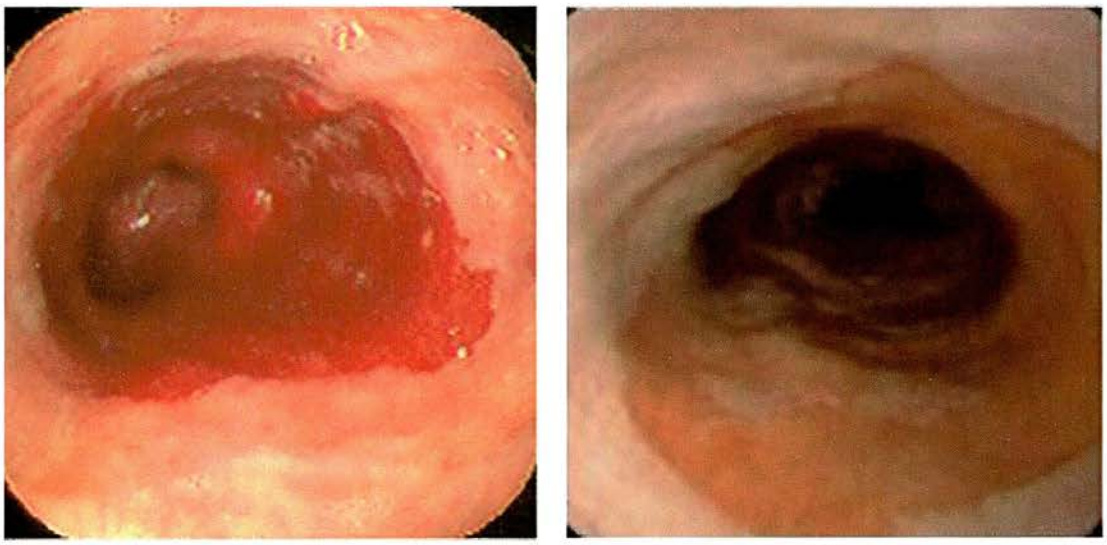

Figure 1.7: Two examples of Barrett's Oesophagus[1]

Although it is accepted that Barrett's Oesophagus is an acquired condition resulting from reflux damage to the normal oesophageal epithelium, it is not understood why only a minority of patients suffering from reflux develops Barrett's.

This condition is identified in approximately 10% of patients who undergo endoscopy for evaluation of symptoms of gastro-intestinal reflux [4]. It has been found that patients with Barrett's are predisposed to the development of adenocarcinoma of the oesophagus and suffer a 30-125 times greater risk than the average population [7]. For this reason, clinicians perform periodic endoscopic surveillance on this group in an attempt to diagnose and effectively treat early-stage adenocarcinoma. Presently, surveillance for pre-cancerous tissue within the GI tract involves carrying out yearly or two-yearly observations. Because pre-cancerous tissue and in-situ carcinoma are usually not macroscopically evident by eye, the clinician takes multiple random biopsies at 2-cm intervals in the hope of detecting any suspicious tissue, which may have developed.

Due to the inherently random distribution of pre-cancerous tissue, there is a considerable sampling error associated with taking indiscriminate biopsies. If the patient has large areas of Barrett's, the procedure is very time consuming. Bleeding also affects the accuracy of the location of the biopsies. Consequently, a more effective screening procedure is required, during endoscopic examinations, to detect pre-cancerous mutations in the tissue.

1.4.2 Ulcerative Colitis

Another high-risk condition is termed *ulcerative colitis*, which is more common in people of Caucasian race, especially in woman and young people, where the peak incidence is between 20 and 25 years. In their lifetime, patients with this condition have an approximately one in three risk of developing carcinoma of the colon. Due to this increased risk, a surgical removal of the colon is recommended to these patients, but the impact of this procedure is severe and not all patients choose this route. Like Barrett's Oesophagus, management of patients suffering from ulcerative colitis includes periodic screening for pre-cancerous changes. Current surveillance programs include regular total endoscopic examinations with multiple biopsies throughout the colon [8]. However, due to the patchy nature of the pre-cancerous tissue, these programs are not always effective.

1.5 Skin Cancer

The skin is a tissue, meaning that it is a collection of cells organised as a unit. New cells are produced through the division of healthy cells and form at the deepest level of the skin and gradually push their way upwards towards the surface as they mature.

The main types of cells found within the skin are basal cells, which form the bottom layer, squamous cells which form the exterior layer of skin and

melanocytes, which produce melanin pigment that colours the skin. Any one of these types of cells can mutate to form skin cancer. When basal and squamous cells become cancerous, they are termed carcinomas, while cancerous melanocytes are termed melanomas.

Basal cell carcinoma, or "rodent ulcer", is the most common form of skin cancer and is unique because it does not spread to other parts of the body. These tumours are easier to treat when detected early. If left for too long, they can cause extensive damage and disfigurement.

Squamous cell carcinomas are less common but more dangerous. They usually occur on the face or hands. If untreated they can spread to other parts of the body and can be fatal. Both basal and squamous cell carcinomas can usually be treated successfully with, for example, radiotherapy or surgery.

Malignant melanoma is the most dangerous form of skin cancer and if untreated can spread to other organs, especially the lymph glands, liver, bones, brain and lungs. The tumours start as small brown or black marks on the skin and are sometimes hard to distinguish from ordinary moles.

Skin cancer is the most common cancer in the UK, with over 40,000 new cases diagnosed every year. The benign forms account for 80% of skin cancers and have a 97% five-year survival rate. The other 20% represent malignant melanoma, which has one of the fastest rates of increase among white races of all the cancers, especially in the young and middle-aged. Every year in the UK about 1500 people die from this form of the disease. In Australia and New Zealand, it is now the commonest cancer affecting young adults.

1.6 Cancer Treatment

Due to the number of different forms of cancer, there are a wide range of treatment techniques available, some of which are more successful than others. A feature that is common to all of these techniques is that the earlier the cancerous tissue is detected, the more effective any form of treatment is likely to be. In the following sections, specific treatments for cancer of the GI tract and the skin are discussed.

1.6.1 Surgery and Cancer Specimens

Treatment for cancer of the oesophagus, stomach and colon depends on a number of factors. Among these are the size, location and extent of the tumour as well as the type of cancer cells. The patient's age and general health is also an important consideration.

The complication associated with cancer of the GI tract is that the symptoms are very late in presenting themselves. Once the patient starts experiencing problems swallowing, digesting food or excreting, the cancer is usually advanced and curative intervention is unlikely. At this stage, the cancer may have spread and the best palliative treatment is surgery.

In the case of the oesophagus, surgery involves the removal of the tumour along with a portion of the oesophagus, the lymph nodes and nearby tissue. The stomach can be connected to the remainder of the oesophagus or in severe cases, a passageway can be constructed between the throat and the stomach, using tissue from another part of the digestive tract. Figure 1.8 shows three examples of cancerous specimens that have been excised.

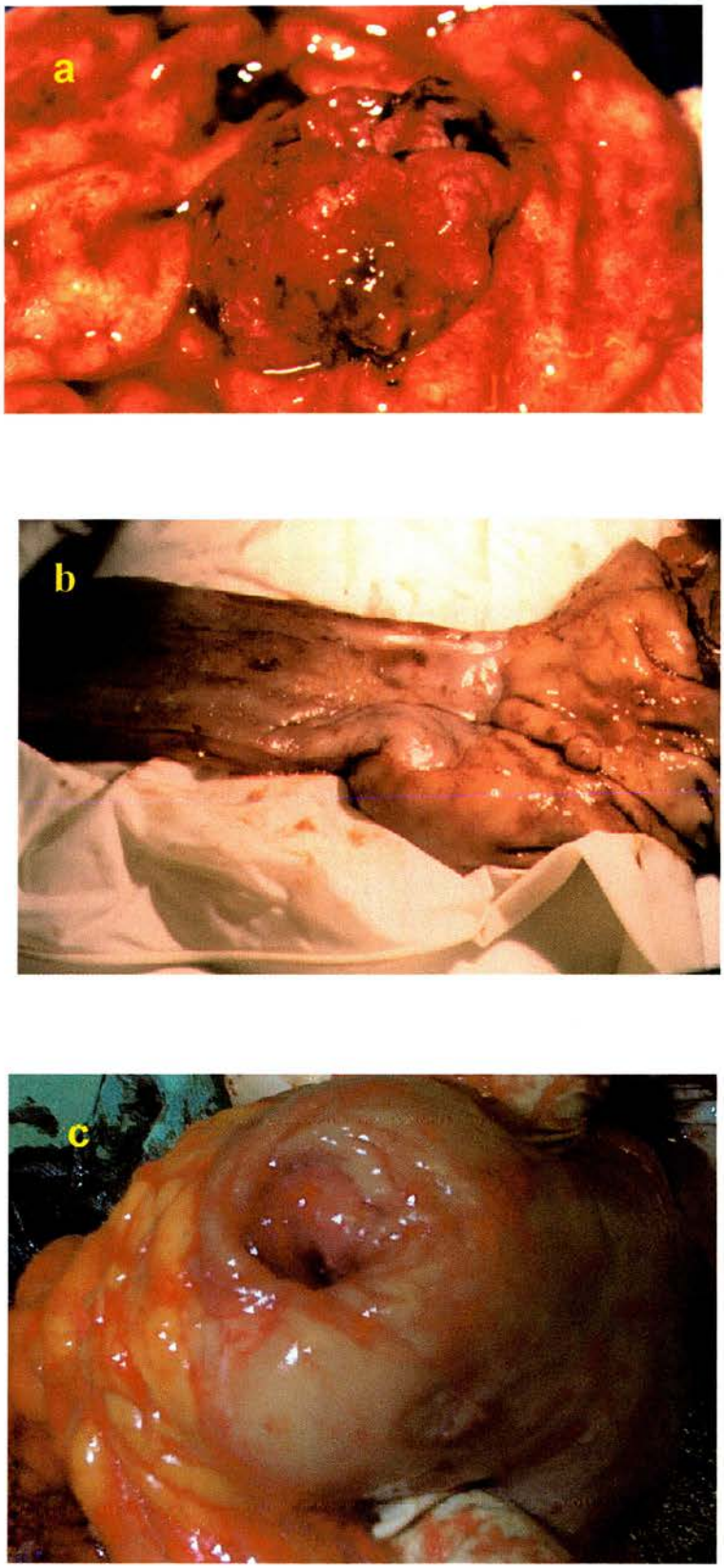

Figure 1.8: Three examples of advanced a) stomach, b) oesophagus and c) colon cancers which have undergone surgical removal

Surgery within the GI tract involves a high morbidity and mortality rate [9] and is further complicated by the fact that most of the patients are elderly and frail. If mild dysplasia, a precursor to cancer, could be effectively detected, alternative, less invasive treatments would be feasible.

For patients unable to undergo surgery, treatment may involve radiotherapy or chemotherapy [10]. Radiotherapy involves the use of powerful X-rays or gamma rays, delivered by an externally applied beam, to irradiate the region of cancerous tumour. This form of treatment acts either by inflicting genetic damage, sufficient to kill cells directly, or by inducing cellular suicide. Radiation can destroy microscopic extensions of cancerous tissue around a tumour that a surgeon might otherwise miss and is a safer option for older frailer patients who might have difficulty recovering from surgery. The drawback of this therapy is that it does not totally eradicate cancer and cannot treat widespread metastasis.

Chemotherapy involves a systemic administration of anti-cancer drugs, which travel through the body via the blood circulatory system. The available chemotherapeutic drugs often fail patients because they kill many healthy cells and thus induce serious side effects. The main disadvantages of both chemotherapy and radiotherapy are that palliative results are not obtained rapidly, the response is often incomplete and the recurrence rate is very high [11].

In some cases, where a tumour is inoperable and blocking the GI tract, the main goal is to provide the most effective palliative treatment. In this instant the surgeon may bypass the blockage or dilate the tract by inserting a stent. This wire mesh expands into the lining of the tract and creates an unobstructed pathway [12]. However, the disadvantage associated with this method is that the tumour can grow through the mesh.

1.6.2 Treating skin cancer

Although skin cancer is extremely common, it has a better prognosis than most types of cancer. Surgery and resection of the lesion is the cornerstone method used for treating skin cancer. Mohs surgery[13] is one method of surgery, which refers to a meticulous histological study of the tissues removed at the time of surgery. The usual approach is to use a fresh frozen tissue technique, where the samples are cut parallel to the skin surface, in contrast to the usual vertical sections, snap frozen and examined for residual tumour cells. In this manner, complete excision can be performed with minimal damage to normal skin.

Cryosurgery is the treatment used for superficial skin cancers and involves freezing the cancerous tissue with liquid nitrogen. For patients with larger cancers on whom surgery will be difficult, radiation therapy is used. Chemotherapy in topical form is most appropriate for the elderly who cannot tolerate other forms of treatment.

The only effective method for treatment of malignant melanoma is a complete surgical removal of the tissue involved. A suspicious lesion is normally removed to establish the diagnosis. If the diagnosis is of a melanoma, then a second surgical procedure involving a wider area of normal skin around the original site must be performed. Curative surgery is incomplete without this wide excision.

1.6.3 Photodynamic Therapy

Photodynamic therapy (PDT) [14,15] for cancer patients is an important cancer treatment. PDT is based on the combination of two modalities, light and a photosensitising drug, which are harmless by themselves but result in a beneficial therapeutic effect when combined. The technique produces local necrosis of tissue using low power light, after prior administration of a

photosensitising drug. The photosensitiser selectively accumulates within the cancerous tissue, which means that the cancer is treated without damaging the surrounding healthy cells.

PDT involves a photochemical rather than a thermal effect. When the photosensitiser is exposed to light within a particular wavelength band, it is transformed into an excited state, from which a reaction produces singlet molecular oxygen and other free radicals. Singlet oxygen is a reactive species with tumour destroying properties.

Over the past ten years, PDT has been mainly used for bladder [16], lung [17] and skin cancers [18]. The photosensitiser used in PDT on most patients is Photofrin. The drawback of Photofrin is the prolonged tissue photosensitivity it induces within patients for up to eight weeks after treatment.

Although Photofrin is the only photosensitiser to receive regulatory approval in any country, it is unlikely to be used widely because of the associated long periods of photosensitivity. Several second-generation drugs are now entering clinical trials, including mTHPC (meso tetrahydroxyphenyl chlorin), Sn Et2 (tin etiopurpurin), BPDMA (benzo-porphyrin derivative monoacid) and AlSPc (aluminium disulphonated phthalocyanine) [15]. These photosensitisers are chemically pure, absorb light at 650nm or longer and induce no, or significantly less, general skin photosensitivity. The advantage of the longer excitation wavelength is that tissue penetration is greater, enabling the treatment of more advanced cancers. Increasing the wavelength at which photosensitisers can be photoactivated also allows the possibility of using new light sources, such as LED's and laser diodes.

One of the most interesting new photosensitisers is 5-aminolevulinic acid (ALA) [19], which is converted in-vivo into the photoactive derivative, protoporphyrin IX (PpIX). The main advantage of ALA, unlike other photosensitisers, is that the skin does not remain photosensitive for long periods after treatment.

Due to the low penetration depth associated with PDT, it is especially suited for treatment of early tumours. Therefore, the number of patients eligible for PDT will increase provided the early detection of malignancies improves.

1.7 Fluorescence detection

It was evident from the discussion concerning cancer treatment that all methods are more successful on early rather than advanced cancers. When a malignant tumour causes clinical symptoms, it is usually large enough to be located via endoscopy, X-ray, computerised tomography or magnetic resonance imaging. However, there are no established protocols for the detection of pre-cancerous tissue.

Fluorescence detection is a technique, which relies on induced fluorescence, to provide the necessary optical contrast for the identification of pre-cancerous tissue. This induced contrast can be achieved through the excitation of either a pre-administered photosensitiser or the molecules native to tissue. When the photosensitiser or native molecules are excited by local exposure of light of the appropriate wavelength, they emit a characteristic fluorescence signature that enables differentiation between the cancerous and healthy tissue.

The potential applications for fluorescence detection, apart from diagnosing pre-cancerous tissue, are providing guidance in localising the optimum sites for biopsy, defining the surgical margins for tumour removal and optimising and monitoring PDT treatments. The advantages of this technique are the high signal sensitivity, the suitability for examination of tissue surfaces and the flexibility in the anatomical site that can be investigated.

The molecules used in fluorescence detection, to provide the optical contrast, can be considered in two main categories; endogenous molecules

that are responsible for native tissue fluorescence and molecules administered as exogenous drugs, such as the photosensitisers used for PDT.

In the following two sections the fluorescence detection techniques associated with an exogenous fluorophore, (administered photosensitiser) and naturally occurring molecules (endogenous molecules) will be discussed.

1.7.1 Exogenous fluorescence

This section concentrates on the detection of cancer via the use of an externally administered photosensitiser. Although photosensitisers are used for treatment purposes in PDT, their tumour localising and fluorescence characteristics make them suitable candidates for detection of cancerous tissue.

The use of an externally applied photosensitiser is advantageous as it is designed to specifically target cancerous tissue and its behaviour can be fully characterised both inside and out of the body. The induced fluorescence from a photosensitiser is also much larger than the background autofluorescence signal originating from the tissue. One of the first exogenous photosensitisers to act as a tumour marker and provide an optical contrast between the cancerous and healthy tissue was Haematoporphyrin Derivative (HpD). HpD is a complex collection of porphyrins, which was first described in 1961 [20] and was subsequently evaluated for detection of cancers in various organs.

In 1968, a 75%-80% correlation was found between the observed induced red florescence and the malignant biopsy specimens in 226 patients [21]. These patients had all been injected with haematoporphyrin derivative.

Although these early photosensitisers provided an optical contrast, enabling

differentiation of cancerous tissue, the patients remained hyper-photosensitive for long periods after administration. This side effect may be tolerated for treatment purposes but is inappropriate if the photosensitiser is to be used as part of a routine screening program.

The ideal photosensitiser for the purposes of fluorescence detection should have a high selectivity for malignant tissue and a short retention time within the body as well as be non-toxic. To aid the development of cost-effective equipment, the photosensitiser should also have a strong absorption and emission peak, which are spectrally separate. Since fluorescence detection is not an established technique, the photosensitisers are not specifically designed for detection purposes but rather for PDT, thus phototoxicity and doubtful tumour selectivity are inherent drawbacks to this method.

The most promising compound identified so far is 5-aminolevulinic acid (ALA). ALA based studies have been the most active area of clinical PDT and fluorescence detection research over the past five years. ALA is presently the preferred photosensitiser for detection purposes, as the patient's skin does not remain photosensitive for long periods after administration. This section will concentrate on details of ALA as it is the only photosensitiser used on patients within the department of surgery and dermatology at Ninewells Hospital and hence is used throughout this study.

5-Aminolevulinic Acid (ALA)

An excessive exogenous supply of ALA bypasses an inhibitory feedback loop in the biosynthesis of haeme and induces preferential accumulation of the fluorescent precursor Protoporphyrin IX (PpIX) in malignant tissue [19]. Thus the ALA is the "pro drug" and the PpIX is responsible for the photosensitiser properties.

Haeme biosynthesis is essential to every cell. In the first step of the haeme biosynthetic pathway, ALA is formed from the glycine and succinyl

coenzyme A. The last step is the incorporation of iron into protoporphyrin IX (PpIX), under the action of the enzyme ferrochelatase. The synthesis of ALA is the rate- limiting step. However, this step can be overcome if large quantities of ALA are provided. Due to the limited capacity of ferrochelatase, an exogenous excessive supply of ALA has been proven to stimulate the production of the intermediate precursor of haeme, PpIX [22]. Porphobilinogen deamise is another enzyme in the haeme synthesis pathway. Its activity is higher in some tumours, whereas that of ferrochelatase is lower, so that PpIX accumulates with some degree of selectivity in such tumours. Figure 1.9 illustrates the basic steps involved in the production of PpIX.

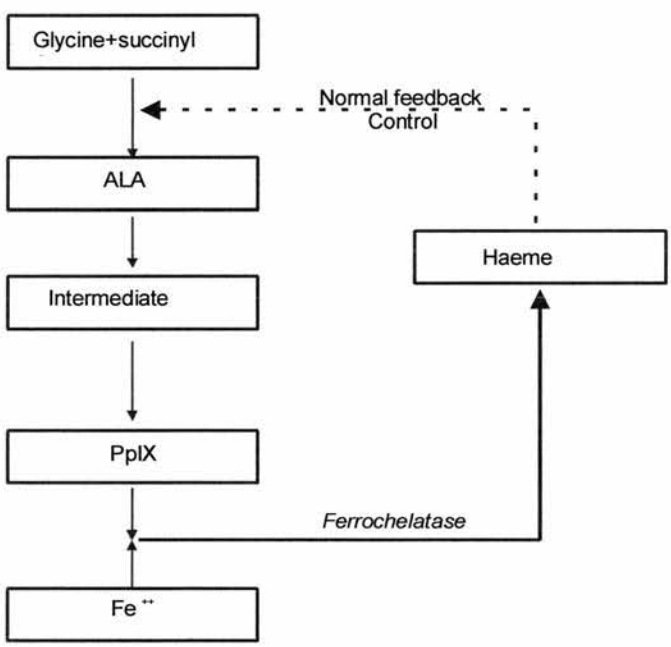

Figure 1.9: Production of PpIX from exogenous ALA

ALA can be applied topically, subcutaneously, or orally for the skin and other organs, such as the GI tract. ALA is hydrophilic and does not easily penetrate through intact skin [23]or through cell membranes [24]. When ALA is applied topically to cutaneous tumours, the tumour selectivity is therefore enhanced by an increased permeability of the skin tumour.

Within the study of the GI tract, the ALA was dissolved in a glass of orange juice and administered to the patient. The dosage of ALA ranged from 3mg

per kg body weight to 40mg per kg body weight. Ethical approval was granted for a maximum of 20mg per kg to be used for detection of cancers in the oesophagus and stomach and 40mg per kg to be used for observation of cancers of the colon. The elapsed time between ALA administration and subsequent observation was varied between one and eight hours.

For the detection of cancer on the skin, an oil-in-water cream containing ALA was topically applied to the region of interest. The concentration of ALA in the cream was 20% and a dosage of 50mg per cm^2 was used. After ALA administration, the region of interest was covered with a thin occlusive dressing (Tegaderm, 3M, UK) to prevent the cream from being smeared off. After an application time ranging from three to twenty hours, the dressing was removed and the cancer was observed with the detection unit.

Inducing fluorescence

The absorption and emission spectral data for PpIX is shown in figure 1.10 below.

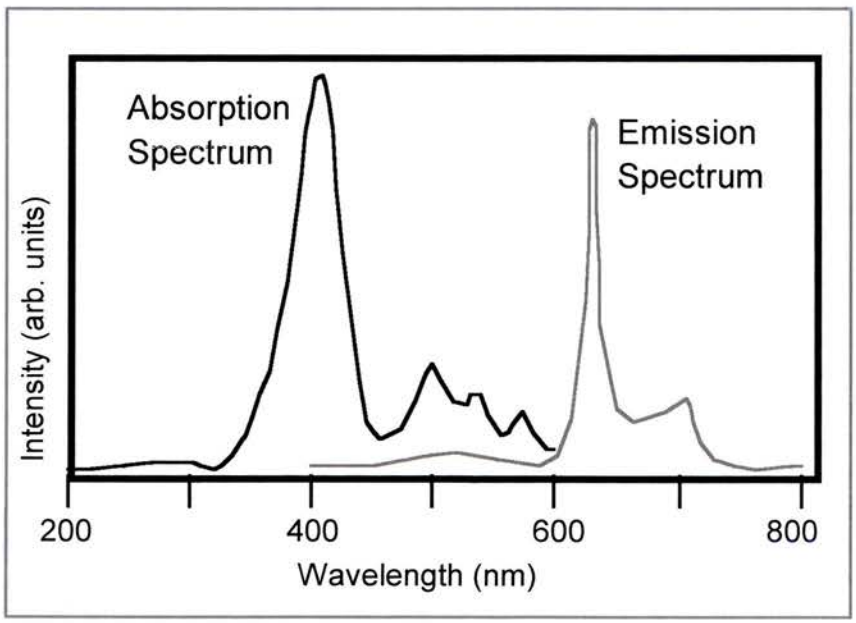

Figure 1.10: Spectral data for PpIX[25]

It is evident from the spectral data that PpIX has a strong absorption peak between 390 and 410nm. Excitation at the violet end of the spectrum induces a characteristic bimodal emission at predominantly 638nm.

Although light excitation in the violet region of the spectrum will induce the maximum fluorescence from the PpIX, it will not penetrate very deeply into the tissue. Light fluence in tissue decreases exponentially with distance and the effective penetration depth is inversely proportional to the effective attenuation coefficient.

The effective attenuation is influenced by scattering and absorption within the tissue, which in turn is affected by endogenous tissue molecules. Both of these parameters differ from tissue to tissue, with the liver, for example, affording especially poor light penetration due to its high haemoglobin content and brain tissue being particularly light scattering. On average, however, penetration is about 1-3mm at 630nm, the wavelength used for PDT with Photofrin, while penetration is approximately twice this value at 700-850nm. At 400nm, the penetration depth within tissue is a fraction of a millimetre and thus, only superficial cancerous tissue on the surface will be detected.

1.7.2 Endogenous fluorescence (Autofluorescence)

This section concentrates on the use of naturally occurring molecules to produce the optical contrast necessary to differentiate cancerous tissue from healthy tissue. The main advantage of using autofluorescence to diagnose cancerous tissue is that no drug is required.

Tissue contains a complex mixture of substances, involving a large number of molecules and potential fluorophores. When the tissue is excited with UV or violet light, a blue/ green fluorescence is emitted that arises from the superposition of the fluorescence of a number of native molecules. Because the molecules excitation and emission bands are broad and often show

spectral overlapping, a distinction between which are responsible for the fluorescence is difficult.

These native fluorescing molecules are associated with the structural arrangement of the tissues or the cellular metabolic processes. The most important molecules involved in the structural matrix are collagen and elastin, whereas those involved in the cellular metabolism include nictotinamide adenine dinucleotide (NADH) and flavins. Various porphyrins are also naturally present within the body. Figure 1.11 shows the spectral data for various endogenous tissue molecules.

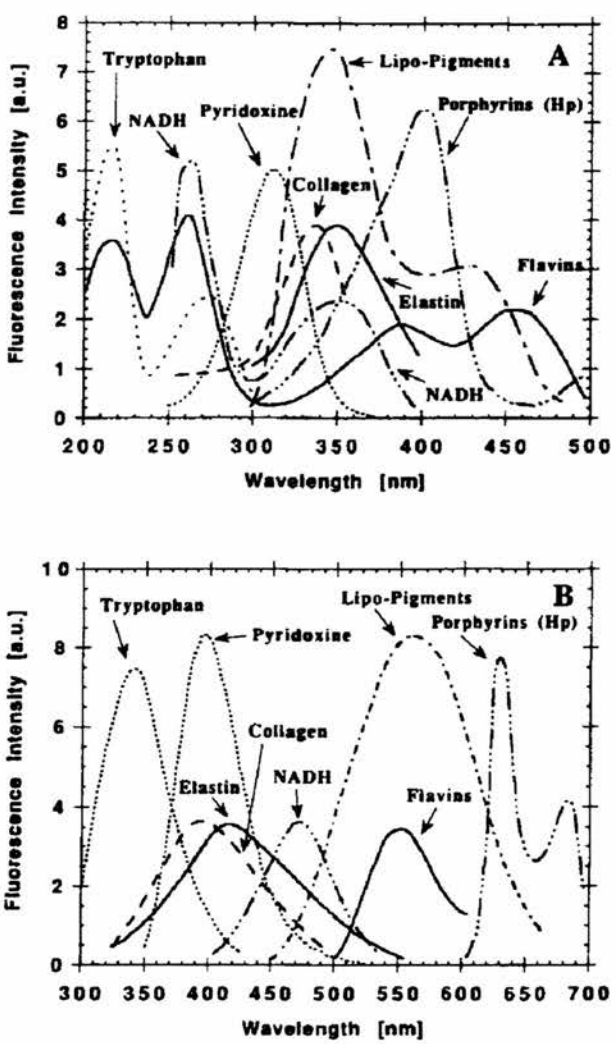

Figure1.11: Fluorescence a) excitation and b) emission spectra of various endogenous tissue molecules. Spectral shapes are shown for the best relative excitation/ emission conditions [26]

The detection of pre-malignant lesions or early cancer using autofluorescence depends on changes in one or more of the following;

1) the molecule concentration or spatial distribution,
2) the metabolic status e.g. NADH is fluorescent only in its reduced form,
3) the biochemical/biophysical microenvironment of the tissue, which may alter the fluorophore quantum yield, spectral peak positions and line widths,
4) the tissue architecture, such as mucosal thickening or loss of layered structure, which affects the relative contributions to the measured fluorescent signal and
5) the wavelength dependent light attenuation due to the concentration and distribution of (non fluorescent) chromophores, particularly haemoglobin[26].

For example, if one were to image the autofluorescence within the wavelength band between 450 and 550nm, a reduced intensity would be recorded within the cancerous tissue, relative to the healthy tissue. This is because epithelial tumours, even in early stages are often characterised by a thickening of the tissue, which acts as a shield to the connective tissue fluorescence.

Due to the small penetration of UV light into tissue, only the tissue surface down to a small fraction of a mm is probed, making the method very sensitive to early and thin malignant and pre malignant layers. Also the degree to which the fluorescence signal measured in vivo is altered by cancerous changes, depends strongly on the excitation and emission wavelengths used because these determine which are the dominant molecules involved.

1.8 Summary

Although there are over a hundred different forms of cancer, some of which are more lethal than others, the principal fact is the earlier that cancer is detected the more effective any form of treatment will be.

Due to the diverse characteristics associated with the various forms of cancer, one is unlikely to develop a single screening programme or mode of treatment that is appropriate for all cancers. For this reason, this chapter concentrated on cancers of the GI tract and skin and their equivalent treatments.

Fluorescence detection is the principle on which the research discussed in this thesis is based. The aim was to detect pre-cancerous tissue in the GI tract and on the skin, exploiting the photochemical reaction comprising a photosensitiser and suitable excitation light. This is not a new concept for detecting cancer but is relatively unexplored. In chapter 2 the detection systems, based on fluorescence detection, which have been developed to diagnose pre-cancerous tissue are described in detail.

1.9 References

[1] Picture obtained from World Wide Web.

[2] C. R. Kapadia, F. W. Cutruzzola, K. M. O'Brian, M. L. Stetz, R. Enriquez, L. I. Deckelbaum. "Laser induced fluorescence spectroscopy of human colonic mucosa." Gastroenterology, 1990, **99**, 150.

[3] N. E. Day. "The geographic pathology of cancer of the oesophagus." *Br. Med. Bull.*, 1984, **40**, 329.

[4] C. Stael von Holstein, A. M. K Nilsson, S. Andersson-Engels, R. Willen, B. Walther, K. Svanberg. "Detection of adenocarcinoma in Barrett's oesophagus by means of laser induced fluorescence." *Gut*, 1996, **39**, 711.

[5] B. A. Lashner. "Colorectal cancer in ulcerative colitis patients: survival curves and surveillance." *Cleveland Clin. J. Med.*, 1994, **61**, 272.

[6] C. R. Boland. " The biology of colorectal cancer." *Cancer*, 1993, **71**, 4180.

[7] W. Hameeteman, G. Tygat, H. Houthoff, J. van den Tweel. "Barrett's oesophagus. Development of dysplasia and adenocarcinoma." *Gastroenterology*, 1989, **96**, 1249.

[8] R. J. Dickingson et al. "Colonoscopy and the detection of dysplasia in patients with longstanding ulcerative colitis." *Lancet*, 1980, **20**, 620.

[9] A. Watson. "A study of the quality and duration of survival following resection, endoscopic intubation and surgical intubation in oesophageal carcinoma." Br. J. Surg., 1982, **69**, 585.

[10] P. Spinelli, M. Dal Fante, A. Mancini, F. G. Cerrai. "Palliation of oesophageal cancer: Endoscopic laser therapy." *Diseases of the Esophagus*, 1996, **9**, 98.

[11] R. Lambert. "Palliation of carcinoma of the oesophagus:is there a hope for cure?" *Am. J. Gastroenterol.*, 1994, **89**, S27.

[12] R. Madhotra, A. Raouf, R. Sturgess, N. Krasner. "Laser therapy in maintenance of the patency of expandable metal stents." *Lasers Med. Sci.*, 1999, **14**, 20.

[13] R. M. Mackie. "Skin Cancer." second edition, 1996, Martin Dunitz.

[14] B. Henderson, T. Dougherty. "How does photodynamic therapy work?" *Photochemistry and Photobiology*, 1992, **55**, 145.

[15] J.J. Schuitmaker, P. Baas, H.L.L.M. Van Leengoed, F.W. Van der Meulen, W. M. Star, N. van Zandwijk. "Photodynamic therapy: A promising new modality for the treatment of cancer." *J. Photochemistry and Photobiology B*, 1996, **34**, 3.

---

[16] J. F. Kelly, J. F. Snell. "Hematoporphyrin derivative:a possible aid in the diagnosis and therapy of carcinoma of the bladder." *J. Urol.,* 1976, **115**, 150.

[17] T. G. Sutedja, P. E. Postmus. "Photodynamic therapy in lung cancer. A review." *J. Photochemistry and Photobiology B:Biology*, 1996, **36**, 199.

[18] R. M. Szeimes, P. Calzavara-Pinton, S. Karrer, B. Ortel, M. Landthaler. "Topical photodynamic therapy in dermatology." *J. Photochemistry and Photobiology B:Biology*, 1996, **36**, 213.

[19] Q. Peng, T. Warloe, K. Berg, J. Moan, M. Kongshaug, K. E. Giercksky, J. M. Nesland. "5-Aminolevulinic acid-based photodynamic therapy." *Cancer,* 1997, **79**, 2282.

[20] R.L Lipson, E. J. Baldes, A. M. Olsen. "Hematoporphyrin Derivative: A new aid for endoscopic detection of malignant disease." *J. Thoracic and Cardiovas. Surg*, 1961, **42**, 5, 623.

[21] H. B. Gregorie, E. O. Jorger, J. L. Ward. "Hematoporphyrin derivative fluorescence in malignant neoplasms." *Ann. Surg.,* 1968, **167**, 829.

[22] A. M. del C. Batlle, "Porphyrins, porphyrias, cancer and photodynamic therapy-a model for carcinogenesis." *J. Photochem. Photobiol.B: Biol.*, 1993, **20**, 5.

[23] J. C. Kennedy, R.H. Pottier, D.C. Pross. "Photodynamic therapy with endogenous protoporphyrin IX: basic principle and present clinical experience." *J. Photochem Photobiol B*, 1990, **6**, 143.

[24] J. M Gaullier, K.Berg, Q. Peng, H. Anholt, P.K. Selbo, L. M. Ma. "The use of esters of 5-aminolevulinic acid to improve photodynamic therapy on cells in culture." *Cancer Res.*, 1997, **57**, 1481.

[25] Spectral data provided by the biochemist (Luke) in the department of surgery at Ninewells Hospital.

[26] G. A. Wagnieres, W. M. Star, B. C. Wilson. "In vivo fluorescence spectroscopy and imaging for oncological applications." *Photochemistry and Photobiology*, 1998, **68**, 603.

CHAPTER TWO

REVIEW OF CANCER DETECTION SYSTEMS

The development of a unit for the early detection of cancer involves more than designing a system to pinpoint the location of transplanted cancerous cells, within a synthetic tissue sample. The major challenge is to design a system that effectively detects cancer in humans, is conducive to the intended clinical environment and is economically viable to the end user. To ensure that the system will be used within the clinical setting, it must be easily operated and maintained; the clinician ought to have full control of the instrument and the diagnosis should be repeatable and obtained in real-time.

The large numbers of cancer detection methods investigated over the past thirty years are indicative of the challenge of the task. To date, experience shows that optical techniques offer the most suitable diagnosis, as they are quick, non-invasive and relatively cost effective. These techniques are easily tailored for use within the GI tract and on the skin as access and observations can be achieved endoscopically or directly.

2.1 Introduction

In this chapter, the subject matter is concentrated on optical methods, reported to date, for the characterisation of tissue in the GI tract and on the skin. Such demarcation of tissue is achieved through spectroscopic analysis, which is the measurement of the interaction of specific spectral bands with biological tissue. Spectral analysis of tissue relies on identifying an optical characteristic that differentiates healthy from abnormal tissue.

A number of optical techniques have been reported to identify pre-cancerous tissue within the GI tract and on the skin. These include fluorescence spectroscopy, elastic scattering spectroscopy, optical coherence tomography and Raman spectroscopy. The differences in these techniques are simply a matter of scale, where elastic scattering relies on the properties of whole cells and the average properties of large groups of cells. By contrast, Raman spectroscopy focuses on the subcellular molecular differences between cancerous and healthy tissue.

The major types of tissue spectroscopy are detailed below along with a review of the detection systems reported in the literature.

2.2 Fluorescence Spectroscopy

Fluorescence spectroscopy is utilised for the diagnosis of tissue pathology, as fluorescence is sensitive to the biochemical make-up of the tissue. Fluorescence spectroscopy exploits the principles of fluorescence detection, discussed in chapter one, to distinguish cancerous and healthy tissue. Fluorescence detection relies on inducing fluorescence by the excitation of light-sensitive molecules, with light of a specific wavelength band and subsequently characterising the emission. The induced fluorescence signature, originating from exogenous or endogenous molecules, enables differentiation between cancerous and healthy tissue.

While fluorescence, Raman and elastic scattering have all been investigated as methods for distinguishing malignant tissue, the earliest work and the majority of in-vivo work done to date by various groups has utilised light induced fluorescence spectroscopy.

Detection can be performed using a single excitation and emission wavelength, although to extract further information several excitation-emission pairs may be used. Additional information can also be provided by monitoring the lifetime of the induced fluorescence.

Fluorescence analysis is performed either as a point-by-point measurement or by imaging a larger tissue surface area. Both techniques are used either directly or via an endoscope. If a fibre probe is used, then the fluorescence is measured at a single tissue site, whereas if filtered imaging technology is used, then the result is spectrally selective imaging of larger tissue surface areas. Typically in a point measurement, the entire fluorescence spectrum is recorded for a given excitation wavelength and this can be repeated quickly for additional excitation wavelengths. However, when the tissue surface is imaged, smaller combinations of illumination and emission wavelengths are recorded. Thus, point measurements provide a large range of spectral data about one tissue site, whereas spectral imaging provides less spectral information but for a larger surface area of tissue.

Current systems vary from simple and relatively inexpensive units, using a filtered lamp and photodiode detector, to highly complex and expensive multispectral imaging systems, involving sophisticated laser sources, sensitive array detectors and computerised image processing to measure fluorescence decay lifetimes. No matter which method is used, the common goal for all detection systems is to obtain the maximum discrimination of the tumour signal from the surrounding healthy tissue signal. It is important to establish reliable limits for defining a positive fluorescence signal by comparative studies with histology.

In the following sections a number of different fluorescence methods used for the detection of pre-cancerous tissue within the GI tract and on the skin are discussed. These methods are applicable to both the monitoring of autofluorescence, from endogenous molecules and induced fluorescence from exogenous photosensitisers. However, the faintness of autofluorescence, the complex interactions between the different molecules and optical properties affecting the fluorescence signal, mean that highly sensitive and sophisticated instruments are needed to provide quantitative information.

2.2.1 Fluorescence ratio technique

One of the earliest systems reviewed in the literature was developed by Lipson et al. in 1961[1] and used haematoporphyrin derivative as the photosensitiser. A filtered 200 W high-pressure mercury arclamp provided the excitation light and was introduced into the endoscope via a transparent quartz rod. The white light necessary for viewing was supplied by an otoscope bulb and could be interchanged with the excitation light, to enable transmission down the same quartz rod. The clinician observed the induced contrast between the cancerous and healthy tissue by viewing the image at the endoscopic eyepiece through a filter, which transmitted the long wavelength spectral band. This method was not adequately sensitive or user-friendly but demonstrated the application of the principles of fluorescence detection, for the purposes of detecting cancer within the GI tract.

Over the subsequent years, the equipment evolved and the detection of the fluorescence signal became more advanced. In 1980, Kinsey and Cortese[2] reported a non-imaging technique for the early detection of cancer using an endoscope. This method involved the clinician monitoring the induced fluorescence by listening to an audio signal, whose frequency was controlled

by the intensity of the detected fluorescence. However, it was established that such techniques suffered from strong dependence on the distance from the endoscope tip to the suspected tumour site, on the angular orientation of the surfaces and the fluorescence excitation power. Profio et al.[3] overcame this problem by taking a ratio of the induced fluorescence signal and the reflected violet excitation light, for which the theory is discussed below.

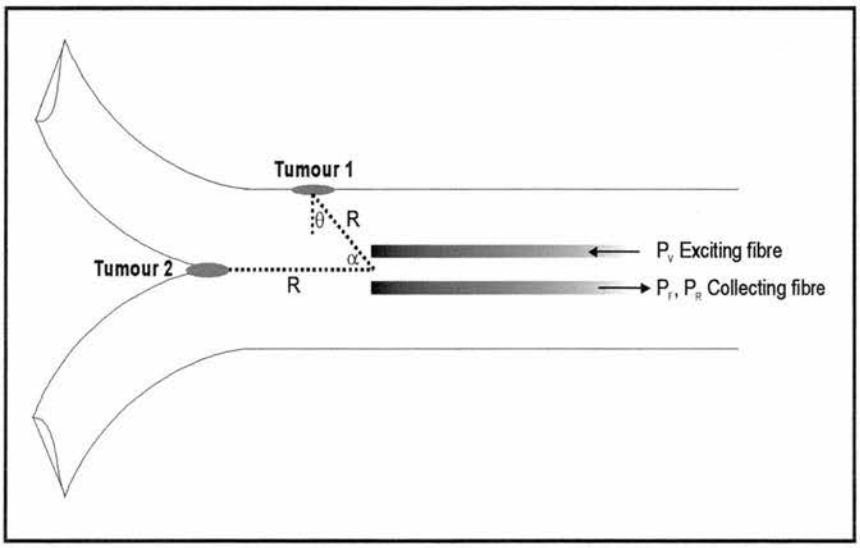

Figure 2.1: Geometry for fluorescence and reflectance measurements[3]

A typical measurement geometry is shown in figure 2.1, where the exciting and collecting fibres are inserted into the body through an endoscope. The one fibre transmits the violet light, with a power P_V to the tumour area, while the other fibre collects the induced red fluorescence of power P_F and the reflected violet light of power P_R from the tumour area. The distance from the fibres to the two tumour sites is R.

The fluorescence emission from a unit area is dependent on the violet irradiance E_V, the fluorescence yield Y and the angle of emission according to an assumed angular distribution g (Θ). The collecting fibre will transmit a fraction of the fluorescence, dependent on the solid angle subtended by the fibre and the angle of incidence on the fibre, which is also α. If this fraction is c (α)/R^2, where $1/R^2$ expresses the spreading of the light when the fibre is considered to be a point source. The fluorescence power per unit area of

emitting tumour surface is,

$$P_F = const.E_V Yg(\Theta)\frac{c(\alpha)}{R^2}.$$

The area contributing to the total fluorescence signal power, P_F, increases as R^2, so for a uniformly emitting flat area;

$$P_F \propto \frac{1}{R^2}.$$

For a unit area of tumour,

$$P_F \propto \frac{1}{R^4}.$$

There is a strong dependence on the distance R and on functions of α and Θ.

Now consider the reflected violet power collected by the fibre. The reflected power contributed by unit area of tumour surface is,

$$P_R = const.E_V R_V h(\Theta)\frac{c(\alpha)}{R^2}$$

where R_V is the violet reflectivity, h (Θ) is the angular distribution of the reflected violet and the other factors are the same as for the fluorescence as the same collecting fibre is used. Again, the reflected power collected may vary as $1/R^4$ (small area only) to $1/R^2$ (large area illuminated by the violet). If one takes the ratio of P_F to P_R, then

$$\frac{P_F}{P_R} = \frac{Yg(\Theta)}{R_V h(\Theta)}$$

because the violet irradiance and light collection efficiency are the same for

both. The distance dependence and part of the angular dependence cancels. If, in addition, the angular distribution of emission is the same then $g(\Theta)=h(\Theta)$ and

$$\frac{P_F}{P_R}=\frac{Y}{R_V}.$$

In as much as this holds for each surface element, it holds for all elements collectively. It is only necessary then to separate the induced red fluorescence from the reflected violet and ratio the corresponding signals. By using such a dimensionless ratio, immunity is provided against variation in distance, fibre-tip target, surface effects and drifts in lamp intensity during an endoscopic procedure.

Such fluorescence-ratio systems were used directly or with an endoscope, while exciting the fluorescence with a laser or incoherent light source. Although this instrument removed the dependence on distance, angle and source power, the output was influenced by the tissue reflectivity of the violet light and fluorescence yield. The reflectivity of a large tumour is likely to differ from that of a small tumour, which complicated the process of distinguishing the audio signal associated with different size tumours. Thus, it is evident that audio techniques required considerable training and skill before the clinician was able to associate a certain tone from the loud speaker with a tumour site. For these reasons, audio-output techniques [2,3,4] suffered ambiguity and were not optimal for straightforward implementation into the clinical environment.

Profio [5] subsequently altered this system by displaying the output signal as an image. To avoid the dependence of the ratio on the reflectivity of the tissue, the instrument was modified to ratio the red-to-green (562±20nm) signal.

A number of other systems, which used this fluorescence-ratio technique, have been reported in the literature. One system was designed for the

detection of cancerous tissue within Barrett's Oesophagus [6]. This system used a combination of Photofrin with a nitrogen pumped dye laser (405nm). The intensity of red induced fluorescence at 630nm was ratioed with the broad autofluorescence peak at 500nm. Because the intensity of the autofluorescence, within the healthy tissue, was on average 6.5 times higher than that in the cancerous tissue, the resulting signal efficiently distinguished adenocarcinoma from Barrett's and normal tissue.

The drawback of this system involved the fact that it recorded point measurements and only 30 sites were evaluated during a 15-minute endoscopic session. This procedure was too slow in a routine clinical setting and made it difficult to cover the whole area of Barrett's. The consequences of point monitoring systems are the length of the procedures and the fact that biopsies cannot be taken as the measurement probe occupies the biopsy channel of the endoscope. There are a number of issues associated with a lengthy diagnosis, such as cost, time, inconvenience and patient waiting lists, which affect both the patient and the clinician. It is vital that the implications of using each technique and piece of equipment are considered at every stage of the developmental process. If this does not occur, then issues such as those mentioned above will prevent the system being accepted into clinical environments.

For medical diagnostics, imaging systems are clearly advantageous over point monitoring instrumentation. However, a system based on spectral imaging poses some problems, since a choice has to be made as to which are the most appropriate spectral bands to monitor. Some detection units used more than two spectral bands for the detection of cancerous tissue. Two such systems were developed by Svanberg et al. [7,8] and Zeng et al. [9]. In the former system, four filtered images were simultaneously captured by a gated intensified CCD camera, via image splitting optics consisting of four individually adjustable mirror segments. The fluorescence was induced by light at 390nm produced by a frequency-doubled alexandrite laser. Three of the images were processed to form the following optimised contrast function

of the measured spectral intensities at 630nm, 600nm and 470nm,

$$\text{Signal}=\frac{I(630nm)-k_1 I(600nm)}{k_2 I(470nm)}.$$

k_1 and k_2 were constants with different values for different applications. The optimised function was displayed as a false colour image. This showed promising results because both the fluorescence from the photosensitiser and autofluorescence from the native tissue molecules contributed to the demarcation of the tumour.

The system by Zeng[9] utilised only the tissue autofluorescence and incorporated three imaging modes, including two ratios between different spectral regions. The first imaging mode consisted of the conventional white light imaging, while the second was based on the ratio of the red and green fluorescence band. The third imaging mode was a ratio of the green fluorescence and red-near-IR reflectance image, which acted as a reference image for normalisation purposes. The unit consisted of a filtered mercury arclamp, two intensified CCD cameras, a colour camera, a fibre optic endoscope and computer based control facilities.

Although the above systems appear to be successful at diagnosing cancerous tissue, attributes such as the size, weight and cost of the equipment represent definite problems. The use of the frequency-doubled alexandrite laser, in the Svanberg unit, meant that the system was cumbersome, expensive and required specialised skills for its operation and maintenance. The consequence of coupling three cameras to the end of the endoscope in the Zeng system was the increased weight of the endoscopic unit, which restricted endoscopic manipulation by the clinician.

2.2.2 Differential Normalised Fluorescence (DNF)

Differential normalised fluorescence (DNF) [10,11,12] demarcates cancerous tissue by assessing the difference between a normalised fluorescence spectrum and an average spectrum (baseline curve), recorded from a number of healthy tissue sites. The measured fluorescence spectrum is normalised by dividing the intensity at each emission wavelength by the integrated area under the total spectrum (430nm to 720nm). This has the effect of making each measurement less dependent on the intensity, while amplifying the spectral structure of the fluorescence signal. A baseline curve is calculated by measuring the mean average of normalised fluorescence spectra recorded from normal tissue samples. The DNF curve for a tissue sample is determined by finding the difference between the normalised tissue spectrum and the baseline curve. Example sets of graphs are shown in figure 2.2.

The equipment used consisted of a pulsed nitrogen pumped dye laser (410nm) and an intensified photodiode array coupled to a fibre optic probe. The placing of the probe in contact with tissue, triggering the laser pulses and collecting the fluorescence emission required 5 to 10 seconds per location. Hence, a long procedure was necessary to ensure rigorous screening, which involved extra cost to the health service provider and longer patient waiting lists.

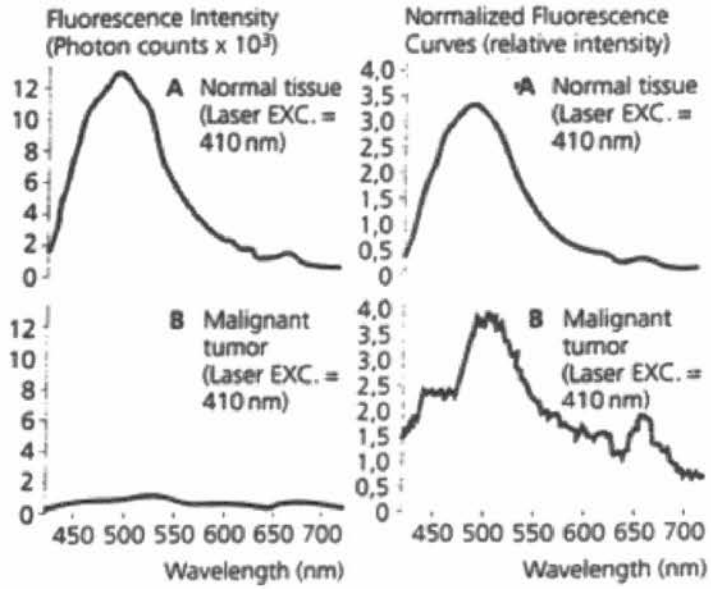

Figure 2.2: Differential normalised fluorescence compensates for the weaker intensity of fluorescence over dysplastic or malignant areas[13].

2.2.3 Fluorescence Lifetime Imaging

The selectivity criterion for the early detection of cancer, using fluorescence spectroscopy, can be found either in the spectral or in the time domain. The majority of research documented, to date, has exploited the spectral domain for the detection of cancerous tissue. However, some research groups have been utilising the time domain approach. This technique is known as fluorescence lifetime imaging (FLIM) and relies on measuring the lifetime of a fluorescence signal, rather than the intensity.

Fluorescence lifetimes can be measured in the frequency [14,15] or the temporal domain [16,17,18,19,20,21]. In the frequency domain, samples are typically excited with a sinusoidally modulated continuous wave laser and the fluorescence lifetime is inferred by measuring the phase change and modulation depth of the emitted fluorescence signal. In the time domain, samples are excited with a short light pulse and the temporal decay of the resulting fluorescence is directly recorded. The use of a spatially resolved detector, in either domain, provides a fluorescence lifetime map or image.

The lifetime of fluorescence originating from either endogenous or exogenous molecules can be measured to distinguish the cancerous tissue from the surrounding healthy tissue. If an exogenous photosensitiser is administered, it emits a long lifetime fluorescence that differs, in both spectrum and time decay, from the natural fluorescence of biological tissue, which has a much shorter lifetime [18]. Thus, the exogenous fluorescence is acquired after a suitable delay, when the short living emission is no longer present. In the case of endogenous molecules, the fluorescence lifetimes of certain native molecules are altered according to the degree of malignancy of the tissue and can thus be used to distinguish the cancerous and healthy tissue.

An example of a system working in the time domain is that developed at Imperial College by French and colleagues [20], who excited endogenous fluorescence with 10ps pulses at 415nm. These pulses were generated by amplifying 100fs pulses, from a commercial femtosecond Ti:sapphire laser, in a Cr:LiSAF regenerative amplifier and then frequency doubling to the blue. After each excitation pulse, the emitted fluorescence distribution was imaged onto a time-gated image intensifier. By recording a series of time gated images, the temporal decay of the fluorescence was measured simultaneously for each pixel in the field of view. A value for the fluorescence lifetime was determined for each of these pixels using a mathematical algorithm. The distribution of the fluorescence lifetime was displayed either as a colour map or in greyscale. It is reported that this system is able to image lifetime differences of as small as 10psec. When using this method, the endogenous fluorescence does not impair the tumour diagnosis. Figure 2.3 illustrates the principle of time domain FLIM.

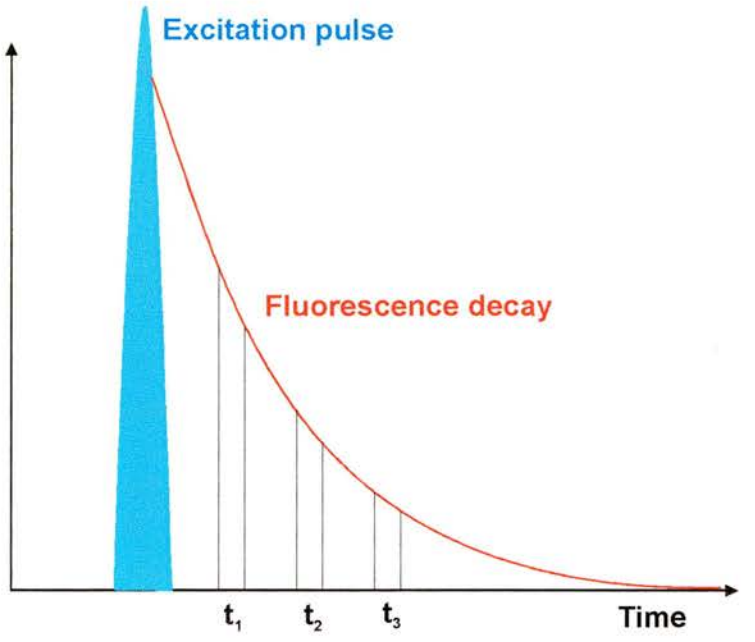

Figure 2.3: Graph illustrating the principle of time domain-fluorescence lifetime imaging

One example of a detection unit working in the frequency domain is that reported by Mizeret and colleagues [14]. This unit measured the fluorescence lifetimes of endogenous molecules to distinguish the cancerous and healthy tissue. Typical fluorescence lifetimes of such biological molecules range from tens of picoseconds to tens of nanoseconds. This technique consisted of modulating the excitation light and measuring the phase shift or the demodulation of the fluorescence from which the lifetimes were deduced.

The excitation was provided by a continuous wave laser such as Ar+, Kr+ or dye laser, which was modulated in amplitude by an electro-optic modulator. Two images were recorded on separate intensified CCD cameras. The one image was of the excitation light backscattered by the tissue and was considered as the reference image. The second image contained the information about the phase shift and demodulation of the emitted fluorescence, where the gain of this second image intensifier was modulated at the same frequency as the excitation light. The phase between the two modulations was adjusted by a phase shifter. The resulting steady-state fluorescence image was recorded by the CCD camera and the fluorescence

signal was measured with respect to the backscattered image. The relative phase and modulation of the fluorescence signal was calculated and used to determine the effective fluorescence lifetime images.

Fluorescence lifetime imaging is an exceptionally high-resolution technique that offers great potential for the in-vivo detection of early cancer. However, a number of inherent drawbacks associated with such systems prevent widespread use within the clinical environment. This technique utilises complex equipment that is not economically viable, to the health provider, for incorporation within a cancer-screening programme. There are very few in-vivo studies reported in the literature that defend this methods effectiveness for use in the clinical environment. Due to the cost and complexity associated with this technique, perhaps it could be used to provide further diagnostic information after an initial cancer diagnosis using another detection method.

2.2.4 Two-Wavelength Excitation

One of the problems, which arise with detection methods relying on the use of an exogenous photosensitiser, is loss of optical contrast between the healthy and cancerous tissue. This reduction in optical contrast is due to the presence of a background autofluorescence originating from the endogenous molecules present in the body.

Braumgartner et al. [22] reported in 1987 how they used two-wavelength excitation to overcome the problem of loss of contrast due to the presence of autofluorescence. The photosensitiser used was a mixture of dihaematoporphyrin-ether and dihaematoporphyrin-ester (DHE) and was efficiently excited with violet (405nm) light. After performing experiments in the bladder, it was observed that the intensity of the excited autofluorescence was similar with both blue (470nm) and violet light. Whereas, the excitation efficiency of DHE in tissue, was five times higher

with violet light than with blue light. Thus, subtraction of the blue light excited fluorescence from the violet light excited fluorescence resulted in a spectrum originating from the DHE only. Therefore, the sensitivity of the detection unit was increased as the system eliminated the autofluorescence, while the intensified camera imaged the induced DHE fluorescence. The full spectral fluorescence bandwidth of the DHE lies between 600 and 700nm. Figure 2.4 illustrates graphically the principle of two-wavelength excitation.

A modified krypton-ion laser provided the excitation and an electronic circuit allowed for switching between the violet and blue light by tilting the resonator mirrors alternately. The electronics permitted switching every 40milliseconds; thus enabling the display of difference images every 80 milliseconds.

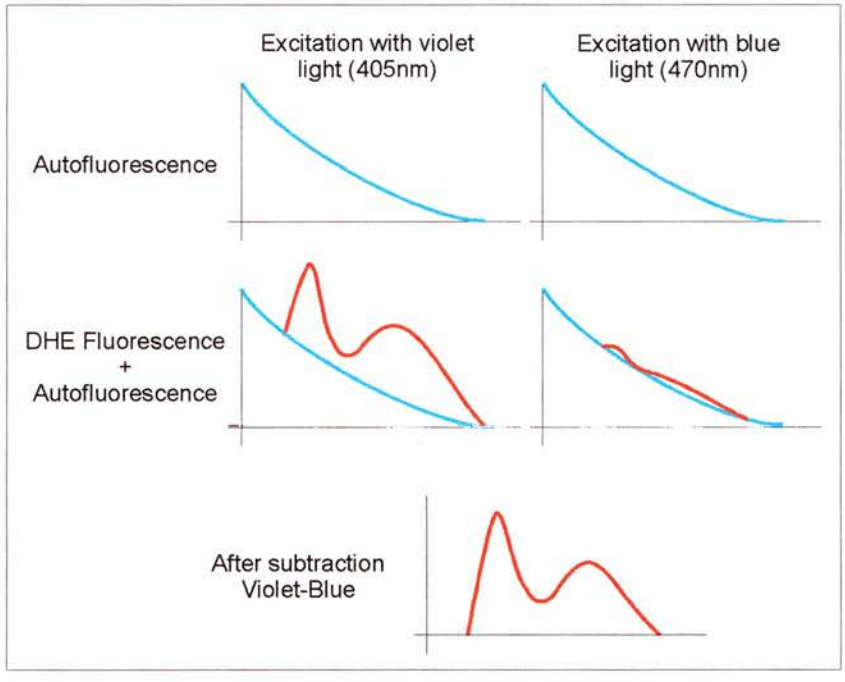

Figure 2.4: Principle of fluorescence excitation of DHE in tissue with two different wavelength ranges and subsequent subtraction for elimination of autofluorescence[22]

Due to the continual muscular movements within the GI tract, this system suffered pixel alignment problems between the consecutively acquired images. Hence, identical pixel subtraction was exceptionally difficult to

achieve. Also, the large expense associated with the laser system and the necessary modifications to enable emission of both violet and blue light, meant that this system was inappropriate for the clinical environment.

2.3 Elastic Scattering Spectroscopy

Elastic scattering spectroscopy (ESS) [23,24,25] takes advantage of the theory first described by Gustov Mie in 1808. This effect describes how the scattering of light is wavelength dependent and the greatest scattering occurs in photons of wavelength similar to the size of the particles, through which the light is passing. The wavelengths in the 320-900nm range are similar in size to cell nuclei and intracellular particles.

The most likely mechanism of interaction for light in tissue is elastic scattering. Hence, ESS ignores the relatively weak autofluorescence signal and instead measures the elastic optical transport of tissue, which consists of data of elastic scattering and absorption characteristics. The majority of cancers exhibit significant architectural changes at the cellular and subcellular level. Thus, ESS presents a graphic and objective representation of the same characteristics that a pathologist would view under the microscope, such as enlargement of cell nuclei, cell crowding and disorientation of architecture.

White light or more specific wavelengths may be used to irradiate the tissue. The scattered light from the tissue under observation is returned to a spectrometer by a fibre and the intensity of light is displayed over a broad wavelength range. The principle of ESS is illustrated in figure 2.5.

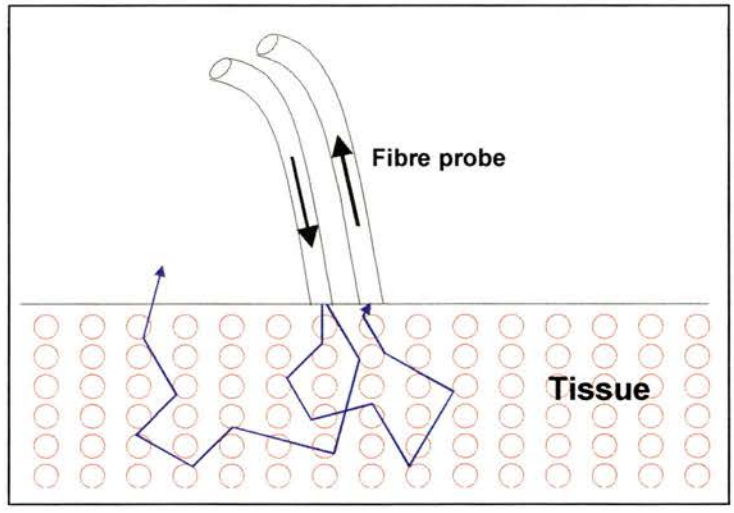

Figure 2.5: Illustration of the principles of ESS with light delivery fibre and scattered light collection fibre

In clinical demonstrations [26], the probe was designed to be in contact with the tissue and had separate illumination and scattered light collection fibres. Hence, no light was collected from surface reflections. With ESS the resulting effective path length of the collected photons was generally several times greater than the actual separation of the fibre tips. Consequently, the system was sensitive to the optical absorption bands of the tissue components over its effective operating range of 300-750nm.

Elastic scattering spectroscopy is possibly the cheapest and most accessible detection technique. The signals are large, the information can be gathered rapidly and the equipment is relatively inexpensive. However, the disadvantages of this detection method lie in its point monitoring nature and its lack of specificity, which restricts its use for detecting pre-cancerous tissue within the clinical environment.

2.4 Optical Coherence Tomography (OCT)

Optical coherence tomography (OCT) [27,28,29,30] involved using near-infrared photons to provide micrometer scale, cross-sectional images in biological systems. The ultra-high-resolution imaging capabilities of OCT provided

diagnostic information on tissue microstructure that was comparable to conventional histology. Imaging of structures deep in the body was not possible due to light scattering but many parts could be accessed both directly and by use of an endoscope.

OCT is based on a classical optical measurement technique known as white light interferometry, which was first described by Newton. The OCT system was similar to a Michelson-type Interferometer and used fibre optics and a compact diode light source. Light from the source was fibre coupled and split evenly by an optical fibre splitter. One of the fibres directed light to the tissue being imaged and the other fibre to a moving reference mirror. The position of the reference mirror was precisely controlled by system electronics and a computer. The light signal reflected from the tissue was recombined with the signal reflected from the reference mirror. Interference between these two reflected light signals occurred only when the two path lengths were matched to within the coherence length of the light source. This allowed a precise determination of the distance within the tissue from which the light was reflected. OCT therefore measured the intensity of backscattered light from within the tissue plotted as a function of depth.

The light beam was scanned across the tissue and the axial reflectance profiles at several transverse positions were recorded by computer. The acquisition times ranged from 10 to 45 seconds depending on the size of the image. The result was a two dimensional cross sectional representation of the optical backscattering properties of the tissue. This was displayed as a grey scale or false colour image. Figure 2.6 illustrates the equipment used for OCT.

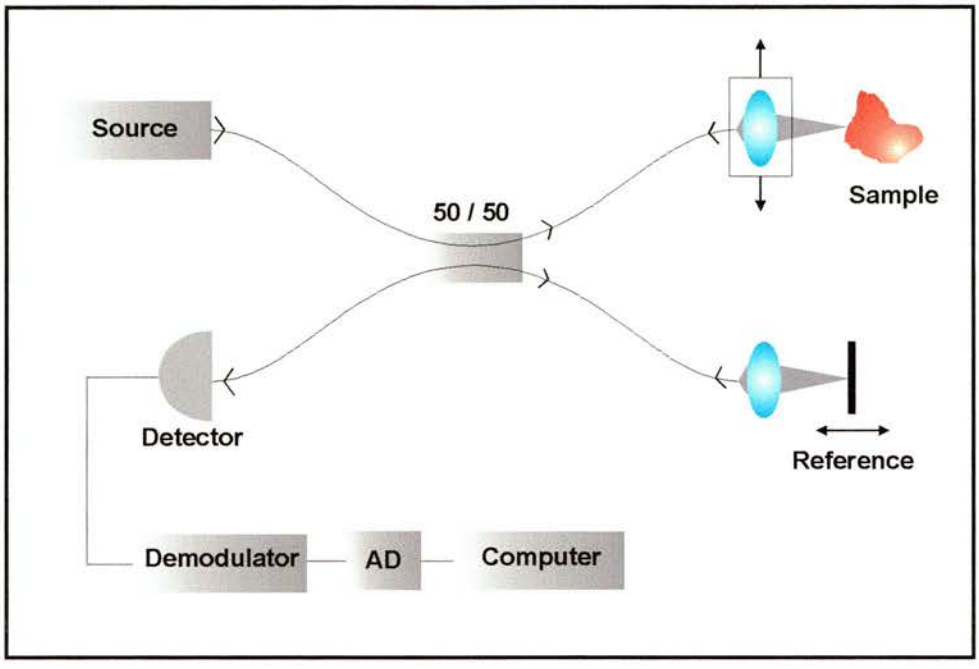

Figure 2.6: Equipment set-up used for OCT

The axial resolution of the OCT imaging was determined by the coherence length of the light used. For a typical system that used a compact diode light source, the axial resolution was between 10 and 20μm. If alternative light sources, such as ultra short pulsed lasers were used, the axial resolution was between 2 and 4μm.

Although tissue strongly absorbs visible wavelengths of light, most tissues are relatively non-absorbing at infrared wavelengths. The depth of imaging in this technique is restricted by the optical scattering within tissue rather than the absorption. Scattering restricts the depth of imaging as it causes attenuation of the light as well as randomisation of image information. If light at optimised wavelengths is used, imaging depths of 1 to 2 mm can be achieved.

The concept of OCT was pioneered by J. Fujimoto and colleagues at the Massachusetts Institute of Technology [31] for the imaging of ocular structures, for example for corneal profiling.

OCT has the potential to detect subtle structural changes within tissue. However, for the early detection of pre-cancerous tissue, the measurement of biochemical rather than structural abnormalities may be necessary. OCT is robust, portable and low cost and can be readily interfaced with optical fibre techniques and endoscopes. However, the limitations of the system involve achieving adequate imaging speed for clinical applications and the relatively shallow depth of penetration of light.

The most likely use for OCT will be in the staging of gastrointestinal cancers, after they have been discovered using other methods. This could be achieved using the technique to measure the depth of abnormal growth at a particular position within the GI tract.

2.5 Raman Spectroscopy

Raman light scattering techniques and infrared absorption are used to determine the vibrational modes of molecules in order to gain information on their shape, symmetry and bond character. A Raman spectrum is generated by a frequency shift in the excitation light (a form of inelastic scattering) created by the vibrational and rotational frequency of the molecules within the tissue. Raman spectroscopy [32,33] involves exciting tissue with monochromatic light and measuring the frequency shift of the scattered photons. Since most biological molecules are Raman active, a distinctive spectral signature can be measured that represents a form of optical biochemistry.

If a monochromatic beam of photons passes through any medium, a proportion will be scattered in all directions. The scattered photons will consist of radiation of the incident frequency, known, as Rayleigh scattering (elastic process), while a small component will emerge with discrete frequencies slightly below that of the incident, known as Raman scattering.

Figure 2.7 illustrates the principles associated with the detection of Raman scattering.

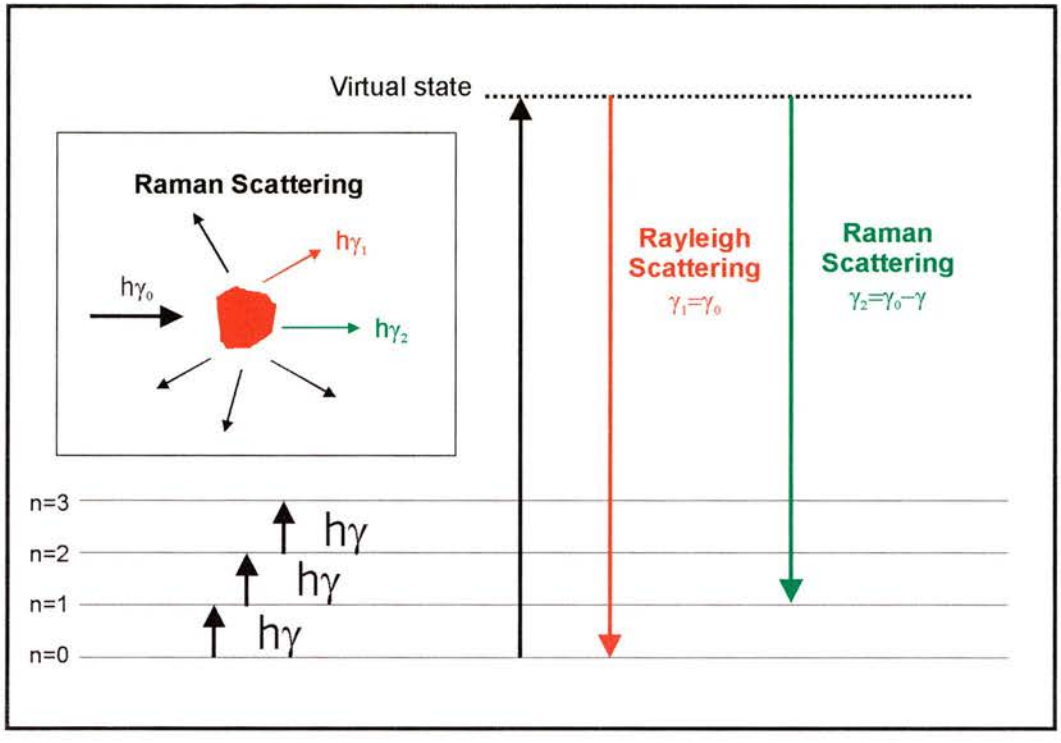

Figure 2.7: Diagram showing energy levels and the Rayleigh and Raman scattering from a tissue sample[34]

Figure 2.7 illustrates how the molecules within tissue are excited to a virtual state after illumination with monochromatic light. From such a state, most molecules relax down to the ground state, scattering light with unchanged wavelength (Rayleigh Scattering). However, some molecules relax into an excited vibration state, sending out a photon with lower energy than the incoming photon (Raman Scattering). The energy difference is the vibration energy. By measuring the energies of all Raman scattered photons; a vibration spectrum can be obtained.

The Raman effect occurs without photon absorption by the molecule but rather the molecule is perturbed by the photon and it is induced to undergo a vibrational or rotational transition. The energy shift associated with Raman scattering is independent of the exciting frequency and is characteristic of

the scattering molecules [35]. For the detection of cancer, suitable molecules for this study include proteins, nucleic acids, nucleosomes and cell membranes [13].

Detection systems measure the energies of all Raman scattered photons and display a Raman spectrum plot. The displayed spectrum is a plot of the scattered intensity as a function of energy difference between the incident and scattered photons. The loss or gain in the photon energies corresponds to the difference in the initial and final vibrational energy levels of molecules participating in the interaction. A Raman peak is spectrally narrow, easy to resolve and sensitive to molecular structure and the surrounding environment. Raman spectroscopy techniques can thus provide specific histological information about the tissue.

Since tissue is inhomogeneous in composition and highly scattering, the full analysis of Raman signals requires an understanding of tissue optical parameters. Raman signals are inherently weak and in addition, early diagnosis of disease requires detection of tissue molecular constituents present in low concentrations. The complex nature of tissue composition results in absorption of light throughout the entire UV-visible region and the subsequent intense fluorescence emission strongly interferes with weak Raman signals.

The drawback of this method is that Raman scattering is an inherently weak process and is typically 10^{-9} to 10^{-6} of the Rayleigh background. It is therefore difficult to observe without intense monochromatic excitation and a sensitive detector.

2.6 Summary

For a cancer detection system to be successfully incorporated within a screening programme, it must within seconds and with a high degree of sensitivity and specificity, accurately and easily produce an answer to the question of whether tissue is cancerous. The device must be economically viable, user-friendly and durable enough to withstand use within the clinical environment. The system must be able to provide more information than that which is already apparent to a trained endoscopist's eye and must have been proved successful during in-vivo trials.

Elastic scattering spectroscopy is possibly the cheapest and most convenient cancer detection technique, which probes the morphological characteristics of cancer and pre-cancerous cells as well as changes in tissue microstructure [36]. However, it is a point measurement system, which makes the diagnosis slow and somewhat random. Optical coherence tomography has the potential to detect structural changes within the tissue. However, due to the nature of pre-cancerous cells, detection of biochemical rather than structural changes may be necessary. The main attraction of OCT is its use in the staging of cancers after they have been diagnosed through other techniques. Although Raman spectroscopy shows potential for diagnosis within localised sites, technical problems need to be overcome to enable routine in-vivo measurements.

One of the main problems with most reported cancer detection techniques is that they have not undergone in-vivo trials. Transplantable tumours inbred in mice and rats are the most frequently used animal models for pre-clinical studies on detection units and can provide a valuable insight into the applications of the system. However, there are several problems associated with these trials as the tumours are rarely transplanted into the tissue of origin. The transplanted cancers are not the same as pre-cancerous tissue in terms of biochemistry and the tumours are usually well demarcated and

mostly not invasive. For this reason, care must be taken in extrapolating data obtained in these models to the clinical situation.

Many groups also carry out the majority of system trials on resected specimens and seldom on living patients. However, it has been shown in a number of studies [37] that significant changes in the fluorescence spectra occur after a specimen has been removed from the body. Because fluorescence signals are in general sensitive to physical factors such as pH and oxidative state, fluorescence data obtained from ex-vivo samples may not accurately reflect the in-vivo situation. Based on these observations, one must be cautious about using any diagnostic algorithm developed from ex-vivo specimens for assessing tissue in vivo. This suggests that it is vital that only systems, which have undergone rigorous in-vivo testing, are considered as potential cancer detection systems.

The different cancer detection techniques are generally a matter of scale, with some methods probing the properties of whole cells and others measuring the subcellular molecular properties. For this reason, as with cancer treatments, the different parts of the anatomy and types of tissue require distinct detection methods that provide specific diagnostic data. Thus, although the methods discussed above are not appropriate for incorporation into a cancer-screening programme, they may be used by the clinician to provide more in depth data, after an initial diagnosis.

The clinical advantages of fluorescence imaging techniques include; high signal sensitivity, suitability for examination of tissue surfaces, flexibility in the anatomical site investigated, reduction in the use of random tissue biopsies and the ease of use by the clinician. Although fluorescence diagnostics cannot replace biopsies and histology, it can guide the physician during endoscopy in selecting biopsy sites in suspicious areas. If multiple biopsies are taken from such an area, the probability of finding early malignant tumours is very high as compared with the random biopsy approach.

Cancer screening programmes, using fluorescence imaging provides the potential for reduced healthcare costs, due to its minimally invasive nature, the speed of diagnosis and the improved patient outcome. However, it is critical that the clinical studies to evaluate fluorescence spectroscopy and imaging are performed in a medically relevant context.

Following a comprehensive consideration of all of these facts, it was decided that the cancer detection systems developed in this project would exploit the principles of fluorescence detection and thus fluorescence imaging. In the four chapters that follow, two detection systems developed through this research are discussed and important results are highlighted.

2.7 References

[1] R.L. Lipson, E. J. Baldes, A. M. Olsen. "Hematoporphyrin Derivative: A new aid for endoscopic detection of malignant disease." *J. Thoracic. and Cardiovas. Surg.*, 1961, **42**, 623.

[2] J.H. Kinsey, D.A. Cortese. "Endoscopic system for simultaneous visual examination and electronic detection of fluorescence." *Rev. Sci. Instrum.*, 1980, **51**, 10.

[3] A.E. Profio, D.R. Doiron, J. Sarnaik. "Fluorometer for endoscopic diagnosis of tumours." *Med. Phys.*, 1984, **11**, 4.

[4] P. S. Andersson, S. Montan, T. Persson, S. Svanberg, S. Tapper, S. E. Karlsson. "Fluorescence endoscopy instrumentation for improved tissue characterisation." *Med. Phys.*, 1987, **14**, 4.

[5] A. E. Profio. " Laser excited fluorescence of hematoporphyrinDerivative for diagnosis of cancer." *IEEE Journal of Quantum Electronics*, 1984, **QE-20**, 1502.

[6] C. Stael von Holstein, A. M. K. Nilsson, S. Andersson-Engels, R. Willen, B. Walther, K. Svanberg. "Detection of adenocarcinoma in Barrett's oesophagus by means of laser induced fluorescence." *Gut*, 1996, **39**, 711.

[7] S. Andersson-Engels, J. Johnasson, K. Svanberg, S. Svanberg. "Fluorescence imaging and point measurements of tissue: Applications to the demarcation of malignant tumours and atherosclerotic lesions from normal tissue." *Photochemistry and Photobiology,* 1991, **53**, 807.

[8] K. Svanberg, I. Wang, S. Colleen, I. Idvall, C. Ingvar, R. Rydell, D. Jocham, H. Diddens, S. Bown, G. Gregory, S. Montan, S. Andersson-Engels, S. Svanberg. "Clinical multicolour fluorescence imaging of malignant tumours-initial experience." *Acta. Radiologica.*, 1998, **39**, 2.

[9] H. Zeng, A. Weiss, R. Cline and C.E. MacAulay. "Real-time endoscopic fluorescence imaging for early cancer detection in the gastrointestinal tract." *Bioimaging*, 1998, **6**, 151.

[10] T. Vo-Dinh, M. Panjehpour, B. F. Overholt, C. Farris, F. P. Buckley, R. Sneed. "In vivo cancer diagnosis of the esophagus using differential normalized fluorescence (DNF) indicies." *Lasers in Surgery and Medicine*, 1995, **16**, 41.

[11] M. Panjehpour, B. F. Overholt, T. Vo Dinh, R. C. Haggitt, D. H. Edwards, F. P. Buckley. "Endoscopic Fluorescence Detection of high-grade Dysplasia in Barretts Esophagus." *Gastroenterology*, 1996, **111**, 93.

[12] T. Vo Dinh, M. Panjehpour, B. F. Overholt, F. P. Buckley. "Laser-Induced differential fluorescence for cancer diagnosis without biopsy." *Applied Spectroscopy*, 1997, **51**, 58.

[13] A. G. Bohorfoush. "Tissue Spectroscopy for Gastrointestinal Diseases." *Endoscopy*, 1996, **28**, 372.

[14] J. Mizeret, G. Wagnieres, T. Stepinac, H. Van den Bergh. "Endoscopic tissue characterisation by frequency-domain fluorescence lifetime (FD-FLIM)." *Lasers in Medical Science*, 1997, **12**, 209.

[15] J. R. Lakowski, H. Szmacinski, K. Nowaczyk, K. W. Berndt, M. Johnson. "Fluorescence lifetime imaging." *Anal. Biochem.*, 1992, **202**, 316.

[16] R. Cubeddu, G. Canti, A. Pifferi, P. Taroni, G. Valentini. " Fluorescence Lifetime Imaging of Experimental Tumors in Hematoporphyrin Derivative –Sensitized Mice." *Photochemistry and Photobiology*, 1997, **66**, 229.

[17] H. Schneckenburger, K. Konig, K. Kunzi-Rapp, C. Westphal-Frosch, A. Ruck. "Time resolved in vivo fluorescence of photosensitising porphyrins." *J. Photochem. Photobiol. B:Biol.*, 1993, **21**, 143.

[18] R. Cubeddu, G. Canti, P. Taroni, G. Valentini. "Study of porphyrin fluorescence in tissue samples of tumour –bearing mice." *Journal of Photochemistry and Photobiology B:Biology*, 1995, **29**, 171.

[19] K. Dowling, M. J. Dayel, M. J. Lever, P. M. W French, J. D. Hares, A. K. L. Dymoke- Bradshaw. "Fluorescence lifetime imaging with picosecond resolution for biomedical applications." *Optics Letters*, May 1998, **23**, 810.

[20] K. Dowling, S. C. W. Hyde, J. C. Dainty, P. M. W. French, J. D. Hares. "2-D fluorescence lifetime imaging using a time-gated image intensifier." *Optics Communications*, 1997, **135**, 27.

[21] K. Dowling, M. J. Dayel, S. C. W. Hyde, P. M. W. French. "High resolution time-domain fluorescence lifetime imaging for biomedical applications." *Journal of modern optics*, 1999, **46**, 199.

[22] R. Baumgartner, H. Fisslinger, D. Jocham, H. Lenz, L. Ruprecht, H. Stepp, E. Unsold. "A fluorescence imaging device for endoscopic detection of early stage cancer-Instrumental and experimental Studies." *Photochemistry and Photobiology*, 1987, **46**, 759.

[23] J. R. Mourant, I. J. Bigio, J. Boyer, R. L. Conn, T. Johnson, T. Shimada. "Spectroscopic diagnosis of bladder cancer with elastic light scattering." *Lasers Med. Surg.*, 1995, **17**, 350.

[24] J.R. Mourant, J. D. Boyer, T. M. Johnson, J. Lacey, I. J. Bigio. " Detection of gastrointestinal cancer by elastic scattering and absorption spectroscopies with the Los Alamos Optical Biopsy System." *SPIE Proc.*, 1995, **2387**, 210.

[25] I. J. Bigio, J. R. Mourant. "Ultraviolet and visible spectroscopies for tissue diagnostics: fluorescence spectroscopy and elastic- scattering spectroscopy." *Phys. Med. Biol.*, 1997, **42**, 803.

[26] J. R. Mourant, I. J. Bigio, J. Boyer, T. M. Johnson, J. Lacey. "Elastic scattering spectroscopy as a diagnostic for differentiating pathologies in the gastrointestinal tract: Preliminary testing." *J. Biomed. Opt.*, 1996, **1**, 1.

[27] G. J. Tearney, M. E. Brezinski, J. F. Southern et al. "Optical biopsy in human gastrointestinal tissue using optical coherence tomography." *Am. J. Gastroenterol.*, 1997, **92**, 1800.

[28] J. G. Fujimoto, M. E. Brezinski, G. J. Tearny, S. A. Boppart, B. Bouma, M. R. Hee, J. F. Southern, E. A Swanson. "Optical biopsy and imaging using optical coherence tomography." *Nature Medicine*, 1995, **1**, 970.

[29] M. E. Brezinski, G. J. Tearney, B. E Bouma, J. A. Izatt, M. R. Hee, E. A. Swanson, J. F. Southern, J. G. Fugimoto. "Optical coherence tomography for optical biopsy." *Circulation*, 1996, **93**, 1206.

[30] M. E. Brezinski, G. J. Tearney, S. A. Boppart, E. A. Swanson, J. F. Southern, J. G. Fugimoto. "Optical biopsy with optical coherence tomography: feasibility and surgical diagnostics." *J. Surgical Research*, 1997, **71**, 32.

[31] D. Huang, E. A Swanson, C.P Lin, J. S. Schuman, W. G. Stinson, W. Chang, M. R. Hee, T. Flotte, K. Gregory, C. A. Puliafito, J. G. Fujimoto. "Optical coherence tomography." *Science*, 1991, **254**, 1178.

[32] A. Mahadevan-Jensen, R. Richards-Kortum. "Raman spectroscopy for the detection of cancers and precancers." *J. Biomed. Opt.*, 1996, **1**, 31.

[33] A. Mahadevan-Jensen, N. Ramanujam, M. F. Mitchell. "Optical techniques for the diagnosis of cervical precancers: comparison of Raman and fluorescence spectroscopies." *SPIE Proc.*, 1995, **2388**, 110.

[34] Picture from web page www.ifm.liu.se/~hanka/methods/raman.spectroscopy.

[35] H. Barr, T. Dix, N. Stone. "Optical spectroscopy for the early diagnosis of gastrointestinal malignancy." *Lasers Med. Sci.*, 1998, **13**, 3.

[36] J. R. Mourant, I. J. Bigio, J. Boyer, R. L Conn, T. Johnson, T. Shimada. "Spectroscopic diagnosis of bladder cancer with elastic light scattering." *Lasers Med. Surg.*, 1995, **17**, 350.

[37] K. T. Schomacker, J. Frisoli, C. Compton, T. Flotte, J. Richter, N. Nishioka, T. Deutsch. "Ultraviolet Laser- Induced Fluorescence of Colonic Tissue: Basic Biology and Diagnostic Potential." *Lasers in Surgery and Medicine*, 1992,**12**, 63.

CHAPTER THREE

DETECTION SYSTEM FOR THE GI TRACT-DEVELOPMENTAL PROCESS

The development of the endoscopic cancer detection system involved the building of two generations of the instrumentation. In this chapter, the aims and specifications for the endoscopically-based detection system are discussed along with the developmental process used for the construction. The first and second-generation systems will be described in detail, in chapters four and five. The operating principles and equipment common to both detection units are discussed in this chapter.

3.1 Introduction

The objective of the research, detailed in the following two chapters, was to design and develop an endoscopically-coupled system for the detection of pre-cancerous tissue within the GI tract. The system is intended for use within a clinical programme for the screening of patients at high risk of

developing cancer. The specifications set out at the inception of the project were as follows:

- detection equipment should be fully conducive to the clinical environment for which it is intended,
- the equipment should be compatible with standard endoscopic techniques and associated medical procedures,
- the prototype unit should be an economically viable solution to the early detection of cancer,
- minimal specialist training should be required.

The development of medical equipment involves testing each element of the detection unit within the clinical environment. Consequently, there were a number of stages involved in the production of the detection system, before the final product was deemed appropriate for use by the clinicians. The developmental process for the endoscopic detection system involved three distinct stages. These stages were as follows; evaluation of the fundamental principles of the task; construction and testing of the first generation system and the subsequent building of an enhanced second-generation system, where significant modifications were incorporated.

In this chapter, the requirements for an endoscopically-coupled optical detection system are introduced. The subject matter in chapters four and five relate to the specific details of the first and second generation systems and both ex-vivo and in-vivo results associated with the performance of each unit are presented.

3.2 Research areas for system development

After lengthy considerations of cancer detection systems documented in the literature, both the clinicians and ourselves decided at the outset of this project that fluorescence detection was the most favourable technique for the early detection of pre-cancerous tissue. Consequently, the main

components involved in the detection process comprise a photosensitiser, a suitable excitation light source and a flexible endoscope. The flexible endoscope is necessary because it allows the observation of the inside of the GI tract, without the need for invasive surgery. (The construction of this endoscope is discussed in more detail in section 3.2.1.)

As detailed in chapter one, there are a number of photosensitising agents, which can be used to induce an optical contrast between cancerous and healthy tissue. However, 5-aminolevulinic acid (ALA) was considered the most appropriate for the purposes of detection, as it has a high selectivity in cancerous tissue and patients do not remain photosensitive for long periods.

Due to the principles associated with fluorescence detection, the developmental process comprised of six main design areas; the endoscope, illumination, imaging unit, control facilities, endoscopic coupling and light transmission. Each of these categories is illustrated in figure 3.1.

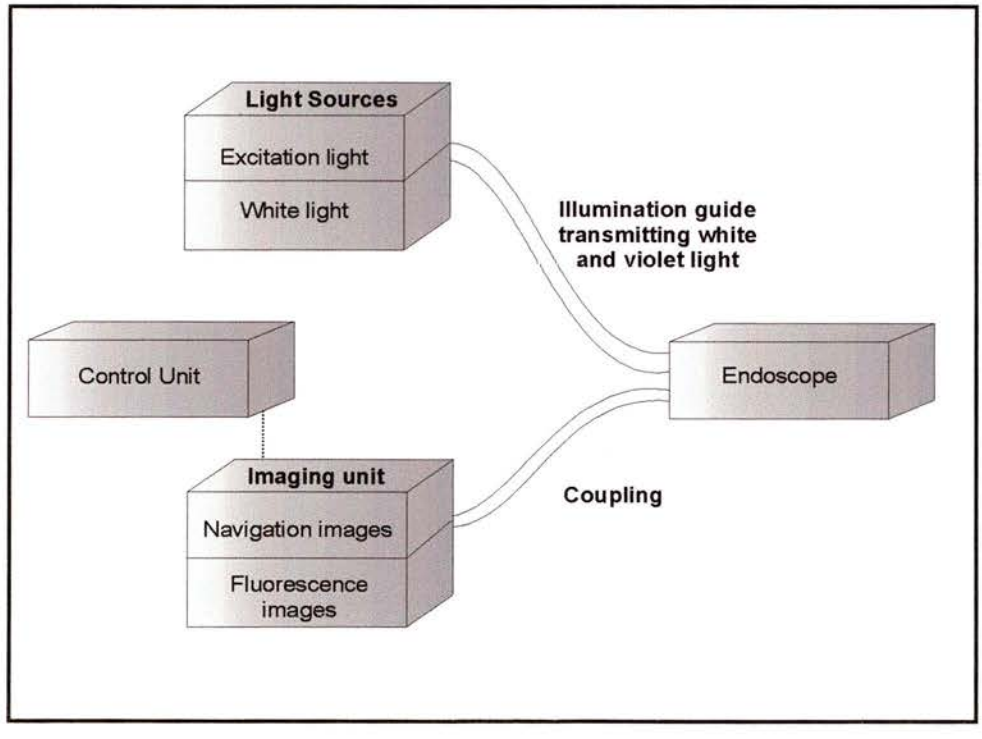

Figure 3.1: Research areas for development of detection system

In the following sections, each design area, illustrated in figure 3.1, is explored in detail.

3.2.1 What is an endoscope?

The endoscope is used by clinicians to observe the tissue and organs within a patient, without the requirement for incision. A number of tools are available to the clinician in order to perform tasks via the endoscope, which would otherwise have to be achieved through more invasive techniques. Endoscopes may be rigid or flexible, depending on the part of the anatomy for which they are intended. Endoscope is the generic name given to a family of instruments, each of which is specific to a certain part of the body. For example, a colonoscope is used for inspection of the colon and a gastroscope is used for the oesophagus and stomach.

The rigid endoscopes [1] use a train of lenses as an image transmission system, while the fully flexible endoscopes, employed in this research, use a specialised coherent fibre bundle. If one observes the end of an illuminated fibre, only a spot of light of a certain colour and intensity is seen. In order to create an image, a large number of fibres are grouped together. The pattern formed by the colour and intensity of the individual fibres is perceived as an image. For the image at the input of the bundle to be duplicated at the exit, it is necessary that the ends of each individual fibre occupy the same relative position at both the entrance and exit of the bundle. For this reason, a bundle of this arrangement is termed a coherent bundle or image bundle.

An image bundle is graded in terms of its resolving power, which is a measure of the image detail transmitted. The resolving power depends on the diameter of the fibre core, the thickness of the cladding and the alignment and orderliness of the packing of the fibres within the bundle. The smaller the fibre and the thinner the cladding, the greater the image resolution. In practice, the thickness of the cladding cannot be less than 1.5

microns for visible light because of production limitations. The number of individual fibres in an image guide ranges from 5000 to 40000. The diameter of the individual fibres varies between 8μm and 12μm, resulting in a bundle diameter of between 0.5 and 3 mm. Thus, if a CCD camera (753x576) is used to image the coherent bundle, the ratio of pixels to fibres in the image bundle would be on average 10:1. However, in reality, the bundle is circular and so the image does not occupy the entire face of the CCD. Thus, the number of pixels to every fibre is approximately half of the above mentioned ratio and so it is possible to see the honey comb effect on the image.

The endoscope also contains a fibre bundle for the coupling of the illumination into the body. The light guide is referred to as incoherent as the arrangement of the fibres is random at each end of the fibre bundle. Consequently, these bundles are very much cheaper to produce and are designed to maximise light carrying capabilities. Since resolution is not a factor, the fibres used are thicker, at 30-70μm and are therefore much more efficient at transmitting light.

A schematic of a typical endoscopic optical system is illustrated in figure 3.2.

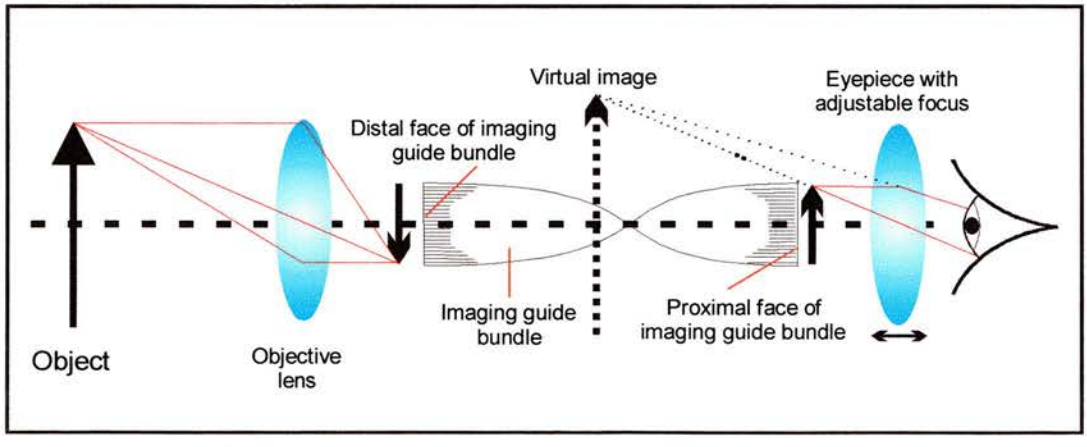

Figure 3.2: A basic endoscope imaging system [1]

Figure 3.2 illustrates the optical system arrangement within an endoscope. The objective lens at the tip of the endoscope forms an image of the object on the distal face of the image guide. This miniature image is limited by the size of the fibre bundle. The light representing this image is transmitted through the image guide and a duplicate is formed on the proximal face of the bundle near the eyepiece. Since the objective lens produces an inverted image on the distal face, the bundle is twisted 180 degrees to produce an upright image at the proximal face. The resulting image is a faithful reproduction of the viewed object; however, it is much too small to view with the naked eye. Thus, the eyepiece is used as a simple magnifying glass, with a magnification ranging between 15x and 30x, to create an enlarged virtual representation of the image resting on the tip of the bundle. This magnified image is easily observed by the endoscopist.

As the distance between the objective lens and the imaging bundle is fixed, there is a limited range, between object and objective lens, over which the object will remain in focus. This limited range of focus is referred to as the optical depth of field. A typical endoscope can focus between three millimetres and infinity from the tip of the instrument. The focal length of the eyepiece determines the magnification of the tiny image on the proximal face of the fibre bundle. The eyepiece also acts as an adjustable focus because the position of the objective lens is fixed. The average field of view of the modern endoscope is between 100 and 140 degrees.

3.2.2 Light sources

The fundamental principle associated with cancer detection is to exploit the optical contrast, either intrinsic (autofluorescence) or induced (exogenous fluorescence), between the lesion and the surrounding healthy tissue.

However, not only is excitation light required to induce fluorescence but also white light, which is fundamental for navigation purposes. During

endoscopic procedures, white light is necessary for the clinician to view the GI tract and navigate through the various structures. In conventional procedures, the light is transmitted to the points of interest via the incoherent fibre bundle incorporated within the endoscope.

The detection unit can only be as effective as the induced contrast between the healthy and cancerous tissue. For this reason, the correct choice of excitation light source was fundamental to the success of the project. As stated above, ALA induced PpIX is used to provide the optical contrast between the healthy and cancerous tissue. It is evident from the spectral curves for PpIX, shown in figure 3.3 that its absorption peaks between 400 and 410nm. For this reason, an excitation source emitting in the violet part of the spectrum was used to induce maximum red fluorescence, between 600 and 700nm, from the PpIX.

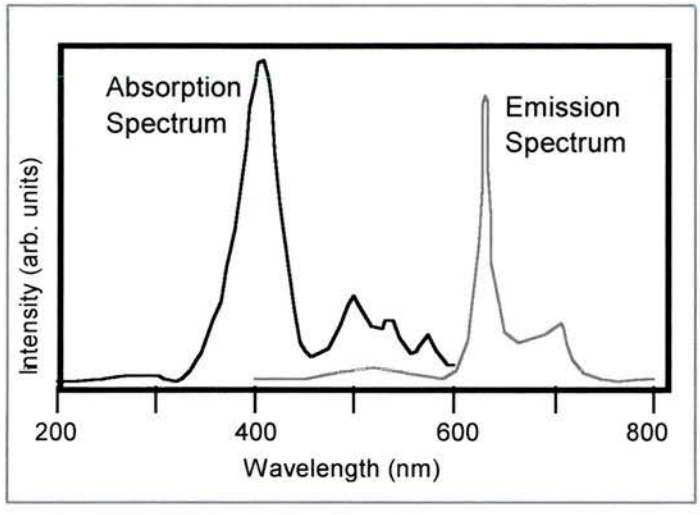

Figure 3.3: Absorption and emission data for protoporphyrin IX (PpIX)[2]

It is worth pointing out that when using short wavelength excitation, the high light attenuation by tissue restricts the measurement to only superficial layers, unless invasive optical fibre probes are used. Non-invasive detection of deep-seated lesions requires more penetrating red/near-infra-red excitation, which reduces the background autofluorescence and makes the

measurements less sensitive to local tissue inhomogenities. However, this was of little concern as we were attempting to detect pre-cancerous tissue in the superficial layers lining the GI tract. High detection efficiency is also possible while using violet light as the excitation and imaging bandwidths are spectrally far apart.

Excitation light source

A number of different light sources, both arclamps and lasers can be used for the excitation of PpIX. Lasers have the advantage of high efficiency coupling into small diameter light guides, allowing for example, use with standard endoscopes. A number of groups have used lasers such as helium cadmium (325nm) [3], pulsed nitrogen pumped dye laser (370nm) [4], argon-ion laser (351-364nm)[5] and krypton-ion laser (406.7 and 413.5nm)[6]. These laser systems are costly and entail high levels of specialist maintenance; for example, the Kr+ laser is inefficient, requiring water-cooling and a specialist technician for its operation. One cancer-detection technique, involving lifetime imaging, uses a commercial frequency-doubled Ti:sapphire laser to provide the excitation light for the photosensitiser [7]. Such a laser system is not conducive to the clinical environment, where expense, mobility and ease of operation are necessary considerations.

My initial investigations involved using a filtered xenon lamp (Storz D-Light), which is marketed by Storz for the excitation of photosensitisers, for cancer detection purposes. However, the low intensity of fluorescence excited meant that the xenon lamp was unsatisfactory. A better option was afforded by using a filtered mercury arclamp for the excitation of the PpIX. This result is understandable when one observes the difference in irradiance between 100W xenon and 100W mercury arclamps. Figure 3.4 illustrates that at 405nm, the peak irradiance of the mercury lamp is ten times higher than that of the xenon lamp. While the integrated output of the mercury lamp, between 380 and 410nm, is approximately two to three times higher than the xenon output. For this reason, I decided to use the mercury arclamp to

excite the PpIX.

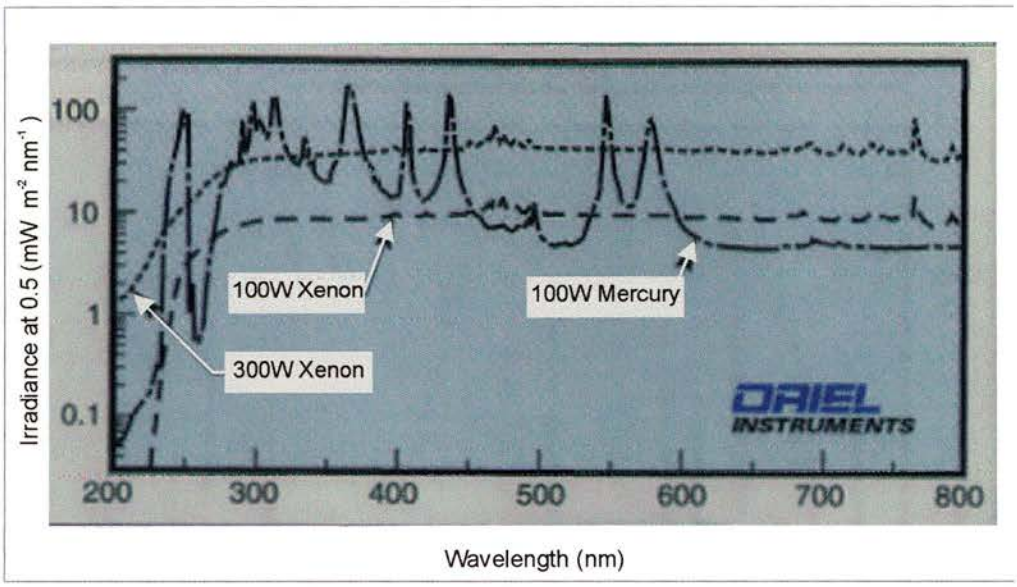

Figure 3.4: Graph comparing the irradiance between Xenon and mercury arclamps [8]

This 100W mercury arclamp had ease of operation and maintenance, modest cost and importantly, an intense emission peak at 405nm, coinciding with the peak absorption of PpIX. Figure 3.5 shows the spectral characteristics of the 100W mercury arclamp (Oriel, UK) used to excite the ALA induced PpIX.

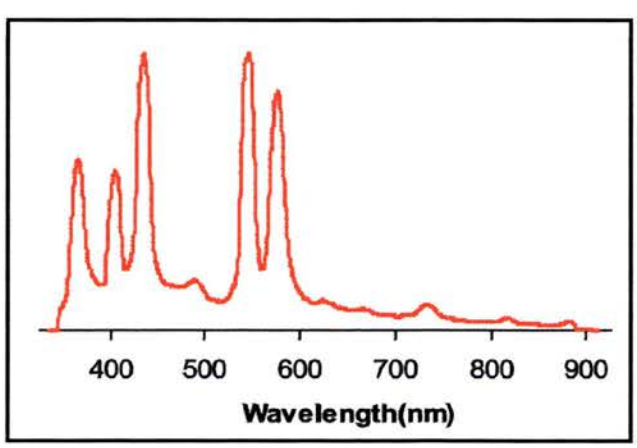

Figure 3.5: Spectrum for 100W mercury arclamp

Figure 3.6 below demonstrates the difference in PpIX fluorescence induced by the commercially available Storz D-Light (xenon source) and the filtered mercury arclamp incorporated within our detection system. I took these photographs of the induced PpIX fluorescence from a resected oesophagus.

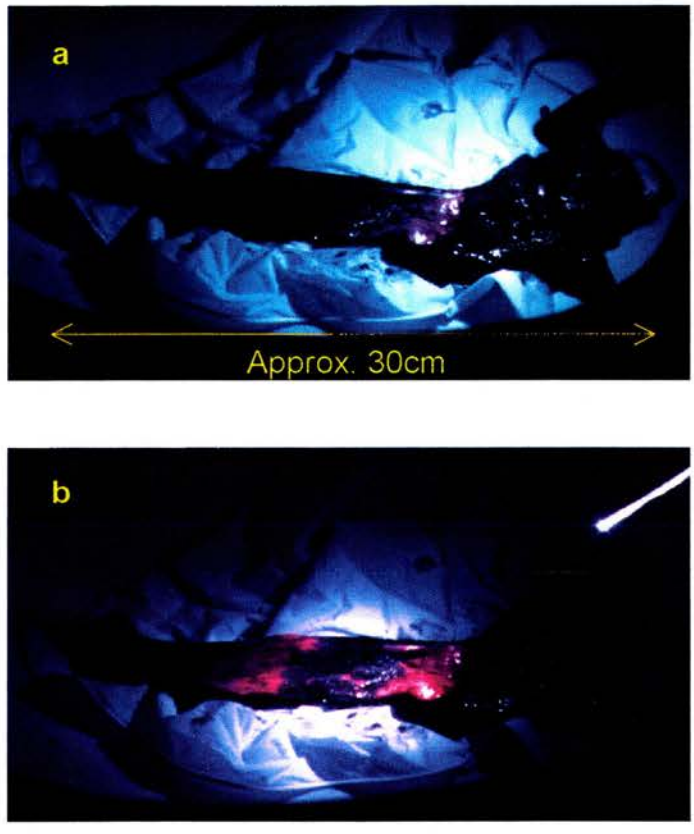

Figure 3.6: Photographs show the fluorescence induced by a) the Storz D-Light and b) the filtered mercury lamp

The second generation endoscopic system incorporates a different and improved filtering technique for the mercury lamp to that in the first generation system. Hence, the filtering of the mercury arclamp is discussed separately in chapters four and five.

White light source

As stated previously, a white light is necessary during standard endoscopic

procedures to enable the clinician to navigate through the GI tract, as well as make any necessary observations. Since white light contains the spectral band between 600 and 660nm, corresponding to the PpIX fluorescence, it cannot be used during fluorescence imaging. Ideally, the mercury arclamp would have provided both the white light illumination and violet excitation light.

In the first generation system, the white light is provided by a separate xenon lamp, whereas the second generation incorporates a custom designed filter, so that the mercury arclamp provides both the navigation and excitation illumination. Again, this will be discussed separately in chapters four and five.

Light Delivery

Illumination of the tissue surface may be achieved in two distinct ways. The first method entails contact between the fibre and the tissue, while the second, used for imaging, illuminates a larger surface area of tissue. Each approach has advantages and limitations. With point measurement, pressure on the tissue may alter the local blood content and so distort the spectrum. Spectral distortion may arise with small area illumination due to edge effects or in large area illumination due to inhomogenities in the tissue optical absorption and/or scattering. With non-contact illumination, the detected signal strength depends on the light source to tissue surface distance. Partial correction for these effects may be achieved by normalising the fluorescence spectrum with the diffuse reflectance or with the tissue autofluorescence.

The time required for a diagnosis is an important consideration because this affects the patients, the clinicians and the hospital. Thus, a non-contact illumination method was used in the detection system as it covers a wider area of tissue, which results in a faster diagnostic process.

It was intended that the endoscope would transmit, via the incoherent fibre bundle, both the violet light necessary for the excitation of the PpIX and the white light. However, after I characterised the transmission of the illumination bundle within the endoscope, it was obvious that other means for coupling the violet light into the body would have to be determined. Figure 3.7 illustrates the decrease in transmission between 700 and 400nm for an illumination bundle in a flexible endoscope. The measured transmission at 400nm was approximately seven times lower than at 600nm, which is a considerable loss of transmitted power.

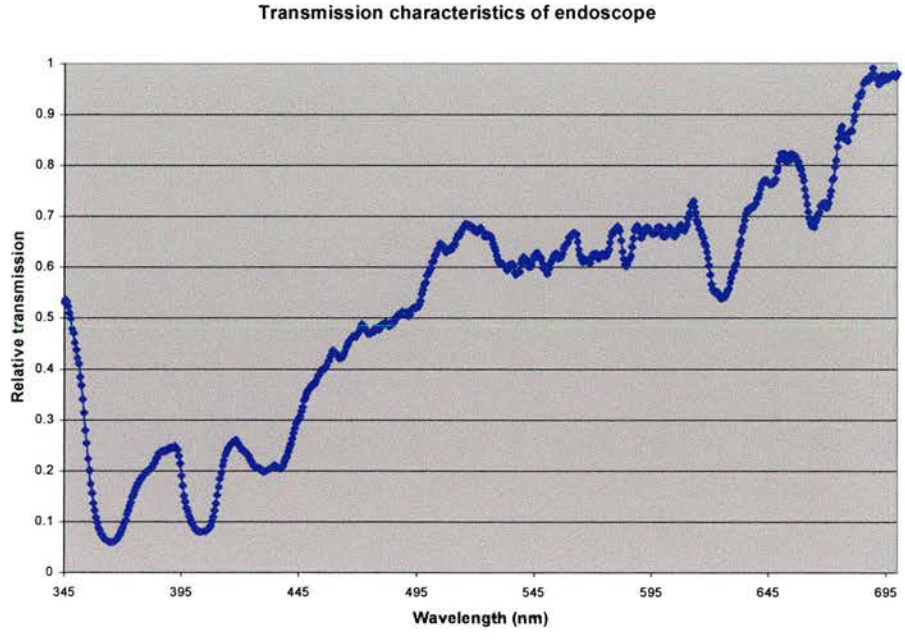

Figure 3.7: Transmission characteristics of an endoscope

As discussed in section 3.2.1, the illumination light is transported into the body via the incoherent illumination bundle in the endoscope. The light losses associated with this procedure are; the fibre transmission losses, the fibre coupling losses and the losses involved with the fill factor of the bundle. It can be assumed that the fill factor losses and the fibre coupling losses are wavelength independent. The relative transmission losses for the illumination bundle in the endoscope are shown in figure 3.7, where the

transmission at 400nm is approximately seven times less than at 633nm. At 633nm, I measured the absolute transmission of the illumination fibre bundle, within the endoscope, to be between 20 and 30 %. Since the fibre transmission can be assumed to be high (>90%) at 633nm, the measured transmission of the illumination bundle is determined by the coupling and fill factor losses.

The methods used to transmit the violet light from the source to the body cavity were different in each generation of the endoscopic system and so are discussed in detail in chapters four and five.

3.2.3 Detection Unit

A successful endoscopically-coupled detection unit will not replace the existing conventional tools available to the clinician but simply add further options to the diagnostic toolbox. For this reason, it is important that the clinician is provided with the conventional high-resolution white light imaging along side the induced fluorescence information.

Conventional colour cameras are based on three spectrally overlapping sensors centred at red, green and blue. Colours in an image are distinguished by the ratios of the three signals. Large changes in colour resulting from small changes in spectral output only occur in the centre of the visible range, where the three spectral bands of the sensors overlap. Extreme reds or blues give poor contrast as only one set of sensors is activated. Thus, a colour camera could not produce high contrast images of the red PpIX fluorescence on a background of red healthy tissue. However, the colour camera was essential for providing white light "navigation" images.

As well as lacking colour selectivity, the colour camera was not adequately sensitive to image the faint red PpIX fluorescence after transmission through

the endoscope. The fluorescence signal arriving at the camera lacks intensity, because early cancerous tissue does not accumulate large quantities of PpIX and any signal experiences appreciable attenuation during transmission through the imaging bundle. For this reason, in addition to the colour camera, an intensified CCD camera is incorporated within the detection unit for the imaging of the PpIX fluorescence.

The camera imaging unit used in the system and its coupling to the endoscope are detailed separately in chapter four.

3.3 System evaluation

As mentioned earlier, medical equipment cannot be fully implemented into the clinical environment before it has undergone a number of phases of testing. Hence, a plan for the evaluation of the equipment had to be incorporated into the developmental process.

Although this endoscopic detection system is intended for use within a cancer-screening programme, one has to first prove that it can detect cancer efficiently. For this reason, all initial system evaluations were carried out on pre-diagnosed cancerous tissue. Only after the system has proved successful at detecting all cancers within the GI tract can it be incorporated into a programme for the screening of persons at high risk of developing cancer.

It is common practice in this field of research to conduct all preliminary studies on animals, transplanted with malignant tissue. However, in this project, it was decided that system trials would take place on resected cancerous human tissue and, at later stages, in cancer patients. Although this involved a number of drawbacks associated with timely access to the hospital environment, patients and time constraints, it was felt that the final detection unit would then be better suited to cancer detection within humans.

In figure 3.8, my developmental planning process is detailed for the endoscopic optical cancer detection system, along with the stages of system evaluation carried out on human tissue.

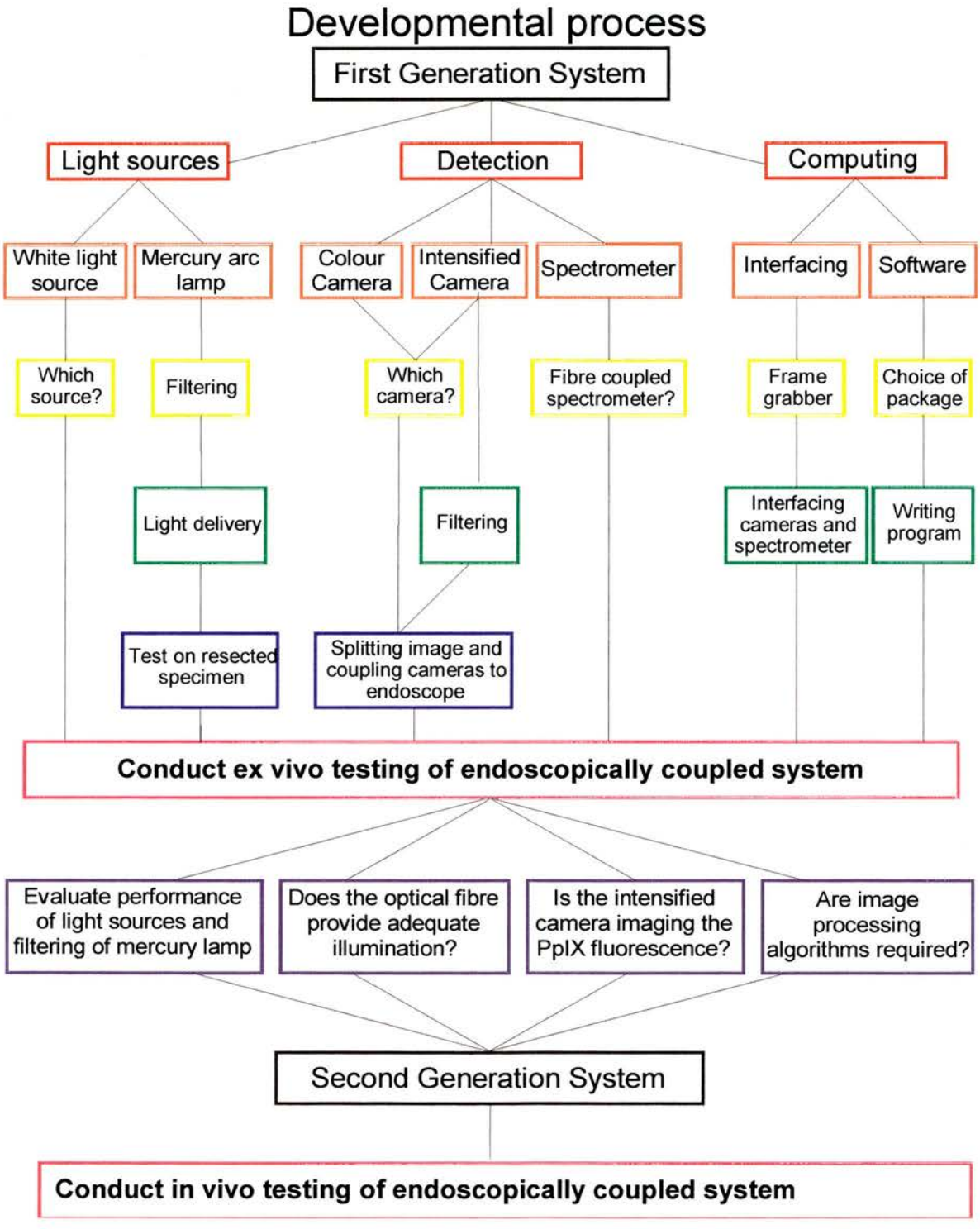

Figure 3.8: Diagram illustrating the developmental process

3.4 Summary

In order to ensure that an endoscopically-coupled detection system was constructed that was appropriate for incorporation into a cancer screening programme in the clinical environment, we collaborated very closely with the clinicians in the department of surgery. This collaboration initially involved analysing the problem as a team and learning from each other about important aspects and potential hurdles within the developmental process.

To ensure that the equipment was conducive to the clinical surroundings, I spent considerable time in the endoscopy suite and operating theatre. This experience enabled us to gain an understanding of the working conditions and equipment that the surgeons are accustomed to using. For example, we quickly learnt that image quality is beneficial when undertaking minimally invasive procedures as they depend on the surgeon observing intricate details from the image. Secondly, due to the extensive range of instrumentation used within surgery, it is vital that all equipment is compact with simple and self-explanatory operation.

The active collaboration with the clinicians was essential in ensuring that the detection unit was appropriate for clinical use and that they continually evaluated its performance on human cancerous tissue.

A more comprehensive description of the development of the endoscopically-coupled cancer detection unit is included in chapters four and five.

3.5 References

[1] I. Kawahara, H. Ichikawa. "Fiberoptic Instrument Technology." Chapter 2. Literature from Olympus Optical C0., Ltd.

[2] Spectral data provided by the biochemist (Luke) in the departemnt of surgery at Ninewells Hospital.

[3] C. R. Kapadia, F. W. Cutruzzola, K. M. O'Brian, M. L. Stetz, R. Enriquez, L. I. Deckelbaum. "Laser induced fluorescence spectroscopy of human colonic mucosa." *Gastroenterology*, 1990, **99**, 150.

[4] K. T. Schomacker, J. Frisoli, C. Compton, T. Flotte, J. Richter, N. Nishioka, T. Deutsch. " Ultraviolet Laser- Induced Fluorescence of Colonic Tissue: Basic Biology and Diagnostic Potential." *Lasers in Surgery and Medicine*, 1992, **12**, 63.

[5] T. J. Romer, M. Fitzmaurice, R. M. Cothren, R. Richards-Kortum, R. Petras, M. V. Sivak, J. R. Kramer. " Laser induced fluorescence microscopy of normal colon and dysplasia in colonic adenomas: implications for spectroscopic diagnosis." *Am. J. Gastroenterol.*, 1995, **90**, 81.

[6] K. J. Brodbeck, A. E. Profio, T. Frewin. "A system for real-time fluorescence imaging in colour for tumour diagnosis." *Med. Phys.*, 1987, **14**, 4.

[7] K. Dowling, M. J. Dayel, M. J. Lever, P. M. W. French, J. D. Hares, A. K. L. Dymoke- Bradshaw. "Fluorescence lifetime imaging with picosecond resolution for biomedical applications." *Optics Letters*, 1998, **23**, 810.

[8] Graph from Oriel Instruments 1999 catalogue.

CHAPTER FOUR

FIRST-GENERATION ENDOSCOPIC CANCER DETECTION SYSTEM

4.1 Introduction

In this chapter, the construction of the first-generation endoscopic cancer detection system is discussed. The fundamental concepts associated with this system, such as the photosensitiser, endoscope, illumination and detection unit were introduced in chapter three, along with strategy for the developmental process.

The following sections include an in-depth analysis of each aspect of the unit and an appraisal of the ex-vivo results gathered during the evaluation stages. This is complemented by a discussion of the limitations of this first-generation system and aspects for further improvement are identified.

4.2 Illumination and delivery

The requirements for the illumination unit included a suitable white light

source for navigation purposes and appropriate filtering of the mercury arclamp, to ensure maximum excitation of the ALA induced PpIX. Due to the poor transmission of the endoscope in the violet spectral region, alternative means for the delivery of the excitation light to the body cavity were necessary.

4.2.1 White light source

As stated previously, a white light is required during standard endoscopic procedures to enable the clinician to navigate through the GI tract. Ideally, the mercury arclamp would provide both the white light illumination and violet excitation light. However, due to the complexity associated with manipulating the filtering of the mercury lamp during a procedure, a separate source was used to provide the white light.

I chose a commercially available Storz xenon light source to provide the white light, due to its broad spectral band and standard endoscopic coupling attachments. Thus, the white light was coupled into the body via the incoherent fibre bundle within the endoscope.

4.2.2 Excitation light source

As discussed in chapter three, a mercury arclamp is used as the excitation source because its high spectral output between 390 and 410nm is well matched to the absorption peak of the photosensitiser, PpIX. Appropriate filtering of the mercury lamp was necessary to maximise the intensity of the induced fluorescence and to ensure the attenuation of all light at wavelengths beyond 450nm. The latter point is important because light originating from the excitation should not interfere with the detection band, which is in the 500 to 700nm region.

Initially, I felt that a 10nm bandwidth interference filter, centred on the

405nm-mercury spectral line would be appropriate to filter the mercury lamp. However, the lack of transmitted optical power resulted in the excitation of inadequately low intensity fluorescence. It appeared that to ensure high intensity fluorescence, the total power of the excitation light was of more importance than the specific spectral bandwidth. Thus, in the first-generation detection system, a 400nm ± 35nm-interference filter (Ealing Electro Optics) was used to spectrally select the output of the excitation mercury lamp. The measured excitation light power at the distal end of the endoscope was 15mW and the spectral output from the filtered mercury lamp is shown in figure 4.1.

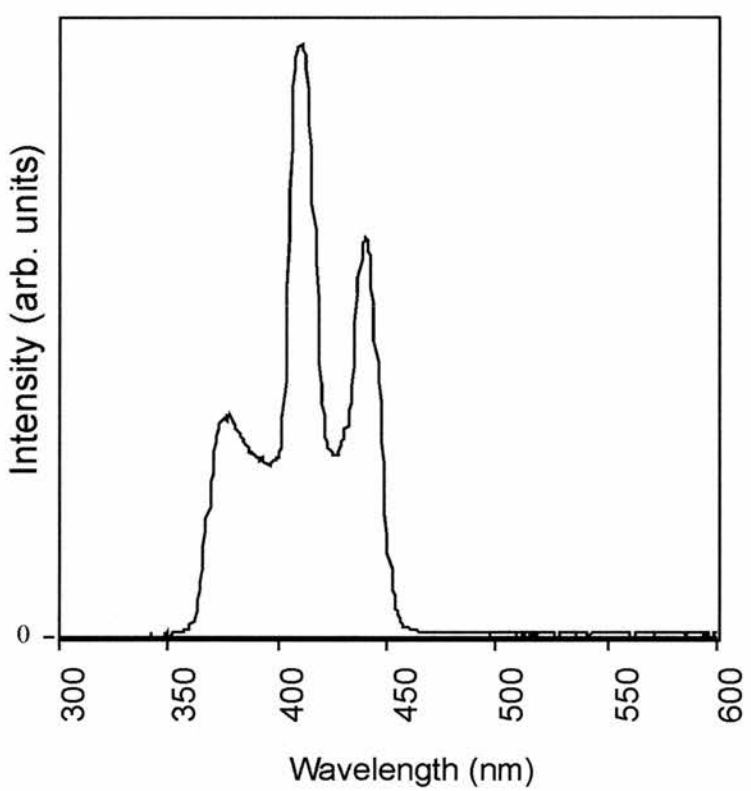

Figure 4.1: Spectrum of 100W filtered mercury arclamp

Light delivery

The poor transmission of the incoherent fibre bundle, within the endoscope, at 400nm ($20\%/7 \approx 3\%$) meant that other means of coupling the violet light

into the body cavity were required. A much more effective method of delivering the filtered light from the lamp to the GI tract involved the use of a dedicated ultraviolet-transmitting optical fibre, inserted into the biopsy channel of the endoscope.

In order to decide what diameter fibre would be most appropriate, we compared the values for the product of the numerical aperture (NA) and aperture for the light through each of the components involved in the unit. If any component has a NA, aperture product that is smaller than that of the light source, the light throughput of the system is not optimised. Therefore, it was possible to determine which component was restricting the throughput of the optical system by analysing the various products.

	NA	**Aperture (mm)**	**NA x Aperture**
100W Hg	0.24	0.25	***0.06***
200W Hg	0.24	2.2	***0.528***
1000W Hg	0.24	3	***0.72***
100W Xe	0.24	0.8	***0.192***
Optical fibre	0.39	1	***0.39***
Endoscope	0.39	3	***1.17***
Laser	λ/d	d	λ

Table 4.1: Comparison of NA aperture product for various components in the optical system (Oriel Research Arclamp Sources). The arclamps aperture is defined by the arc size, while the NA is defined by the collection optics.

Since the product for the 100W mercury lamp is very much less than that for the one millimetre diameter optical fibre, in theory, all the light will be efficiently coupled into the fibre. It is interesting to point out that the use of the 100W xenon lamp would decrease the sensitivity of the system, due to the poor fibre coupling.

It is also apparent from table 4.1 that a higher wattage mercury lamp, used in conjunction with the optical fibre would not result in more light reaching the tissue. In the ideal situation, a 1000W-mercury lamp would be coupled

to a UV transmitting endoscope as this would increase the intensity of the induced fluorescence. As a comparison, the laser is included in the table, as it has the lowest NA aperture product and can therefore be efficiently fibre coupled.

The following specifications for the optical fibre were necessary to ensure effective transmission of the light to the distal end of the scope:

- high *transmission efficiency* around 400nm.
- *large core diameter* to transmit adequate power.
- minimum bend *radius* no greater than that of the endoscope.
- large *numerical aperture* to increase the coupling efficiency.

The maximum bending which can be tolerated by a fibre without fracture is given by

$$R_F = \frac{Ed}{2\sigma}$$

where R_F is the minimum radius of curvature, E is the modulus of elasticity, σ the ultimate failure stress and d is the diameter of the fibre.

In our arrangement, I used a 1mm-diameter, hard clad, multimode, UV transmitting fibre (3M Power-Core, attenuation of 0.08dB/m at 400nm). The fibre had a minimum bend radius of 50mm, which was comparable to that of the endoscope, while the large numerical aperture (0.39) enabled efficient coupling to the mercury lamp via an SMA connector.

The coupling optics of the mercury lamp housing comprise a 1:1 imaging lens system, f/1.8, attached to a 50mm spacer tube and then to a SMA adapter. I attached a SMA connector to each fibre, which enabled a robust, efficient coupling system that required no further adjustments. Figure 4.2 shows the mercury bulb and fibre coupling optics used in the system.

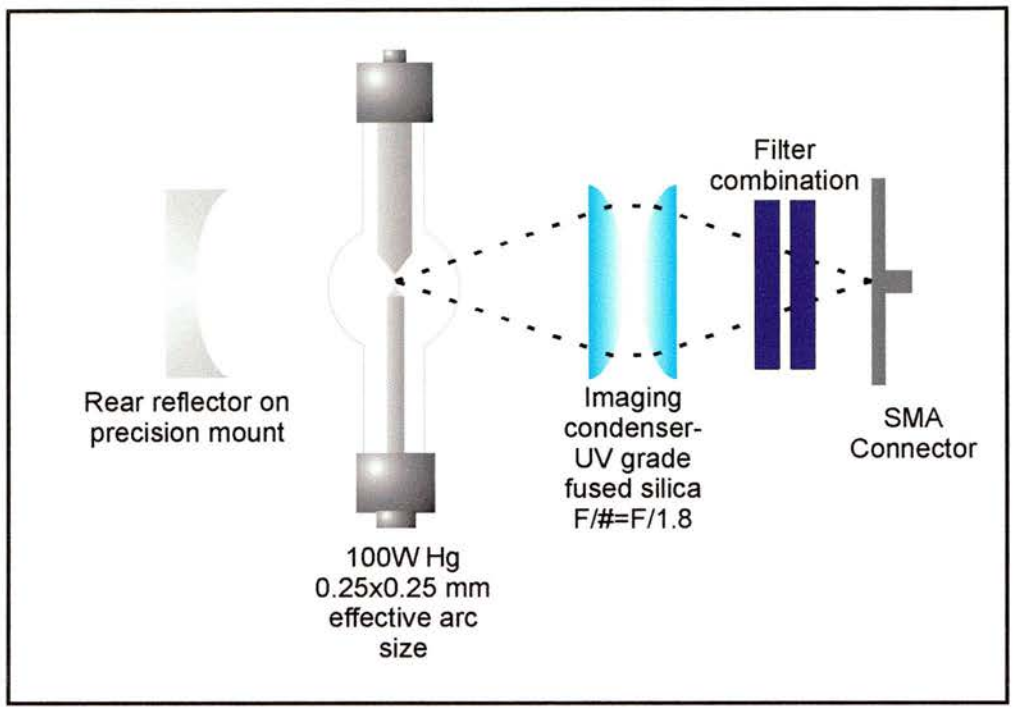

Figure 4.2: Fibre coupling optics used in the mercury arclamp

The figure below illustrates the difference in intensity of fluorescence induced when the excitation light is delivered through the endoscope illumination bundle and through the UV-transmitting fibre.

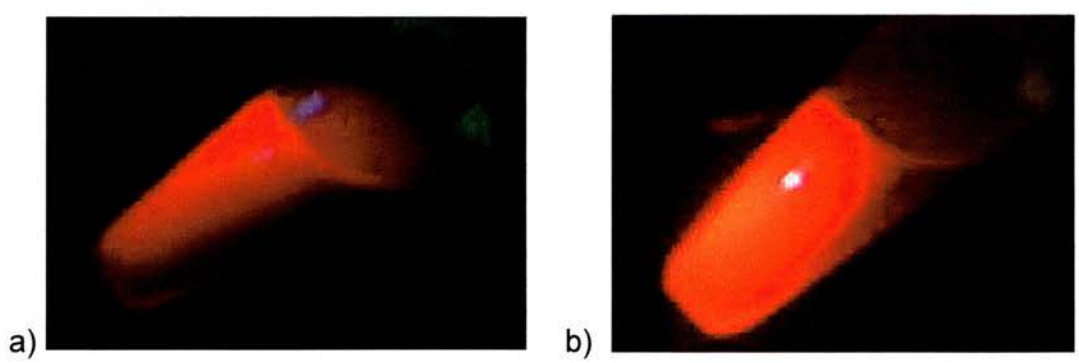

Figure 4.3: Photographs demonstrating intensity induced when transmitting light down a) the illumination bundle of the endoscope and b) down the UV transmitting optical fibre

Figure 4.4 shows the 100 W mercury arclamp and UV transmitting fibre used in this first-generation detection system.

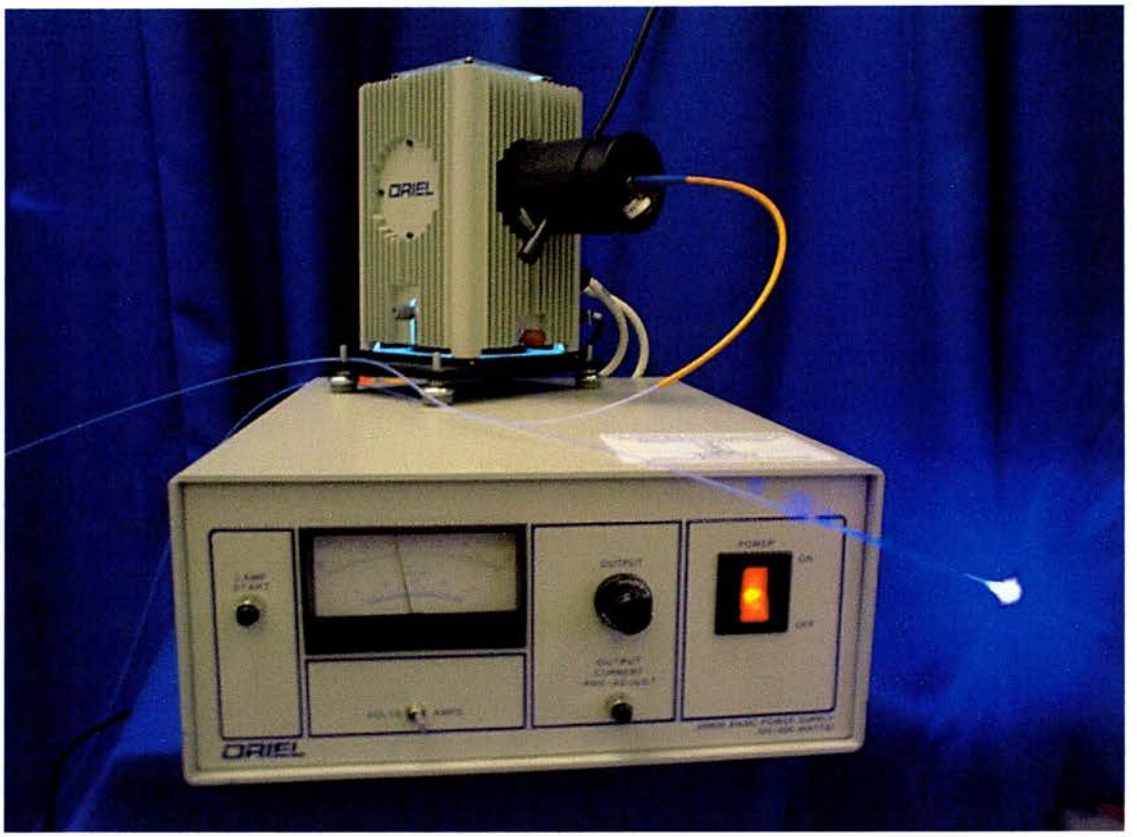

Figure 4.4: Mercury arclamp and fibre

4.3 Detection Unit

As detailed in the previous chapter, the detection unit requires both a colour camera for navigation purposes and an intensified camera to image the low intensity induced fluorescence. This system also incorporated a fibre-coupled spectrometer for the provision of quantitative spectral analysis.

4.3.1 Colour CCD Camera

A colour camera is an essential component of the detection system as surgeons require high-resolution white light colour images for navigation purposes. A remote-head colour CCD camera (Storz, Endovision TELECAM SL), with a ½ inch chip, a resolution of 752x582 pixels and an integrated zoom facility ranging from 25 to 38 mm was used. The dimensions of the remote head camera permitted coupling directly to the end

of the endoscope, whereas this would not have been possible if the camera were heavy and bulky.

4.3.2 Intensified Camera

The intensified camera used in this first-generation system weighed one kilogram and measured 218mm in length (Photon Technology International IC-200). The input light to this camera was filtered in order to detect the intensity of the bimodal emission peak of the fluorescence from the photosensitiser. Since the emission is predominant at 638nm, the use of a 610nm cut-off glass filter, in front of the camera, ensured that all violet excitation and light scattered by the tissue was removed. The filter also blocked scattered light generated by optical components such as lenses, fibres and filters.

The cancerous tissue is signified by a high intensity area in the monochrome image, since the photosensitiser preferentially accumulates in cancerous tissue and the intensified camera is not colour sensitive. The use of this camera made the entire detection unit more sensitive to a fluorescent signal than would otherwise be possible with the naked eye or with a colour camera. The main drawback in using an intensified camera in an endoscopically-coupled system is its inherent size and weight.

4.3.3 Optical Head

In conventional endoscopy, a colour camera, focused at infinity, is coupled directly to the output aperture of the eyepiece and an electronic image is relayed to a high definition colour monitor. The requirement for two cameras meant that a combination of beam splitter and lenses was employed to split the image. Initially a Teaching Aid, which is a commercially available beamsplitter with remote viewing bundle, was used to attach the two cameras to the endoscope. However, due to the light losses associated with

transferring the image from one fibre bundle to another, an alternative beamsplitting optical system was constructed. Because both cameras were to be coupled to the end of the endoscope, it was necessary that the optical head was as compact and light as possible.

To maintain image brightness, achromatic doublet lenses either side of a 50/50 beamsplitter imaged the output aperture of the endoscope onto the input apertures of the cameras. Figure 4.5 shows the arrangement of the optical head used to split the image from the endoscope and refocus it onto the two cameras. Due to the focussing optics incorporated within the colour camera, it could be focussed at infinity, whereas a 30mm lens was positioned in front of the intensified camera to focus it at infinity. This optical head was constructed completely from Spindler and Hoyer components and lenses.

Although this optical head was not optimised in terms of compactness or aberrations, it was designed in such a way as to allow flexibility. Due to the adaptability of the optical head, we were able to experiment with a number of different cameras and filters, without the need to build a new optical head.

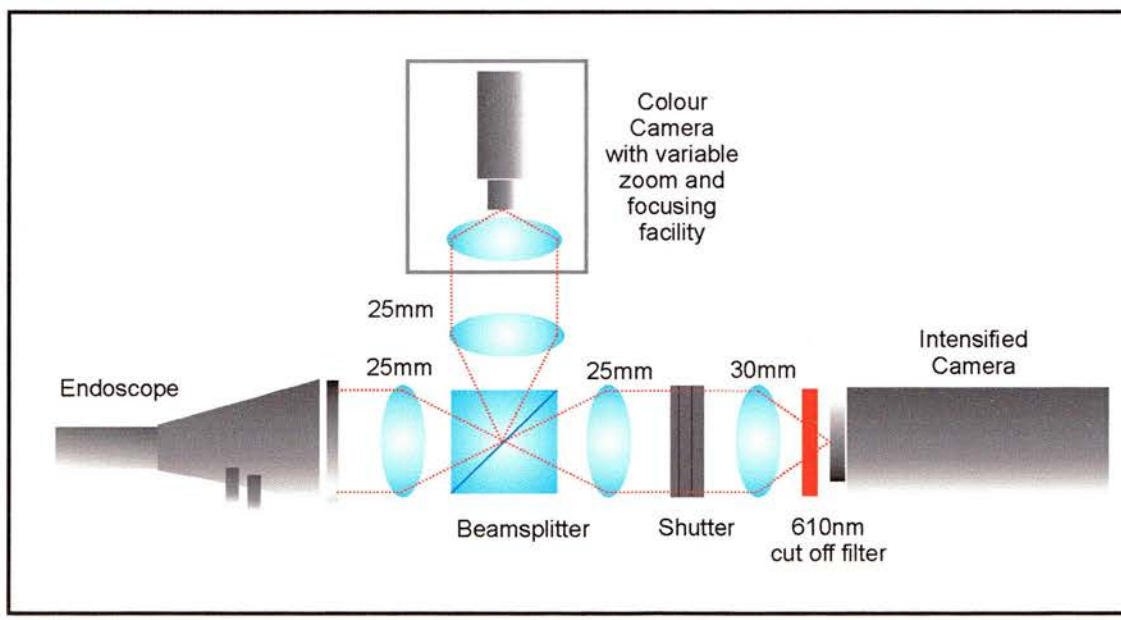

Figure 4.5: Optical head to couple the cameras to the endoscope

An electronic shutter (Ealing 228411) was attached to the intensified camera in order to protect the intensifier faceplate from the high intensity white light, which would cause permanent damage. This shutter was controlled by a footswitch, which when compressed, resulted in the blocking of the white light source and opening of the shutter, to allow the intensified camera to image. On the next compression of the footswitch, the shutter was closed and the white light was unblocked, to allow the colour camera to image. The control of this shutter is discussed in more detail in section 4.4 below.

The focussing of the endoscopically-coupled detection unit involved three distinct stages, which are:

i) focus both the intensified and colour cameras at infinity. The intensified camera is focussed using the lenses in the optical head, while the colour camera has a built in focussing facility.

ii) attach the colour camera and endoscope to the optical head and intensified camera. The eyepiece on the endoscope is used to finely focus the intensified camera, while the colour camera is adjusted using its built-in focus facility.

iii) once both cameras are in focus, the eyepiece is available for subsequent adjustments to the focus of both cameras during clinical procedures.

4.3.4 Fibre-coupled Spectrometer

The incorporation of a spectrometer into the system enhanced the specificity and sensitivity of the detection process and most importantly facilitated the acquisition of quantitative spectrally-related data for each patient. Because the spectrometer was fibre-coupled (Ocean Optics S1000), its fibre pigtail was fed into the biopsy channel of the endoscope. The spectrometer thus enabled quantitative identification of fluorescence originating from tissue under observation. This spectrometer was also very important in the initial ex-vivo experimentation because it enabled identification of the exact

wavelength of PpIX fluorescence and autofluorescence. An example of such spectral data is included in figure 4.6

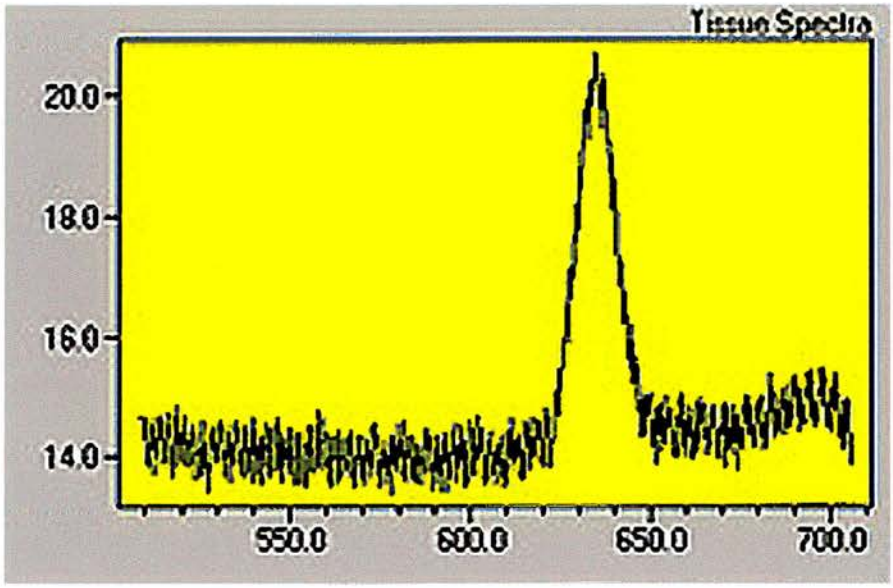

Figure 4.6: An example of spectral data to allow identification of exact wavelength of PpIX fluorescence

4.4 Computer interfacing and software

Prior to embarking on the writing of the software for this detection system, I had no previous computer programming experience. For this reason, I spent three months, in my first year, teaching myself to write computer programs, using the Pascal language. Thus when deciding what programming environment in which to write my software, I chose Borland Delphi as it requires an understanding of Pascal and enables the design of user-friendly interfaces for the end-user.

The first and most time consuming stage in the software design involved interfacing the shuttered intensified camera, the colour camera, the fibre-coupled spectrometer, white light source and footswitch via a frame grabber to a desktop PC (233MHz). (A frame grabber is an analogue to digital

converter optimised for digitising video signals.) A footswitch was incorporated into the system to enable the clinician to control the white light source, shutter and grabbing of relevant images, whilst manipulating the endoscope. The footswitch was fitted with a relay switch and on activation sent a signal to the computer, which in turn controlled, using a voltage signal (TTL), the shutter and white light source.

The software was written to co-ordinate the grabbing of the colour and intensified images, the spectral data, the blocking of the white light source and the operation of the shutter. Thus, while the colour camera was grabbing, the white light source was unblocked and the shutter closed where as, while the intensified camera was grabbing, the white light source was blocked and the shutter open. During the entire procedure, the violet light remained on, as this had no effect on the white light imaging. (A brief explanation of the software and the code used are included in appendix one.)

The design of the software not only involved the displaying of the relevant data but the incorporation of control facilities appropriate for use by the clinicians, in the clinical environment. Clinicians use a diverse range of complex instrumentation and so it is important that the interface between clinician and software is user-friendly, intuitive and shows only the necessary information. I designed the software so that any control required from the clinician could be achieved via manipulation of simple scroll bars and push buttons, on the desktop. In the event that the equipment became uncoordinated, there were reset buttons on the desktop, to enable the surgeons to easily reset the equipment by changing the shutter position and camera operation.

An example of a computer desktop, with which the surgeon interacted, is shown in the figure 4.7. To allow comparison between images, while one camera was grabbing in real-time and displaying to the screen, the last captured image from the other camera was held on the screen. The

software also incorporated facilities to save and store the corresponding images and spectra for patient-related documentation.

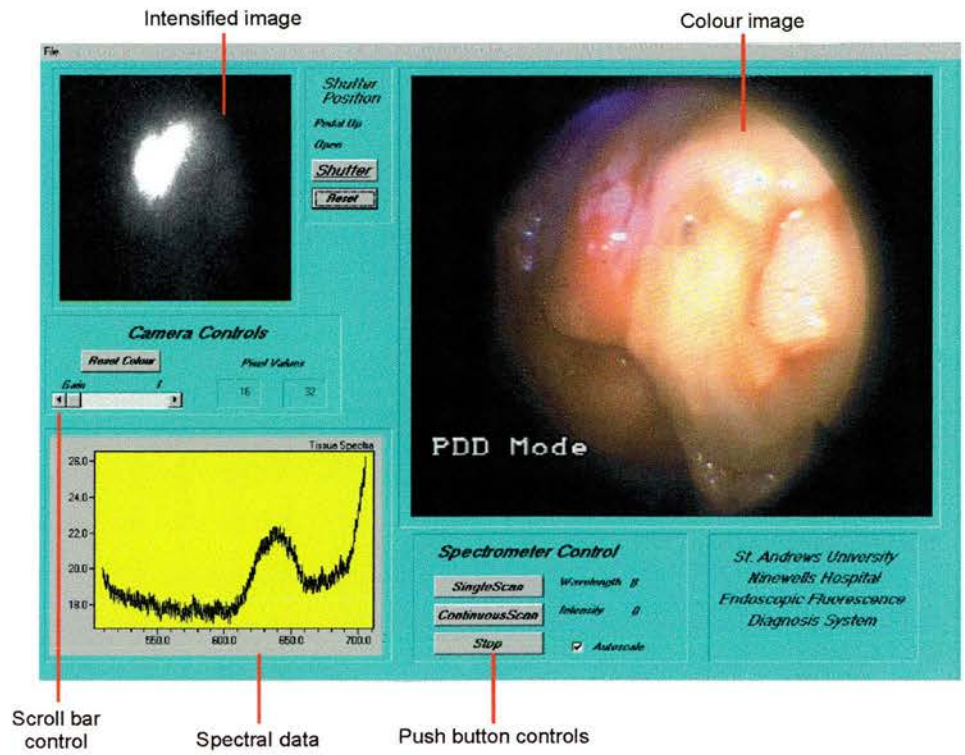

Figure 4.7: An example of a computer desktop with which the surgeon interacts

4.5 System Configuration

The completed configuration of the equipment, detailed in the above sections, is shown in figure 4.8 and a photograph of part of the first-generation system is pictured in figure 4.9. The ex-vivo results on resected specimen recorded using this system are detailed later in the chapter.

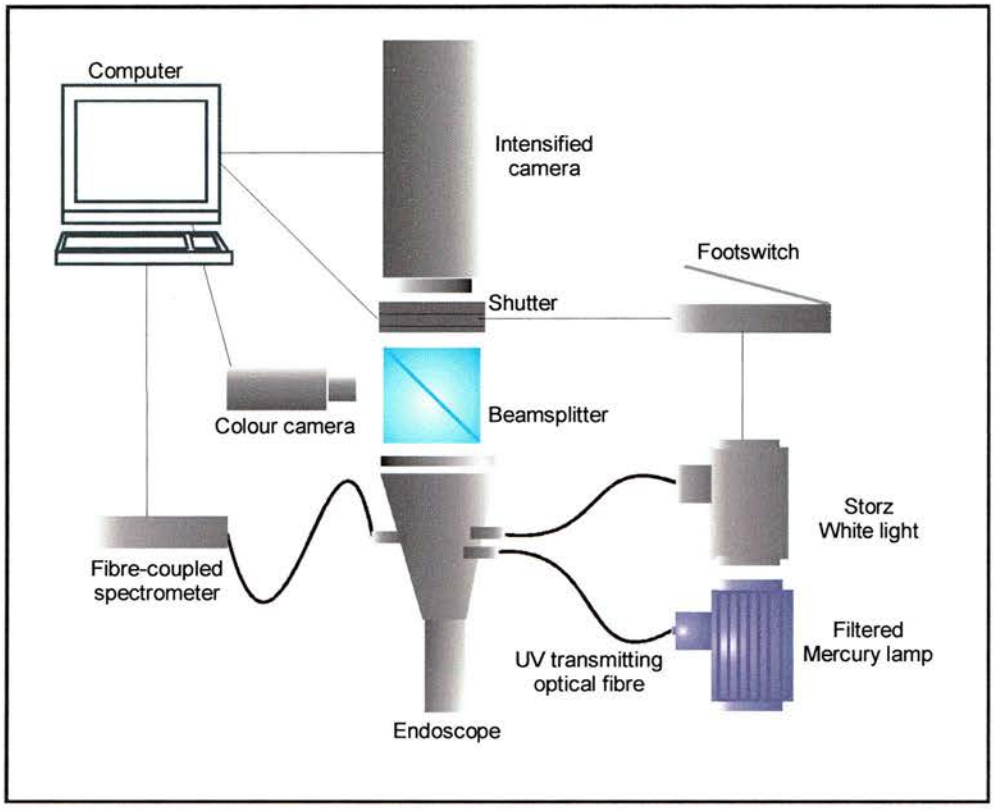

Figure 4.8: System configuration

Figure 4.9: Endoscope, optical head and cameras

4.6 Ex-vivo fluorescence and spectroscopic studies of gastric and oesophageal cancer

Initial system evaluation concentrated on the examination of diagnosed cancers of the oesophagus, stomach and colon. This process involved the clinician administering ALA to the patient prior to the surgical removal of the cancerous specimen. Written informed consent was acquired from each patient before inclusion in the study. Once the cancer was resected, I was able to test the system on the specimen for up to half an hour, before it had to be sent to histology. During this time, fluorescence images were recorded, spectral data documented and biopsies were subsequently taken by the clinician to histologically confirm the fluorescence observations.

For detection purposes within the oesophagus, ALA dosages of between 3 and 20mg per kg body weight were administered orally to patients. This dosage is three times lower than that used for photodynamic therapy and therefore ethically approved for use in cancer screening. The variation in dosage corresponded to the observation of respectively varying intensities of fluorescence. The highest ethically approved dosage of 20mg per kg body weight induced the highest optical contrast and was consequently set as the protocol dosage within the oesophagus, for this study.

The colon on the other hand required a higher orally administered dosage of the ALA. A maximum of 40mg per kg body weight was used for the fluorescence observations within the colon and rectum.

The elapsed time between ALA administration and inspection with the system varied between three and eight hours. Although, we attempted to investigate the influence of the elapsed time on observed PpIX fluorescence, the unpredictability of the length of operations and the difficulty in controlling the environment made this task impractical during these project studies.

4.6.1 Oesophagus

Contrary to expectations, we consistently observed a reversed contrast fluorescence pattern within the oesophagus, where the healthy tissue exhibited the strongest PpIX fluorescence. Figure 4.10(a) illustrates the fluorescence reversal observed in a resected oesophagus. This fluorescent image should be compared against the white light image (figure 4.10(b)) that the clinician would traditionally view.

Despite the unexpected fluorescence reversal, the optical contrast still provided a clear demarcation of the cancerous tissue from the healthy background. Whereas figure 4.10(b) illustrates that, the cancerous tissue cannot be distinguished from the healthy tissue in the white light image. This fluorescence reversal pattern was consistently observed in over thirty oesophageal specimens studied. Where fluorescence was observed, biopsies were taken and histology showed this as healthy tissue, whereas a lack of fluorescence corresponded to cancerous tissue.

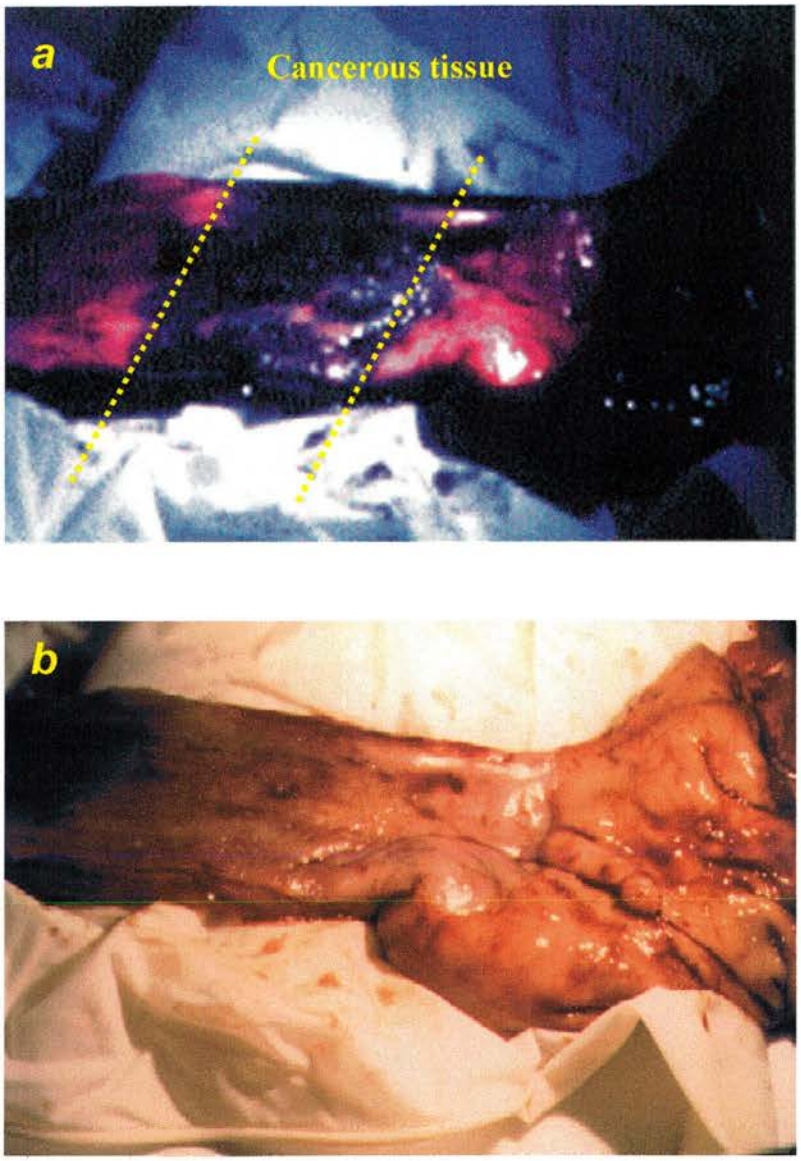

Figure 4.10: Photographs showing a) the fluorescence image and b) the white light image of an oesophagus with a carcinoma

While this contrast reversal does not hamper the detection of cancer through fluorescence imaging, it does have detrimental consequences for PDT. However, it will be seen in chapter five that this fluorescence reversal was not observed in-vivo. Possible explanations for this observation are that the tumours contained large amounts of dead tissue, which did not metabolise the ALA and therefore appeared black on excitation. On resection, the pH, oxidative state and blood flow has been reported to change, which may have effects on the PpIX present within the tumour. (In chapter two some

problems associated with relying on ex-vivo data are discussed.)

The performance of the imaging unit was also evaluated by myself on resected specimens via the endoscopic detection unit. Figure 4.11 shows the colour image under white-light illumination and the fluorescence image under violet-light illumination. Note the marked contrast between the healthy and cancerous tissue can only be observed in the fluorescence image from the filtered intensified camera.

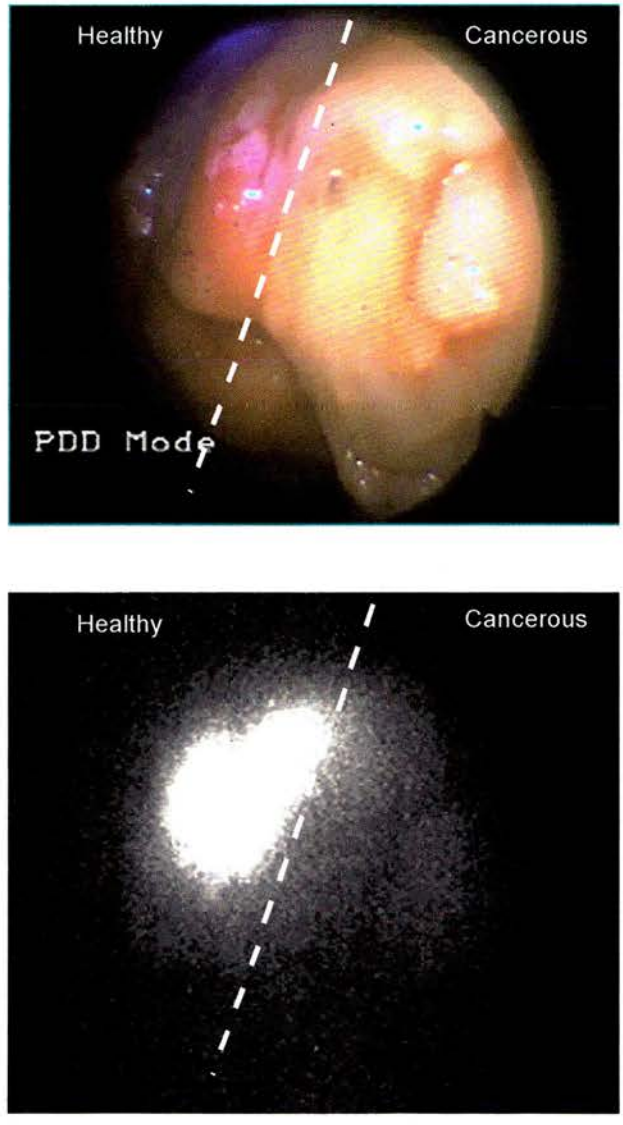

Figure 4.11: Colour and fluorescence image of a cancerous region of the oesophagus

The fibre-coupled spectrometer was also used with the violet illumination to

obtain further data relating to the induced PpIX fluorescence and possible fluorescence originating from endogenous fluorescent molecules. Spectral data was recorded within both the cancerous and healthy tissues and figure 4.12 shows example spectra recorded from both.

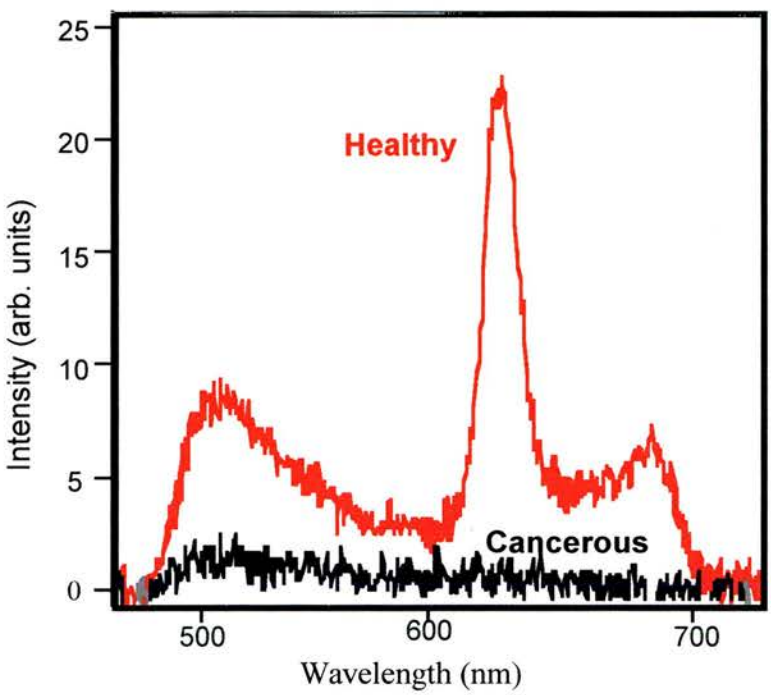

Figure 4.12: Spectra of fluorescence from healthy and cancerous tissue

Figure 4.12 illustrates the characteristic bi-modal emission peak originating from the PpIX within the healthy tissue, while no PpIX fluorescence was recorded in the cancerous tissue. This pattern correlates with the images observed from the filtered intensified camera, where the fluorescence is evident in the healthy tissue only.

A further peak at 500nm is apparent in the spectrum from the healthy tissue, but not in the cancerous tissue spectrum. We deduce that this autofluorescence originates from the endogenous molecules within healthy tissue. (The theory for this observation was discussed in chapter one.)

4.6.2 Colon

Figure 4.13 shows an example of one resected colon, which I analysed with the optical imaging detection system.

Figure 4.13: White light image of resected colon

Within the colon, induced PpIX fluorescence was observed in cancerous tissue, while healthy tissue showed PpIX fluorescence of a very much lower intensity. The intensity of the fluorescence depended on the ALA dosage and the elapsed time between administration of the photosensitiser and observation using the detection system. If the elapsed time before inspection was more than approximately five hours, the optical contrast between the cancerous and healthy tissue was reduced. The maximum allowed ALA dosage of 40mg per kg body weight, proved most successful at inducing an optical contrast.

Again, the fibre-coupled spectrometer was used to collect quantitative spectral data relating to the nature of the induced fluorescence within the

colonic tissue. Figures 4.14 and 4.15 show examples of such spectral data recorded from cancerous and healthy tissue under violet light illumination.

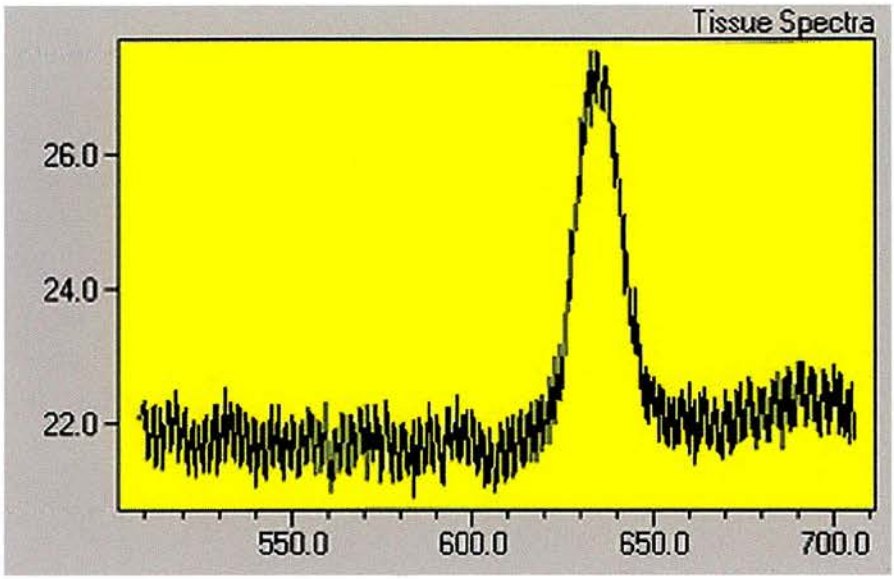

*Figure 4.14: Spectral data from **cancerous tissue** within resected colon*

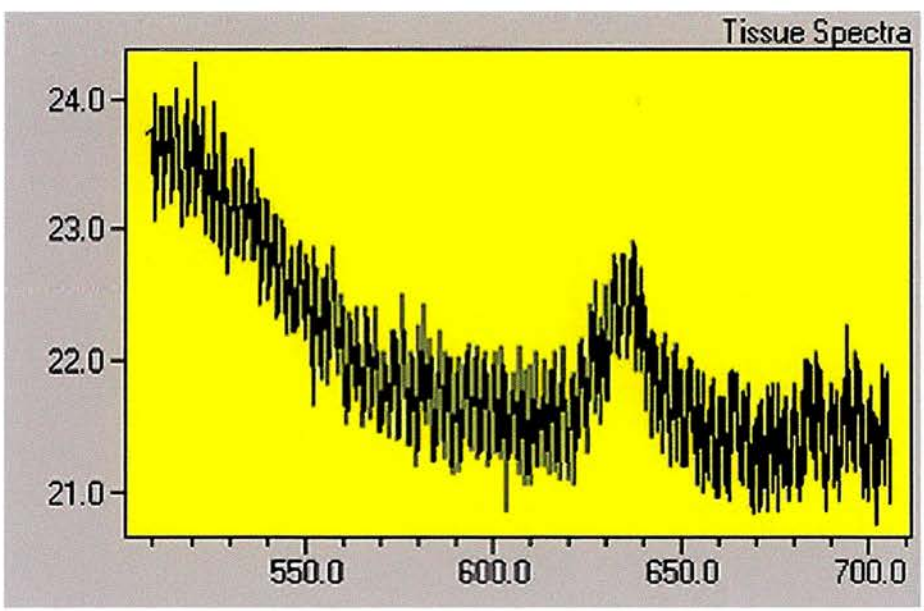

*Figure 4.15: Spectral data from **healthy tissue** within resected colon*

There are a number of characteristics associated with the spectral data shown in figures 4.14 and 4.15, which are worthy of comment. Firstly, the spectral data recorded from the cancerous tissue shows a strong emission

at 638nm and a smaller peak at 690nm, which correspond to the induced fluorescence from the PpIX. Secondly, in the data recorded from the healthy tissue, the PpIX fluorescence is present but at a very much reduced intensity. The third point of interest is the appearance of a spectral peak at 500nm, in the healthy tissue, which it is believed, corresponds to autofluorescence. Figure 4.14 supports the reports that this autofluorescence is not present within cancerous tissue.

Unfortunately, the performance of the detection system was not as convincing in the stomach as in the oesophagus and colon. From a large number of specimens investigated, it was not possible to obtain a high contrast image from stomach tissue. Only a very weak heterogeneous fluorescence was observed in tumours in the stomach. Frequently a weak fluorescence was observed in both the cancerous and healthy tissue. There is no obvious explanation for this pattern other than the tissue in the stomach has a different ALA uptake to the rest of the GI tract.

4.7 Summary

In this chapter, the design of a first-generation, endoscopically-coupled cancer detection system has been described and the results of ex-vivo experimentation on cancerous specimens, within the GI tract, have been presented.

To address the concerns relating to the fluorescence reversal observed within the resected oesophagus, it was vital that the cancer detection system was tested, in vivo, on patients. Although the fluorescence reversal did not affect the potential success of the detection system, given that the optical contrast present enabled detection of the cancer tissue, it contradicted published data and the accepted principles of photodetection.

A number of aspects of the detection system required further development,

before it could be used routinely by the clinician in theatre. These limitations related to the violet light delivery, the consecutive grabbing of the colour and intensified images, the size of the intensified camera and the image processing capabilities.

Although the violet light from the filtered mercury lamp successfully induced PpIX fluorescence, the angle of illumination of the fibre did not correspond to the field of view of the endoscope. Consequently, due to the tubular nature of the oesophagus and colon, there was inadequate violet light incident on the tissue, to induce an optical contrast over the entire viewing angle of the endoscope. This resulted in a very slow inspection process and concerns arose about missing areas of cancerous tissue. Thus, either a fibre with a larger angle of illumination that matched the field of view of the endoscope, or an alternative means of delivering the light was required.

The second complication involved the switching between the white and violet light. The oesophagus does not remain stationary during an endoscopy; it is subject to continuous muscular movement. As a consequence of this, the consecutive switching between white and violet light resulted in images, whose imaging field did not correlate exactly. Pixel alignment between the colour and intensified images is beneficial, as the clinician has to identify the exact location of the suspicious tissue imaged by the intensified camera. Therefore, it was essential that the fluorescence and white light images were captured simultaneously. This must be achieved in such a way that the presence of white light does not saturate the fluorescence images.

Although I wrote the software in this generation system to independently display the fluorescence and white light images, it was intended that the final detection system would display the colour "navigation" image superimposed with the fluorescence data. However, due to the presence of the beamsplitter within the optical head, the colour image was the mirror image of the fluorescence image and hence required pixel reversal. It transpired after much experimentation, that reversal of the colour image, followed by

superposition of the fluorescence data was not possible in real-time. Thus, an alternative method of reversing the colour image was required to free up the computer, for further image processing.

From a user-viewpoint, the clinicians felt that the detection unit attached to the endoscope was rather cumbersome and that the system would be more robust and user-friendly if the unit was smaller with a better weight balance. They also indicated that the endoscopically-coupled detection system would be compatible for use on patients if the issues stated above were improved. In chapter five, the specific improvements made to produce a second-generation version of the detection system is described and the design of this was intended to enable it to be used for in-vivo observations.

CHAPTER FIVE

SECOND-GENERATION ENDOSCOPIC CANCER DETECTION SYSTEM

5.1 Introduction

The development of a second-generation endoscopic cancer detection system is discussed in this chapter. As mentioned in the previous chapter, during the evaluation of the first-generation endoscopic cancer detection system, a number of limitations were identified in its design and performance characteristics. Most importantly, these prevented this system being suitable for routine in-vivo assessments of cancer patients. In this chapter, there is an emphasis on modifications made to the illumination, endoscope, camera and associated image processing in the first generation system, to enable its use on patients in a clinical setting. The results of some in-vivo system evaluations are also presented here.

During the development of this second generation detection system, a new

PhD student, Jacqueline Hewett, joined the project. Thus, Jacqueline contributed to the construction of part of this system, of which her assistance is acknowledged in this chapter.

5.2 Endoscope and violet light delivery

As discussed in chapter three, conventional endoscopes have poor optical transmission in the violet region of the spectrum. This is not surprising given that this spectral region contains little useful visual information for imaging within the human body. The advantage of violet illumination for photodetection has been highlighted in chapter four, however. Unfortunately, the UV transmitting optical fibre, used in the first-generation endoscopic detection system, was not providing adequate optical power over a wide enough angle of illumination. Therefore, an alternative means of delivering the violet light to the GI tract was required. This problem could not be solved using additional optical fibres due to the limited diameter of the biopsy channel.

In order to increase the angle of illumination from the fibre, considerable effort was invested in changing the shape of the fibre tip. However, I was unable to achieve a 120-degree angle of illumination by melting or sanding the tip into different shapes. Even if this had been possible, the available power density of the violet light would have been insufficient to excite adequate fluorescence. Thus, a solution was sought through the investigation of possible modifications to the endoscope. As detailed previously, it is only the imaging fibre bundle, within the endoscope, that has stringent specifications regarding core size and numerical aperture. For the illumination fibre bundle, the restrictions are not so severe. For this reason, it was decided that the fibres comprising the illumination bundle could be exchanged for fibres with enhanced transmission below 450nm.

Storz, the endoscope manufacturer agreed to modify an endoscope by

replacing the illumination fibres, with fibres that met our specifications. The hard clad, multi-mode UV transmitting fibres used in the first-generation system (3M Power-Core, attenuation 0.08dB/m at 400nm) were specified for the illumination bundle. Due to the lens system at the proximal end of the illumination bundle, an angle of illumination covering the ultra-wide imaging field was achieved.

The custom-designed endoscope that Storz supplied had an eight-fold improvement in transmission at 400nm compared with their standard model. The transmission of the custom endoscope relative to the standard endoscope is illustrated in figure 5.1.

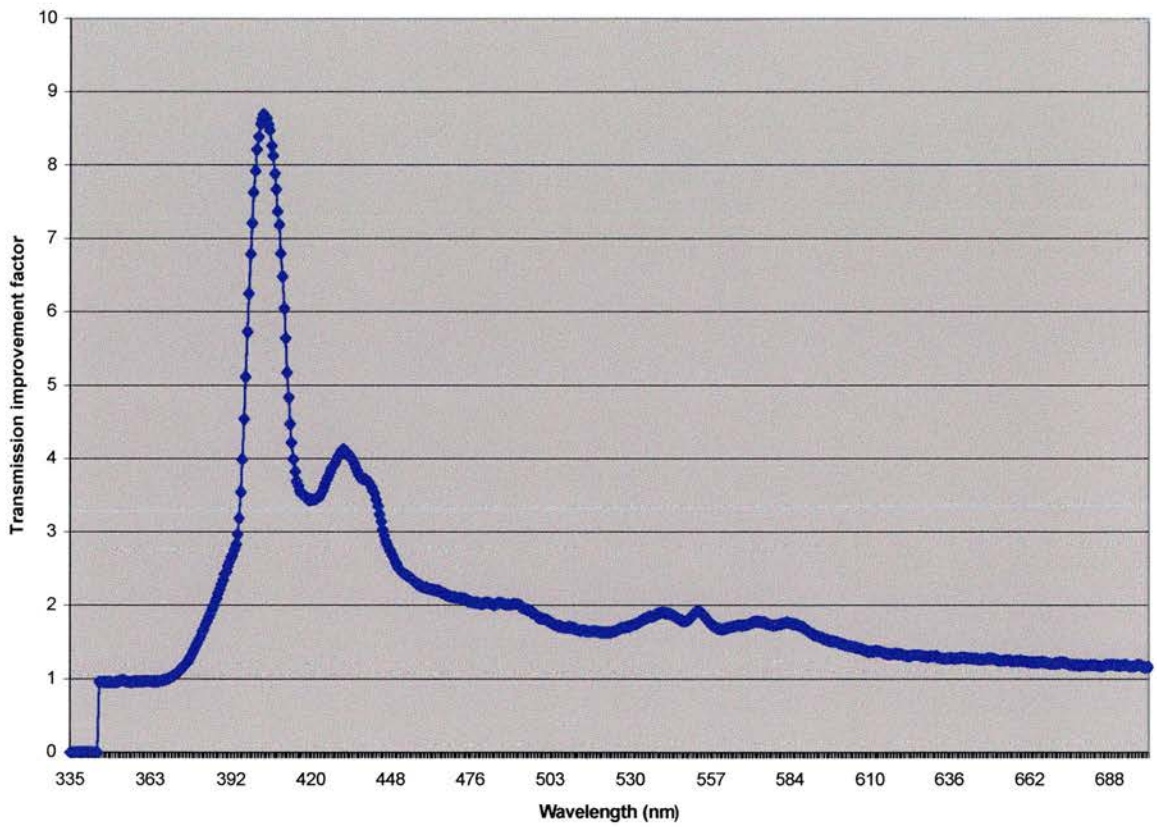

Figure 5.1: Transmission of Storz violet transmitting endoscope relative to standard endoscope.

The incorporation of this new endoscope into the detection system not only

solved the problem relating to the violet light delivery but also meant that the biopsy channel was free to be used conventionally during the endoscopic procedures.

5.3 Light Sources

In the first-generation detection system, the fluorescence and colour images were grabbed consecutively rather than simultaneously. Hence, as discussed previously, the continual muscular movement within the GI tract caused the content of the two images to be uncorrelated. Consequently, image-processing algorithms, such as superposition, could not be carried out due to the lack of pixel registration between the colour and fluorescence images.

This problem was solved through the filtering of the mercury arclamp with a custom-designed multi-layer dielectric mirror (Laseroptik, Germany). This filter transmits the mercury spectrum apart from a 60nm band between 600 and 660nm, which it reflects. Figure 5.2 illustrates the filter transmission characteristics of the Laseroptik filter and of the interference filter for the intensified camera, which will be discussed in the next section.

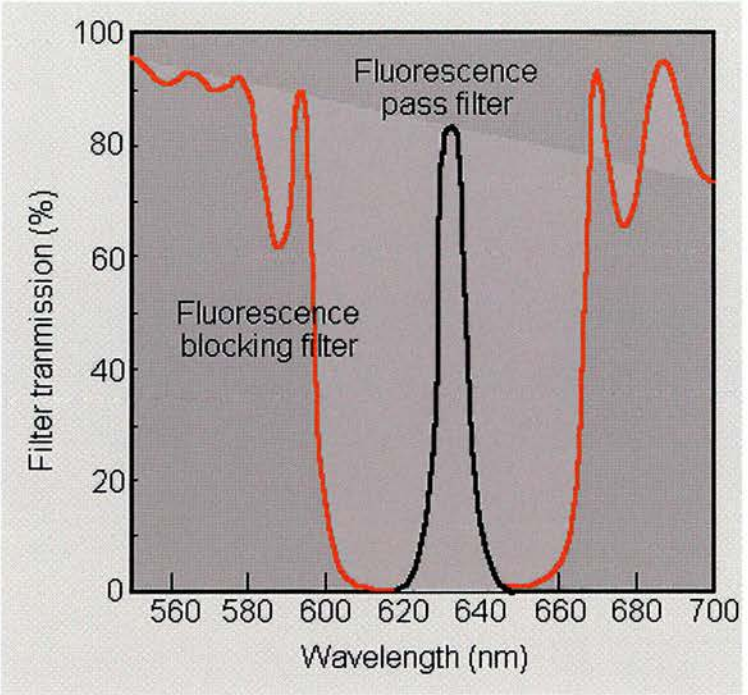

Figure 5.2: The transmission characteristics of the Laseroptik filter (fluorescence blocking) and the pass filter (PpIX fluorescence) used with the intensified camera

Because the filter transmits the mercury spectrum from below 400nm to above 700nm, it is used to provide both the white light for navigation and the violet excitation light. The 60nm spectral band that the filter reflects corresponds to the PpIX emission bandwidth. Thus, the filtered intensified camera detects the PpIX fluorescence only and not the reflected or scattered light from the illumination source.

The missing wavelength band from the illumination does not affect the colour balance of the navigation image. Any slight correction can be achieved by re-normalising the RGB colour balance of the camera against a white reference. Therefore, due to the custom filtering of the mercury lamp, the violet and white illumination are provided by one source, which results in the potential to grab simultaneously, both the fluorescence and navigation images having identical fields of view.

5.4 System Configuration

The configuration of the second-generation detection system is demonstrated in figure 5.3. Each aspect of this system will be discussed in detail in the following sections.

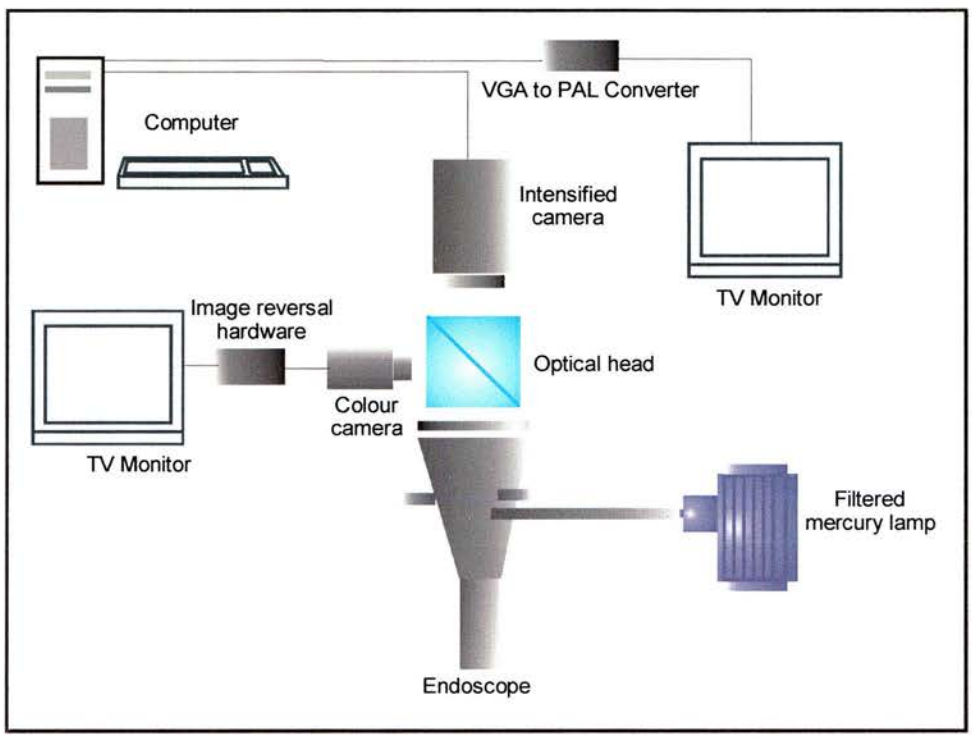

Figure 5.3: Configuration of equipment for second-generation detection system

5.5 Detection Unit

The optical head and miniature colour camera used in the first-generation detection system were incorporated within the second-generation version. However, due to the specialist filtering of the mercury lamp, saturation of the intensified camera no longer occurred and so the electronic shutter was no longer necessary and was removed from the optical head.

A footswitch was incorporated within the first-generation detection system for the switching of the white light source, the control of the shutter and the

grabbing of the images. Now that the violet and white light were simultaneously provided by the mercury lamp, this footswitch was also no longer required.

A remote miniaturised head intensified camera (Photonic Science ISIS 3, 753x576) measuring 115mm by 70mm replaced the original camera, which was too large for the end of the endoscope. The intensified camera was filtered with a 10nm-wide interference filter centred at 633nm, such that only the PpIX fluorescence can be detected. The pass transmission characteristics of this interference filter are shown in figure 5.2.

The fibre-coupled spectrometer was not coupled into this detection unit because it was felt not to add any significant diagnostic value to the detection unit during in-vivo evaluations. Thus, the biopsy channel was free for use by the clinician.

The detection unit used in the second-generation arrangement is illustrated in figure 5.4.

Figure 5.4: Detection unit comprising of optical head, colour and intensified camera, coupled to the violet transmitting endoscope

5.6 Displaying of images

5.6.1 Colour image

As discussed in chapter three, the colour image orientation is the mirror of the intensified image, due to the presence of the beamsplitter within the optical head. In order to free the computer for image processing tasks only, other means of reversing the colour image, to match the orientation of the intensified image, were investigated. Initially, this task was accomplished by reversing the polarity of the horizontal scan coil on a television, such that the resulting image was left-to-right inverted. Problems were still encountered in recording this image with a video recorder because the opposite orientation image was recorded.

Fortunately, Storz, the endoscope manufacturer markets hardware specifically designed to reverse an image, prior to display on a monitor. This equipment comprises of a frame-grabber, which digitises the signal, applies a flip to the matrix and converts it back to an analogue PAL signal, for display on a conventional monitor. Thus, the image from the colour camera is sent, via a composite signal, through the image reversal hardware and to a monitor, where the entire procedure is recorded on a video recorder. This meant that the computer was no longer required for the display of the colour image.

5.6.2 Intensified image

Patient-to-patient variability combined with the demands of the clinical environment means that it is sometimes difficult to ensure that the elapsed time between administration of the ALA and subsequent inspection is optimised, to ensure maximum contrast in the fluorescence image. Consequently, the image intensifier is usually operating near its maximum gain and therefore, the image quality suffers from a characteristic "salt and pepper" noise. This noise arises as a background signal due to thermally

released electrons from the photocathode. Once released, such "noise" electrons propagate through the system, giving rise to an optical output that is indistinguishable from that arising from a "signal" electron. The resulting "salt and pepper" noise appears as brighter pixels, randomly superimposed on top of the image. This noise distracts the operator, particularly when a still image is acquired, since the natural averaging of the eye over several frames no longer occurs.

Consequently, to remove the "salt and pepper noise" and improve the contrast of the fluorescence images, processing is carried out prior to display of the fluorescence data. Due to the inherently random nature of this noise, averaging over a number of frames or pixels improves considerably the image contrast. In the system, the user can choose between two processing algorithms, a rank filter which replaces each pixel with the median value of the surrounding eight or an averaging filter which outputs the average of the last eight frames. Jacqueline helped to write the necessary software for both of these filters, which suppress the "salt and pepper" noise at the expense of spatial or temporal resolution respectively.

The analogue output from the intensified camera is acquired using a high-speed frame grabber incorporating a digital signal processor (Matrox, Genesis). After processing, the digital image is converted to a PAL video signal for display on a conventional high-resolution TV monitor. Given that the colour and intensified images are displayed on TV monitors, the entire procedure can be recorded on a conventional video recorder.

A photograph of the second-generation detection unit in the operating theatre is pictured in figure 5.5.

Figure 5.5: Photograph of detection unit

5.7 System Evaluation

Prior to the system being used within the clinical setting, the clinicians reassured themselves of its safety and operational compatibility within an endoscopic training environment. Within the laboratory, the system was evaluated by ourselves and the clinician, using an endoscopic training aid made from sponge. A hot wire cutter is used to create an irregular channel within the sponge, which resembles an oesophagus or colon. Locations within this model were loaded with a fluorescent agent and using the detection unit, the operator was tasked to find the "tumour" site. Figure 5.6 shows the sponge model used for the initial evaluation of the system.

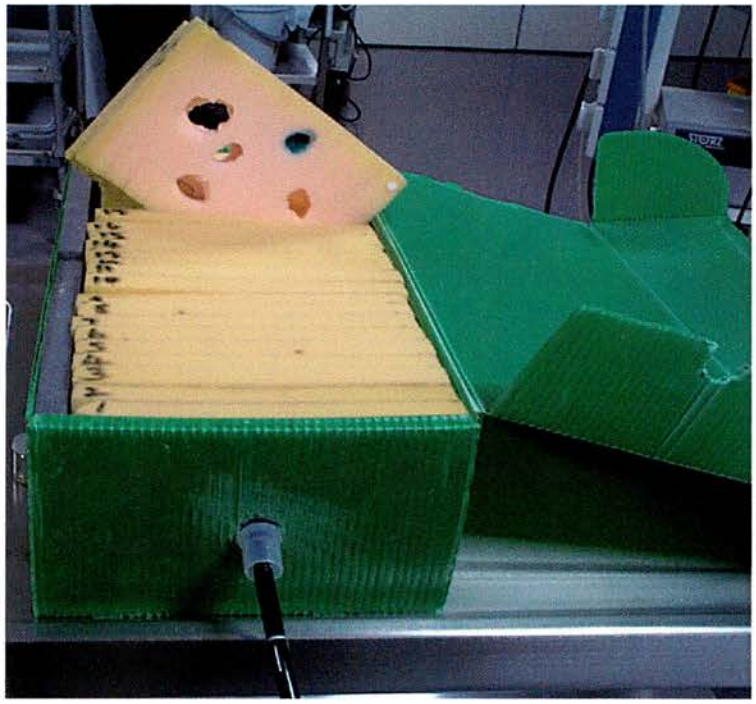

Figure 5.6: Sponge model used as a training aid

Figure 5.7 demonstrates the detection system being tested by a clinician within the sponge model.

Figure 5.7: Clinician evaluating system with sponge model

The navigation and fluorescent images recorded within the sponge aid, marked with fluorescent dye, can be seen in figure 5.8. It should be noted that the fluorescence is not observable within the colour image and correspondingly the fluorescent image is not degraded by scattered or reflected light from the illumination source.

a) 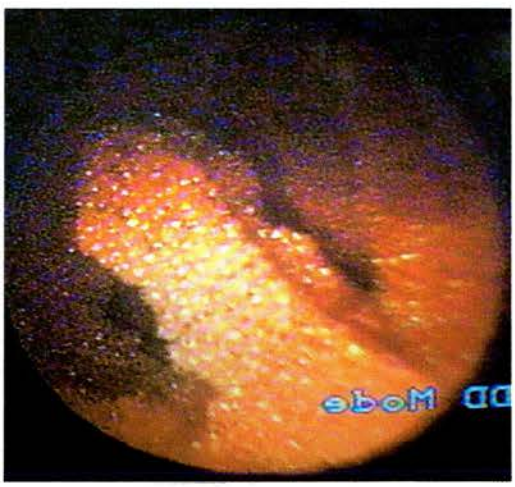 b) 

Figure 5.8: The a) navigation image and b) fluorescence image of a "tumour" site within the foam model

As one notices from figure 5.8, the performance of the system within the sponge model is extremely impressive, with the smallest areas of fluorescent dye appearing with high intensity in the fluorescent images. After witnessing the performance of the system and the encouraging results, the clinicians wanted to implement the unit for patient evaluation.

I estimated the sensitivity of the detection system by considering the efficiencies of the various pieces of equipment incorporated into the system. The following calculations approximate the minimum numbers of emitted fluorescence photons required before a signal is detected by the endoscopic imaging system. Although the figures used, are estimates, it provides an idea of where the emitted fluorescence photons are attenuated in the system.

Figure 5.9 illustrates the geometrical arrangement for the collection of emitted fluorescence photons by the endoscope.

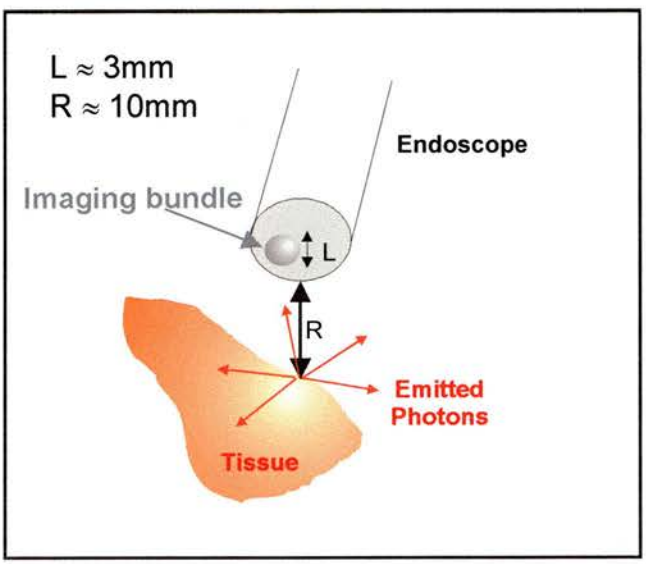

Figure 5.9: Collection geometry of endoscope

Collection efficiency of endoscope = endoscope collection area / Area of sphere of emitted photons

$$= \frac{\pi\left(L/2\right)^2}{4\pi R^2} = \frac{L^2}{16R^2} \approx 0.5\%.$$

Thus, the geometrical loss associated with the collection efficiency of the endoscope is the largest loss in the system.

Taking into consideration the intensifier photocathode efficiency (≈20%), the intensifier gain (≈10^5), the CCD efficiency (≈10%), the full well depth of the CCD (≈ 10^5) and the endoscope transmission (≈20%); the minimum number of fluorescence electrons which are detected at the camera are;

$$\text{Minimum \# of electrons detected} = \frac{\text{Full well depth}}{128} = \frac{10^5}{128} \approx 10^3,$$

the digitisation noise is taken into consideration by dividing the full well depth by 128 rather than 256.

Thus,

$$\text{Min. \# electrons} \approx 10^3 \approx 20\% \times 20\% \times 10^5 \times 10\% \times \text{\# Fluorescence Photons},$$

and therefore the minimum number of fluorescence photons detected at the camera are between 2 and 3. Taking into consideration the geometrical collection efficiency of the endoscope, this estimation shows that, in principle, between 400 and 600 fluorescence photons should be emitted from the tumour site for a fluorescence signal to be detected on the intensified camera.

As mentioned previously, before the detection unit can be relied upon as an integrated part of any screening program, it is necessary to evaluate its performance on previously diagnosed cancers. Figure 5.10 shows the detection unit, ready for use in the operating theatre.

Figure 5.10: Detection unit in an operating theatre

5.8 In-vivo testing

The in-vivo evaluation of the endoscopic detection system was carried out on patients with diagnosed cancers of the GI tract. To confirm that the system located the cancerous tissue, the clinical team carried out an endoscopy, with the detection system, on patients prior to their operations for surgical removal of cancers of the oesophagus, stomach or colon. Figure 5.11 shows the system in use, on a patient within the operating theatre.

Figure 5.11: Detection unit in use on a patient in the operating theatre

A study of the optimum time between ALA administration and observation was attempted. However, we found the experiment impossible to control, due to the unpredictability of the operation times in theatre. The elapsed time between administration and observation varied between three and six hours.

Although this second-generation system is still in the early stages of in-vivo evaluation, initial results have been extremely encouraging. Figure 5.12 is an example of two images that I captured from a patient with cancer of the oesophagus. The region of cancerous tissue is not obvious by eye in the colour image but it is clearly evident in the intensified fluorescence image.

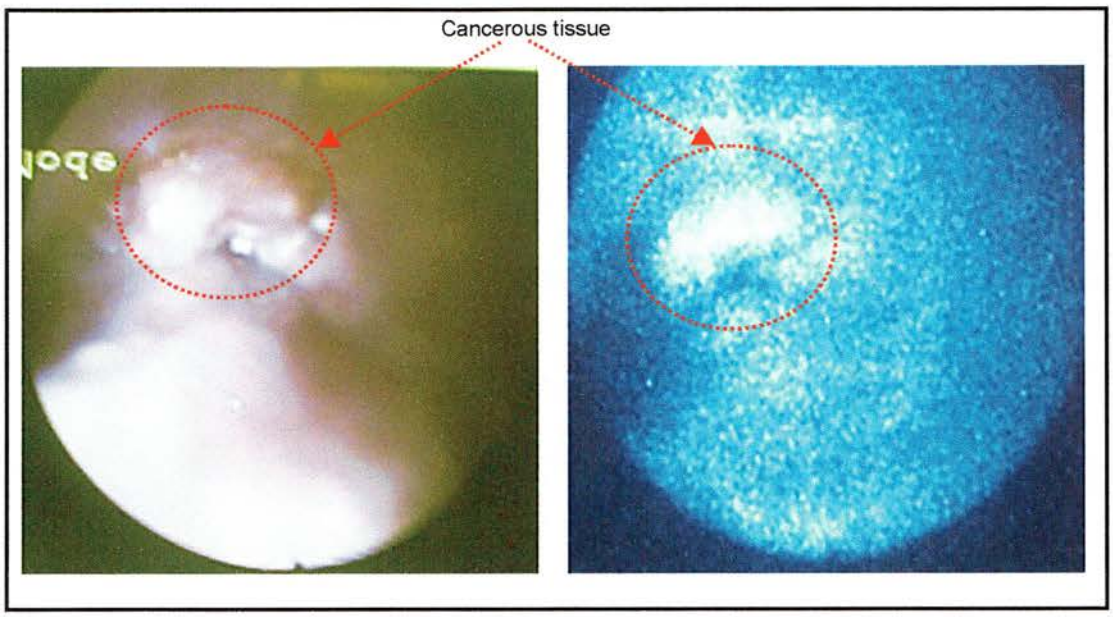

Figure: 5.12: Colour and fluorescence image captured from patient with oesophageal cancer

Further examples of images captured by the detection system are shown in figure 5.13. This patient had stomach cancer, where again the cancer was not obvious in the colour image but could be seen clearly in the intensified image, containing the PpIX fluorescence.

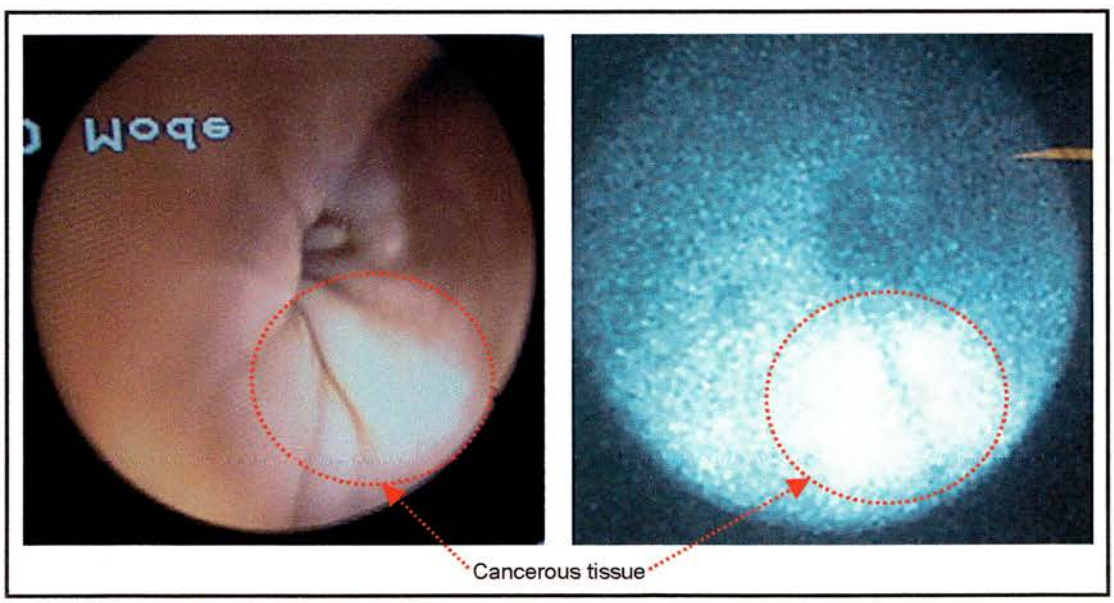

Figure 5.13: Colour and intensified image of cancerous tissue in the stomach

Colon cancer often appears in the form of polyps and while these are easily detected via the colour navigation image, they are not always composed of cancerous tissue. Hence, diagnosis can be achieved through observing the intensity of the fluorescence displayed in the intensified image, where a high intensity region suggests the presence of cancerous tissue. Figure 5.14 illustrates the fluorescence recorded from a polyp in a patient's colon.

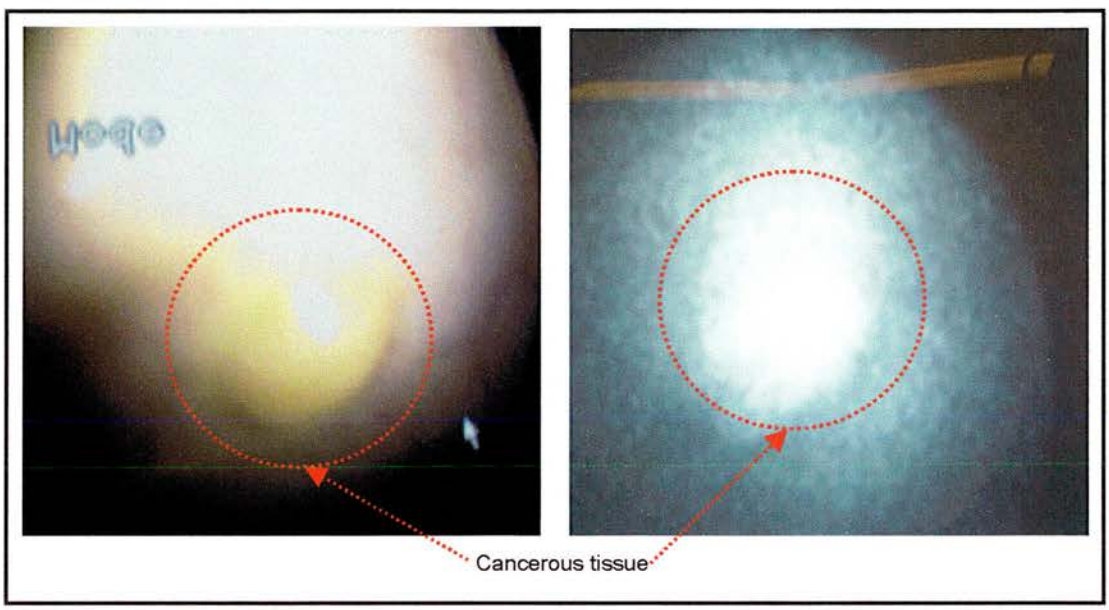

Figure 5.14: Images of a cancerous polyp within a patients colon.

This second-generation detection unit is now located at the hospital, where it is undergoing further evaluation by the clinical team.

5.9 Discussion

The most interesting result gained from the in-vivo testing was that no fluorescence reversal was observed in the oesophagus, unlike the fluorescence pattern in the resected specimens. Thus, it is important to note that while ex-vivo experimentation may be useful; any observed patterns should not be correlated directly with in-vivo behaviour.

The second-generation detection system has now successfully reached the point where no further system development can be embarked upon, until the unit has been fully evaluated by the clinicians. The detection unit proved very successful during its assessment by the clinical staff in the sponge training model. To date, everyone has been encouraged by the performance of the system in patients with diagnosed tumours. It is felt that this endoscopic detection system has the potential to offer an effective solution to the screening of patients who are at high risk of developing cancer within the GI tract.

It is vital to take into consideration that the detection system can only be as accurate as the selectivity afforded by the PpIX. It is reasonable to conclude that because the detection system proved effective for the targeting of areas marked with a fluorescent chemical, within the sponge model, it might also perform effectively in the human body. However, the fluorescence images recorded from within the human body lacked contrast in comparison to those recorded within the sponge model. This would suggest that the ALA-induced PpIX lacks selectivity within the cancerous tissue and consequently, the healthy tissue fluorescence degrades the optical contrast of the images.

Once the system is used as part of the screening programme, studies can be expected to establish the optimum dose of ALA and the time at which maximum contrast can be observed. I found this impossible in this study, as the inspection time could not be controlled due to the unpredictability of timing in the operating theatre.

CHAPTER SIX

MULTI-SPECTRAL IMAGING SYSTEM FOR DERMATOLOGY

In this chapter, the development of a multi-spectral fluorescence imaging system for the detection and observation of skin cancers is discussed. The results obtained through examining patients with this imaging system are presented in detail, along with its potential benefits in dermatological applications.

6.1 Introduction

Non-melanoma skin cancer is the most common form of cancer in fair skinned populations and its incidence is increasing worldwide. At present, an exact cancer diagnosis is only possible after histological examination of the excised tissue. However, the excised tumour frequently proves to be benign and thus surgery, with its inevitable disfigurement, proves to have been unnecessary. It is therefore important to establish a non-invasive, non-destructive technique, which determines, in-situ, a diagnosis of the area of skin in question.

As discussed in chapter one, the principles of fluorescence imaging can be exploited for the purposes of tumour detection and border demarcation. Furthermore, such fluorescence detection in-situ may be used to optimise the conditions necessary for PDT, such as the optimal time for light activation, the rate of PpIX photobleaching and the treatment time.

During the construction of the endoscopic detection system, we recognised the potential of the fluorescence imaging for application to other tissues of the body. Consequently, we initiated collaborations with the Department of Dermatology and Photobiology at Ninewells Hospital in Dundee. Although the hospital had already started treating patients with PDT, they felt that a fluorescence imaging system offered the potential for the optimisation of the PDT procedures. It was also felt that such a system would aid in the diagnosis of cancerous tissue and better demarcate tumour boundaries for surgical purposes.

It was decided that a unit was required that would enable the clinicians to learn from the fluorescence imaging process and optimise the conditions for PDT. The system was to be conducive to the clinical environment in which it would be used, but most importantly, it had to be adequately versatile to enable investigations into the entire fluorescence and PDT process in the skin. It was vital that the equipment could be easily adapted for use on any patient and on any part of the skin.

In this chapter the development of the multi-spectral fluorescence imaging system is discussed along with the results gained using the system on a sample of patients.

6.2 The System

The choice of inspection equipment was not restrained by weight and speed, because the skin does not suffer continuous muscular movements or require endoscopic inspection. Consequently, we decided that not only would the imaging system be designed to monitor the PpIX induced fluorescence but it would also record the autofluorescence induced by the endogenous molecules within the tissue. I felt that the imaging of the reflected excitation light would also provide further useful information.

6.2.1 Optimisation of the excitation light source

ALA is again used as the photosensitising drug in the Department of Photobiology for the purposes of PDT. An initial experiment was conducted to confirm the optimum wavelength of excitation of PpIX. This was achieved using a monochromator, containing a 1600W-xenon lamp, which excited a vial of PpIX at 10nm intervals between 350 and 510nm. The induced fluorescence was recorded with a monochrome camera filtered with a 633±5nm-interference filter. The series of false colour images recorded during the experiment are illustrated in figure 6.1.

As expected, the figure confirms that maximum PpIX fluorescence is induced by light between 400 and 410nm. Hence, the 100W mercury arclamp is appropriate for use within this imaging system, as it is economically viable, easily maintained and operated and has a strong spectral output in the violet band of primary interest.

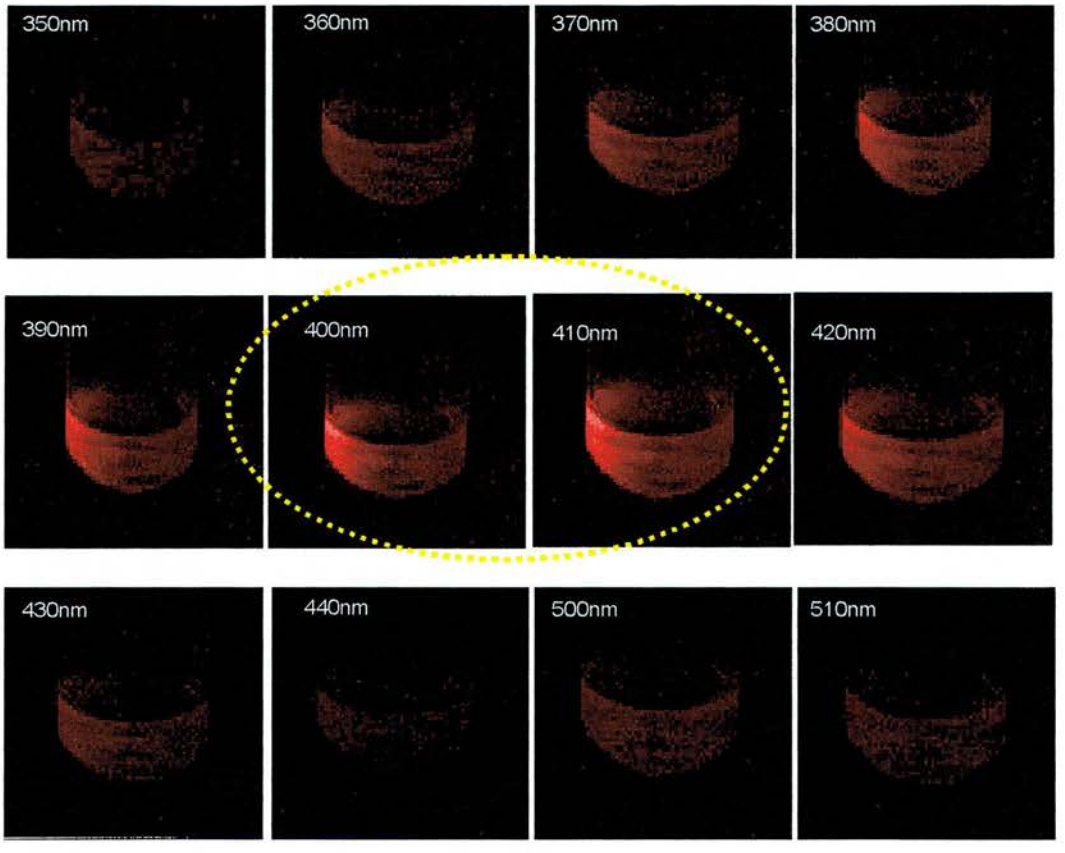

Figure 6.1: Images of PpIX fluorescence induced by a range of excitation wavelengths

When considering the autofluorescence induced at this excitation wavelength, it can be seen from figure 1.11 in chapter one that flavins, porphyrins and lipo-pigments are the endogenous molecules that will be excited. The flavins and the lipo-pigments have a characteristic emission at predominantly 550nm, while the porphyrins emit fluorescence at 630 and 670nm. (These values will be considered later in this chapter).

The next question was "*How should a mercury arclamp be optimally filtered to induce maximum fluorescence from PpIX, without itself having any output in the fluorescence bands of interest?*"

I investigated a number of filters for the filtering of the mercury light source. The most suitable were BG3, BG37, UG5 (Schott glasses) and a 70nm wide interference filter centred at 400nm. Figure 6.2 illustrates the spectral output

of the mercury arclamp filtered with the above mentioned commercially available products (measurements made by Jacqueline).

The measured power from the mercury lamp filtered with each of the filters was as follows:

- BG 37 70mW
- UG 5 80mW
- BG3 100mW
- 400±35nm 24mW.

These power measurements suggested, due to the high power, that BG3 was the most appropriate filter. From figure 6.2, it is implied that the spectral peak at 405nm, corresponding to the mercury lamp filtered with BG37 would induce the maximum PpIX fluorescence.

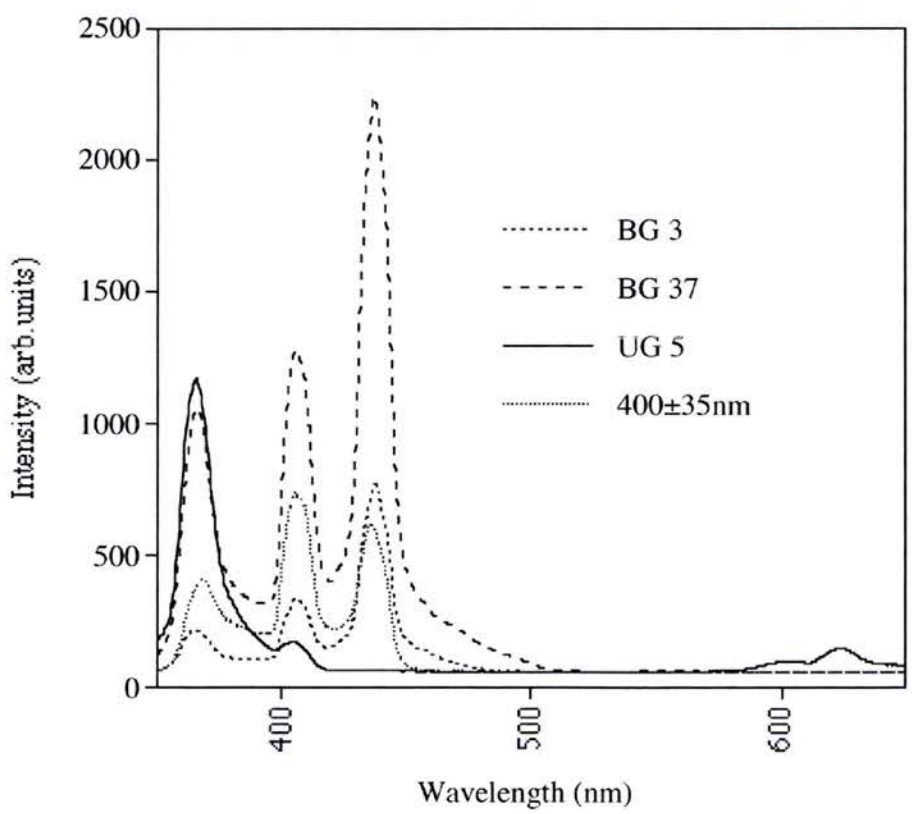

Figure 6.2: Spectra of mercury lamp filtered with five different filters

To determine the optimum filtering of the mercury arclamp a vial containing a PpIX solution was excited with the light from each of the filters with the mercury lamp. I did not carry this experiment out on tissue, as the induced autofluorescence would have affected the results. Figure 6.3 shows images of the PpIX filled vial, recorded with a monochrome camera filtered with a 633nm filter and illuminated using the above mentioned filters in combination with the mercury lamp.

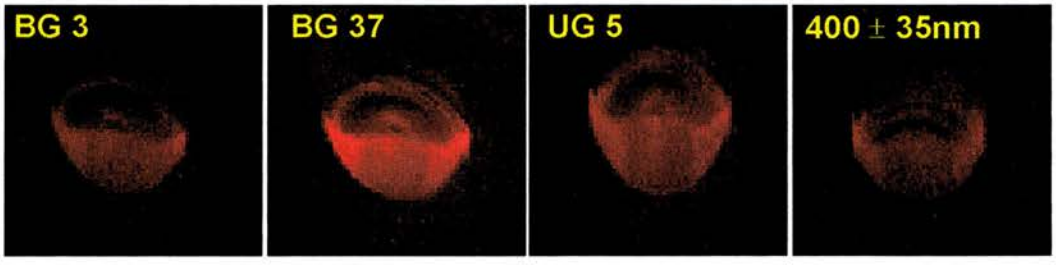

Figure 6.3: Images of vials of PpIX fluorescence induced by mercury lamp filtered with a) BG 3, b) BG 37, c) UG 5 and d) 400nm.

It can be seen from the above figure that BG37 induces the most PpIX fluorescence. However, reference to its spectral transmission in figure 6.2, suggests that the residual transmission of the filter at 500nm may restrict its use for imaging very low autofluorescence levels.

The skin is more assessable than the GI tract and thus, it was possible to conduct rigorous, in-vivo, experiments to determine the optimum filtering of the excitation light. A patient was selected who had a number of histologically confirmed superficial basal cell carcinomas on his back. ALA cream (20%) was applied topically to the lesions using a dosage level of 50mg per cm^2.

From such in-vivo experimentation I determined, that the BG37 filter did not affect the contrast of the autofluorescence images. This result can be observed in figures 6.4 and 6.5, where the BG 37 filtered excitation induces

the maximum PpIX fluorescence, resulting in no loss of contrast in the autofluorescence image. The autofluorescence images were recorded through a monochrome camera filtered with a 540nm±22nm interference filter, as 540nm is one of the peaks excited by the 400nm illumination. The BG 37 filter was therefore selected as the optimum to be used in combination with the mercury arclamp.

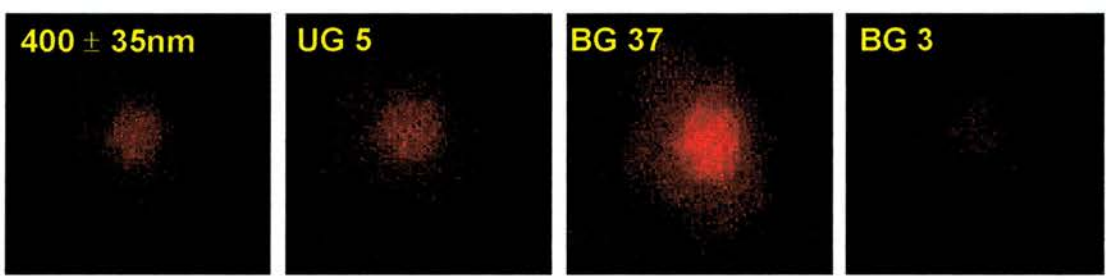

Figure 6.4: Images of PpIX fluorescence induced by mercury lamp filtered with a) 400nm, b) UG 5, c) BG 37, d) BG 3 from a superficial basal cell carcinoma after 4 hours ALA application.

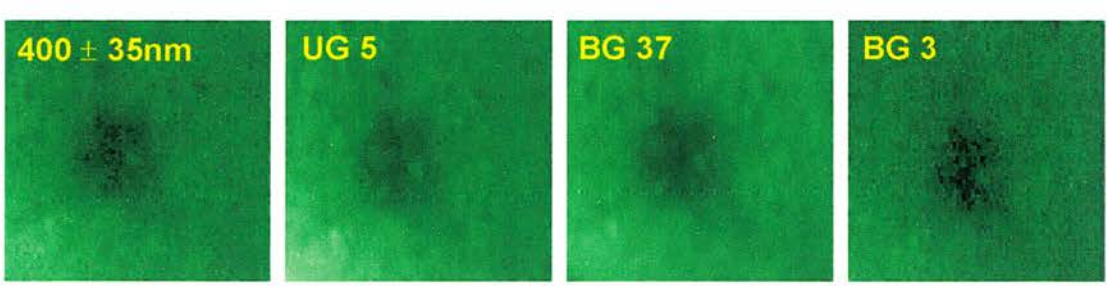

Figure 6.5: Images of autofluorescence induced by mercury lamp filtered with a) 400nm, b) UG 5, c) BG 37, d) BG 3 from a superficial basal cell carcinoma after 4 hours ALA application.

6.2.2 Multi-spectral imaging unit

As discussed previously, this system not only records the PpIX-induced fluorescence but also the autofluorescence from endogenous molecules and

the reflected excitation light.

The induced fluorescence is monitored via imaging because this method enables a quicker and more remote recording of the in-vivo results. The system comprises a low cost, monochrome, CCD array (Cohu CCD 1100) with a variable exposure/integration time. Unlike the GI tract, real-time imaging is not necessary on the skin, as the subject can remain adequately stationary for the recording of results. The integration time can be continuously adjusted from 20 milliseconds to 1 second, without excessive increase in the thermally induced dark level. Consequently, despite the low intensity of the fluorescence, bright, high contrast images can still be obtained.

Monochrome cameras provide only spatial data based on the variation in the intensity of reflected light. By imaging three spectral bands, red, green and blue, which match the sensitivity of the human eye, one is able to analyse an image based on spectral effects that we recognise as colour. While colour cameras image light in the visible wavelengths (450-650nm), the CCD sensors that they are based on can detect light at wavelengths from 400nm to 1100nm. A multispectral CCD camera expands on the concept of the colour camera to enable observation of specific wavebands, which may be beyond the sensitivity of the eye. Thus, the sensitivity of the system can be increased substantially by the targeting of very specific wavebands.

A filter wheel was coupled to the front of the camera to allow insertion of appropriate filters. For the imaging of the autofluorescence a 540±22nm interference filter was used (Ealing, UK), while a 633nm (10nm bandwidth) interference filter was used for the imaging of the PpIX fluorescence. A broadband interference filter centred at 400nm (70nm bandwidth) gave an image of the reflected illumination light distribution, against which the fluorescence image was normalised.

The monochrome camera was interfaced to a desktop PC via a frame

grabber (Kane CX100). Figure 6.6 illustrates the configuration of the multi-spectral imaging system.

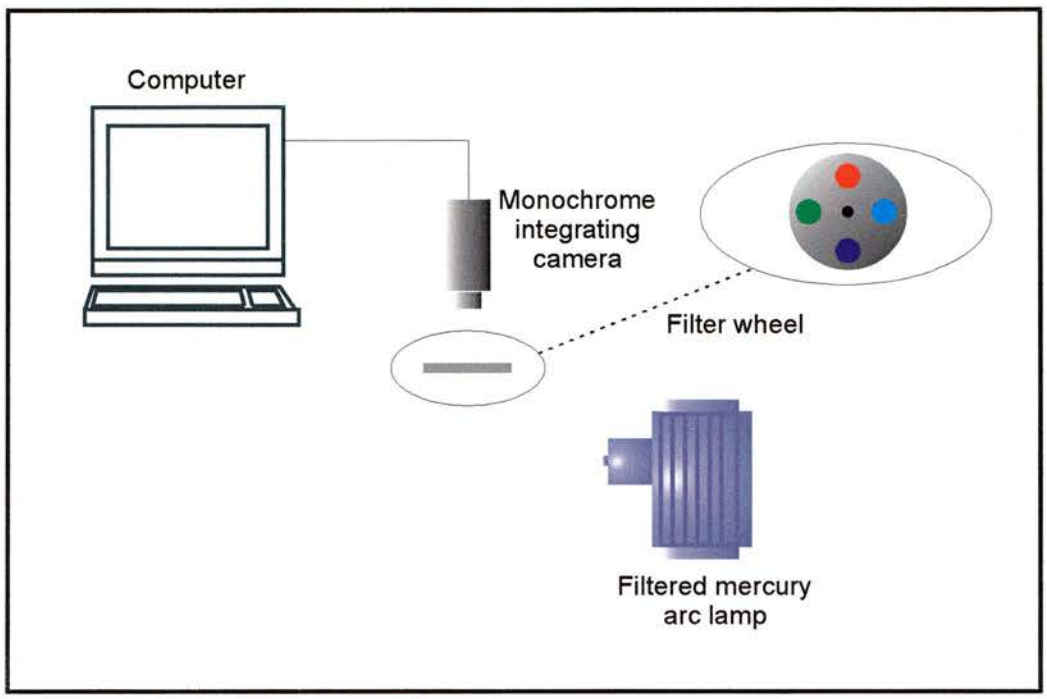

Figure 6.6: System configuration for imaging of skin cancers

Both the colour camera and frame grabber are controlled by software, which I wrote in the Delphi environment. As in the endoscopically coupled counterpart, the software was designed to facilitate a user-friendly interface between the clinician and camera controls. This software has the facility for the display of four images, which may correspond, to different spectral bands. Only one image is grabbed at any one time, while the software displays the previously acquired images from the remaining three spectral bands.

The values for the integration time, gain and offset are controlled via scroll bars and displayed independently for each image. The program also incorporates the facilities to display the intensity values of individual pixels and the spectral data from the fibre-coupled spectrometer. Figure 6.7 displays an example desktop containing an image of a lesion in four different

spectral bands.

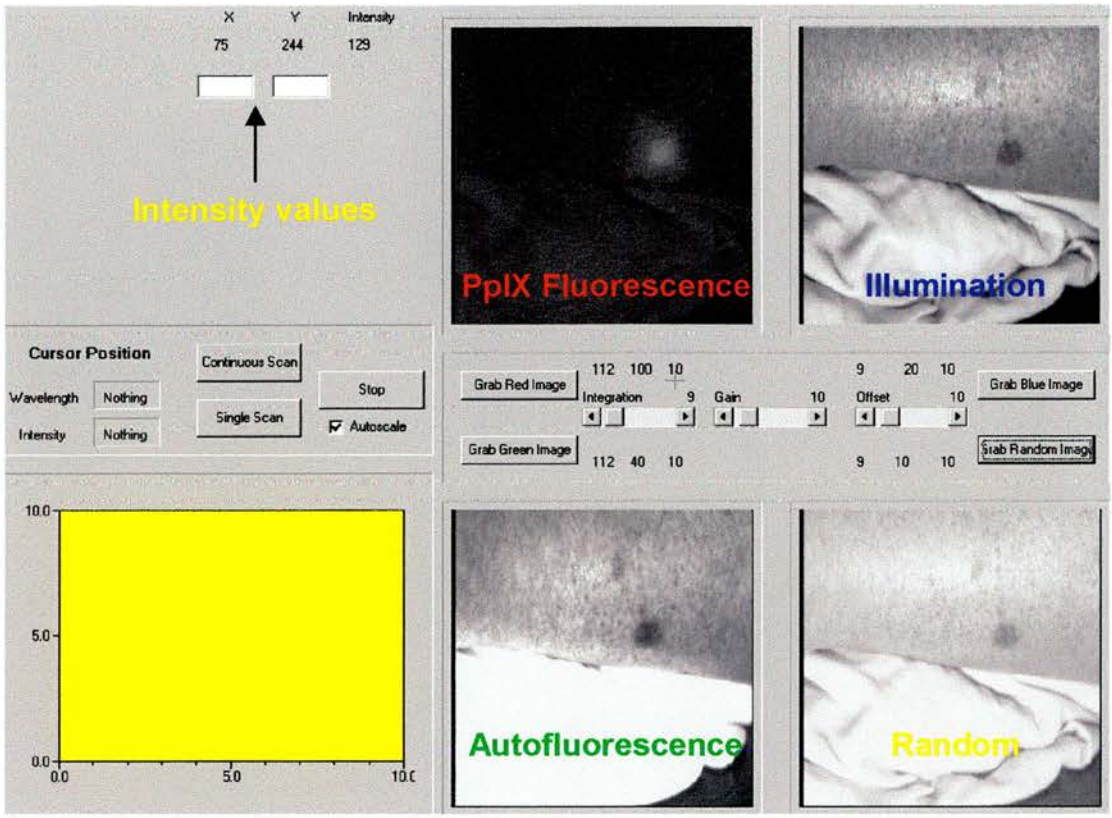

Figure 6.7: Example desktop displaying four spectral bandwidths of a skin lesion

(The code for the software incorporated within this system is included in appendix 2.)

The arrangement for the multi-spectral imaging and illumination unit is demonstrated in figure 6.8. The filtered mercury arclamp was attached to a tripod to allow simple height changes. The CCD camera and filter wheel were coupled to the top of the lamp, which proved convenient as only one instrument required alignment rather than two separate pieces of equipment. A measuring stick was also connected to the mercury lamp to ensure that the patient remains at the same distance during the acquisition of all the images. The arrangement of the equipment also allowed repeatability of the results.

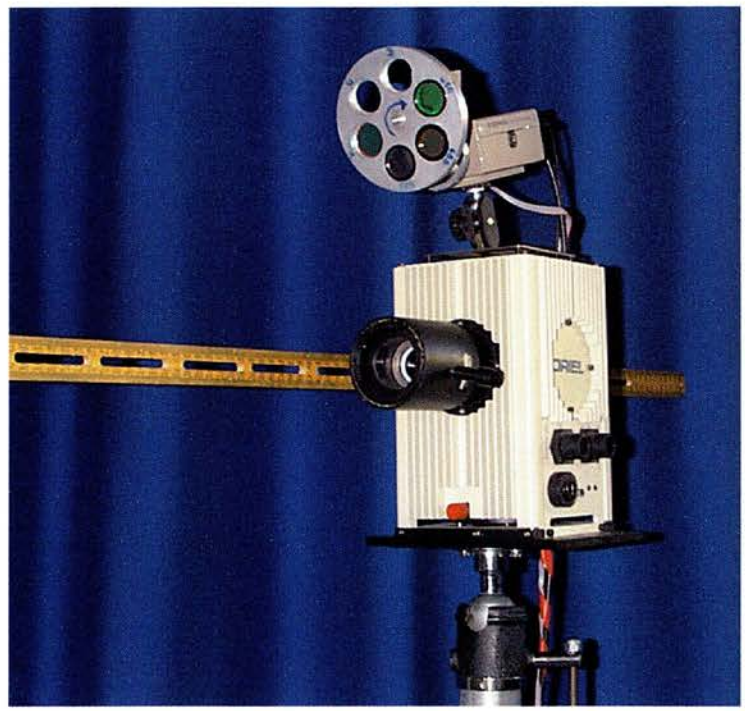

Figure 6.8: Filtered mercury lamp and variable frame-rate camera with incorporated filter wheel

6.3 Results and discussion

We used the multi-spectral imaging system to investigate the relationship between ALA application time, the delay time before observation, the total elapsed time and the optical contrast between cancerous and healthy tissue. We define the application time as the contact period of ALA with the tissue and the delay time as the interval between the end of ALA application and observation. The definition of total elapsed time is the interval between initial ALA administration and subsequent observation (application + delay).

Due to the accessibility of the skin, a number of experiments have been carried out on patients to learn about the variation of the induced fluorescence over time. The patients were prepared for inspection by removing the crusts that covered the lesions, in order to increase the permeability of the lesion and thus facilitate the penetration of ALA. After

ALA administration, the carcinomas were covered with a thin occlusive dressing (Tegaderm, 3M, UK) to prevent the cream being smeared off. The ALA was applied over approximately a $4cm^2$ area, encompassing the lesion and surrounding healthy tissue. Inspection of the lesion involved removing the dressing and any excess cream, examining the area and recording the results via the spectral imaging system.

One such patient who participated in our studies had a large number of superficial basal cell carcinomas on his back. He kindly allowed us to monitor the induced fluorescence within his tumours over a 22-hour period. Figure 6.9 shows the patient in preparation for inspection with the imaging system.

Figure 6.9: Patient in preparation for inspection with multi-spectral imaging system

During this experiment, the ALA application time was varied between 3 and

20 hours and the delay between the end of application and viewing was varied between 0 and 19 hours.

In keeping with the work of other groups, our preliminary results suggested that a fluorescence signature is observable for elapsed times between 4 and 20 hours. After an application time of three hours, no fluorescence was observed in the healthy or cancerous tissue. However, as figure 6.10 portrays, after a one-hour delay time, intense fluorescence was recorded within the same lesion.

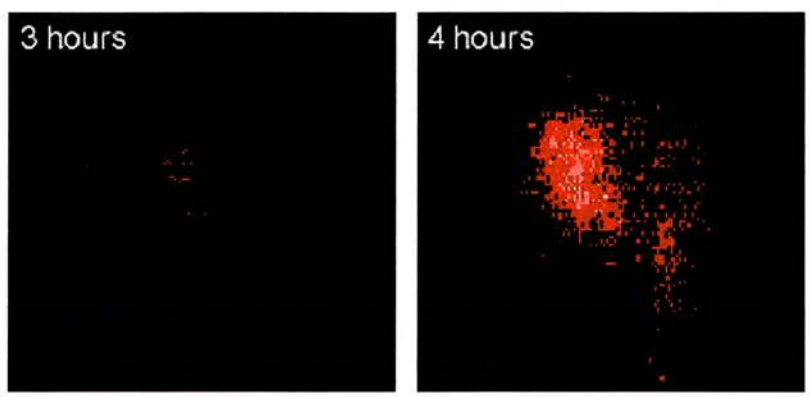

Figure 6.10: Images show the change in fluorescence for an elapsed time between 3 and 4 hours

For ALA elapsed times between four and eight hours, the PpIX fluorescence appeared to be restricted to the tumour site only, resulting in the acquisition of high contrast images. It is important to note that these were macroscopic observations that were not confirmed histologically. High contrast fluorescence images demonstrate the optimum conditions for PDT, as the photoreaction would be restricted to the cancerous tissue only. Figure 6.11 illustrates an example of a high contrast image, achieved after an application time of five hours.

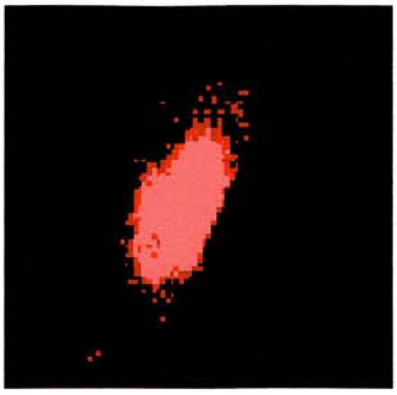

Figure 6.11: Image showing induced fluorescence restricted to tumour after application time of 5 hours

The influence of application time and delay time between ALA administration and observation was investigated and the relationship between them was complex. However, the intensity of the induced PpIX fluorescence was affected more by the total elapsed time, than the two individual times. We observed that for total elapsed times longer than 8 hours, the healthy tissue surrounding the tumour fluoresced. Figure 6.12 illustrates the gradual reduction in optical contrast between lesion and healthy tissue with time.

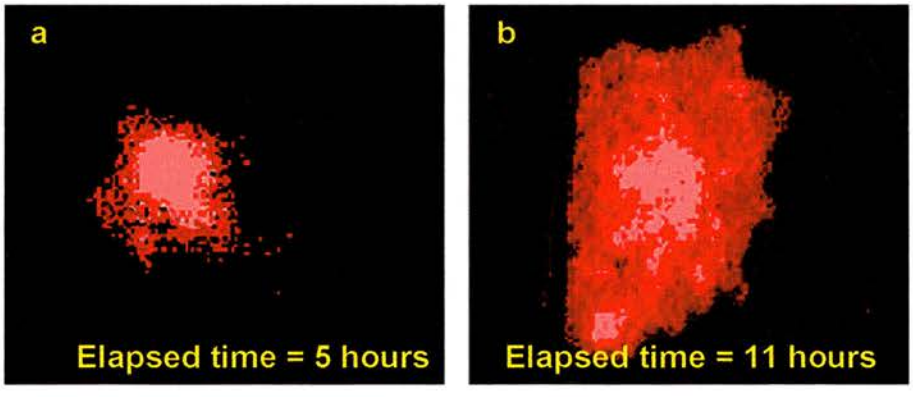

Figure 6.12: Images showing the gradual reduction in optical contrast between an elapsed time of 5 hours and 11 hours.

The growth of induced PpIX fluorescence within the surrounding healthy tissue, seen in figure 6.12(b), corresponded to the area of ALA application. This reduced contrast between cancerous and healthy tissue is unfavourable

for the purposes of PDT, but is potentially useful for diagnostics and the staging of cancer. The healthy tissue PpIX fluorescence can be used to assure the clinician that total ALA coverage of the lesion has been achieved and to enable detection of developing satellite lesions in the vicinity of the main lesion. Figure 6.12b shows a number of fluorescent strands branching out from the main lesion, which could be suspicious but these would require biopsy for confirmation.

The PpIX fluorescence within the healthy tissue did not exceed that observed in the lesion. It was noted that the total area of fluorescence decreased in intensity with elapsed time.

As discussed earlier, autofluorescence can be readily imaged, to provide further information about the tumour. In the small number of patients observed, to date, the autofluorescence was consistently suppressed within the tumour as figure 6.13 demonstrates. This pattern is in agreement with earlier work [1,2].

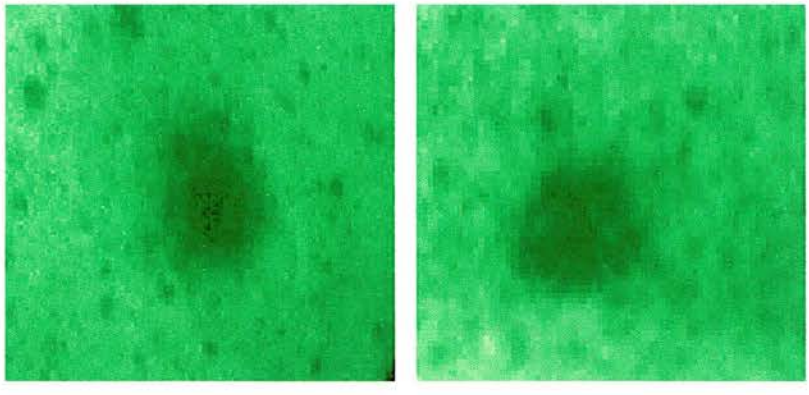

Figure 6.13: Images showing reduction of autofluorescence within basal cell carcinoma on two different patients

The third spectral region of interest is the blue imaging channel. These images are captured through a 400 ± 35nm interference filter. This was intended for use as a guide to the illumination uniformity over the area of observation. However, the patient-to-patient variability of skin reflectivity

affected the results. As figure 6.14 illustrates, on some patients the lesions were highly reflective, while on others the excitation light was strongly absorbed.

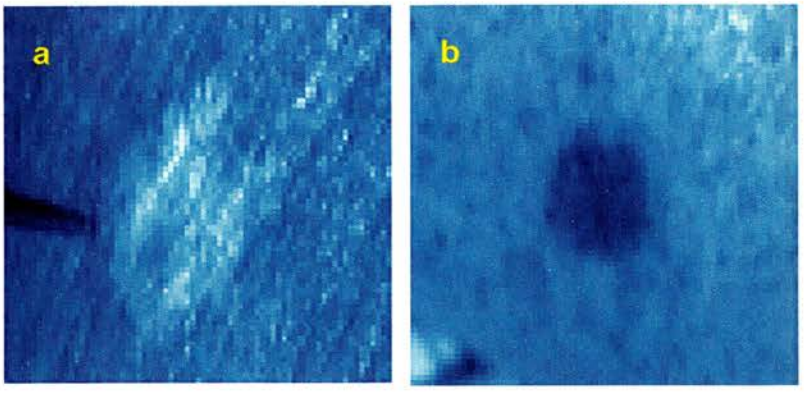

Figure 6.14: Images of illumination channel in two different patients. a) The tumour is highly reflective and b) the tumour absorbs the excitation light.

When the three images, PpIX fluorescence, autofluorescence and illumination, are viewed independently of each other, very little additional information is gained than is available from the PpIX fluorescence image. However, when we carried out image processing on the three images, the apparent contrast between cancerous and healthy regions can be further enhanced. Figure 6.15 illustrates a lesion imaged through the three independent spectral channels.

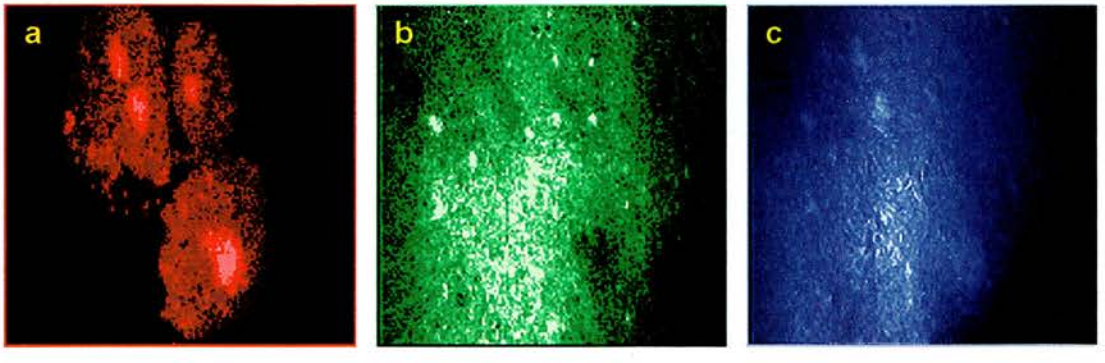

Figure 6.15: Three spectral images of a group of lesions. a) PpIX fluorescence, b) autofluorescence and c) illumination channel

Simple image processing algorithms were carried out on these three spectral images in order to enhance the contrast between the healthy and cancerous tissue. Figure 6.16 shows the result of firstly summing the green and blue images and secondly summing all three images. It is evident that suitable contrast can be achieved without using the PpIX fluorescence image.

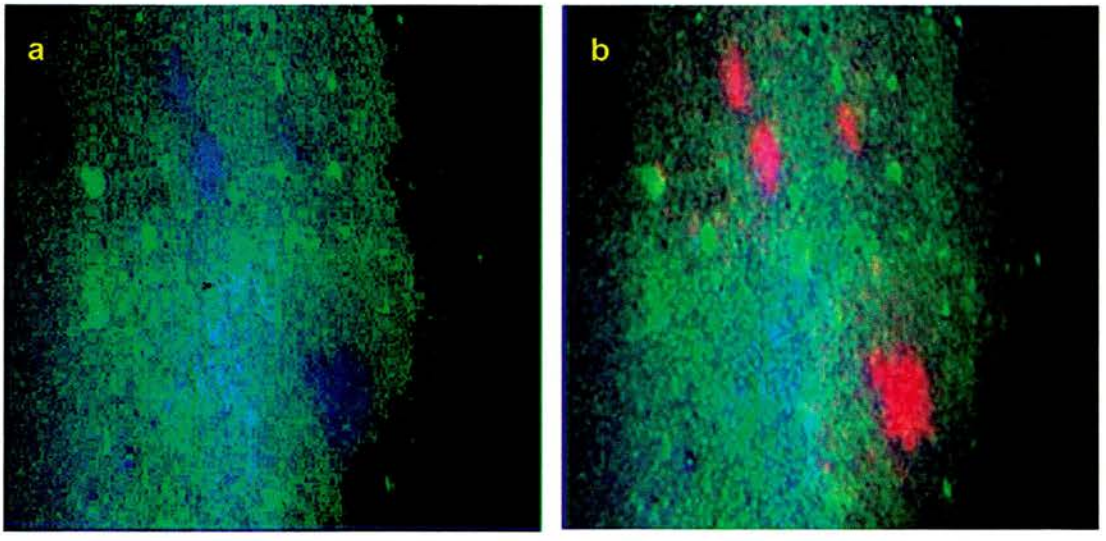

Figure 6.16: Result of summation of a) green and blue image and b) green, blue and red images.

A number of different image-processing techniques were attempted by Jacqueline and myself within Matlab, which is a technical computing environment for numeric computation and visualisation with an integrated image processing toolbox. It was hoped that any successful algorithms could eventually be incorporated into the custom software. The two algorithms producing the highest contrast, between the healthy and cancerous tissue, were the ratio of the red and blue channel and the ratio of the green and blue channel.

Figure 6.17a shows an example of the PpIX fluorescence divided by the illumination, where the boundaries of the four lesions are evident. This image shows clearly the cancerous area as well as the healthy tissue ALA application area, which may be useful to the clinician for different purposes.

Figure 6.17b illustrates a high contrast image, which is the result of the ratio of the autofluorescence and illumination channels. This is an exceptionally interesting result because this image implies that an exogenous photosensitiser is not a necessity for achieving images showing a high contrast between the cancerous and healthy tissue.

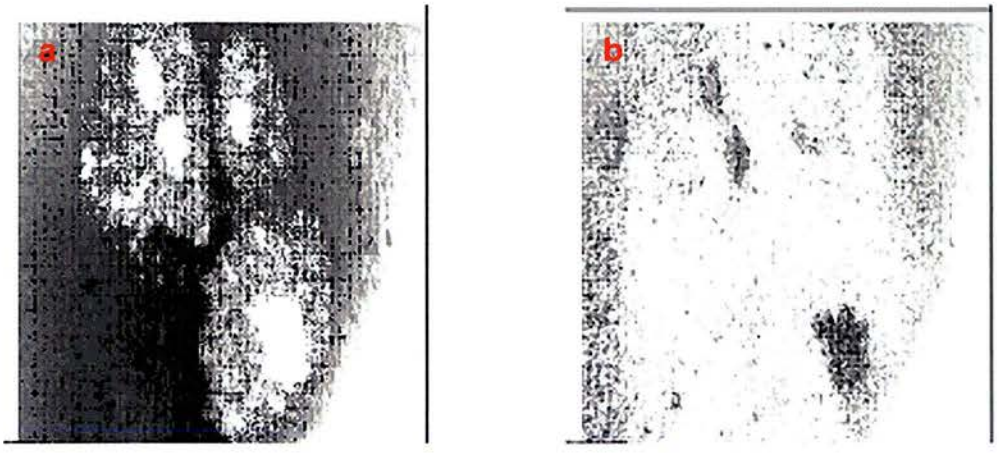

Figure 6.17: Image processing carried out on images in figure 6.15 to enhance optical contrast. (a) PpIX fluorescence divided by illumination and b) Autofluorescence divided by illumination.

The image processing algorithms involving a ratio between two images not only enhance the contrast but also reduce the sensitivity to fluctuations in illumination geometry and uniformity. (The theory covering this principle is discussed in detail in chapter two.)

The multi-spectral imaging system has also been used to image tumour sites both prior to and following PDT procedures. In one such example, the ALA was administered and after an elapsed time of eight hours, the tumour was treated with photodynamic therapy. The tumour was observed with the imaging system prior to treatment and for a continuous eight-hour period following the treatment. Figure 6.18 shows a white light image of the lesion, while figure 6.19 represents the observed PpIX fluorescence during this

period.

Figure 6.18: White light image of treated lesion

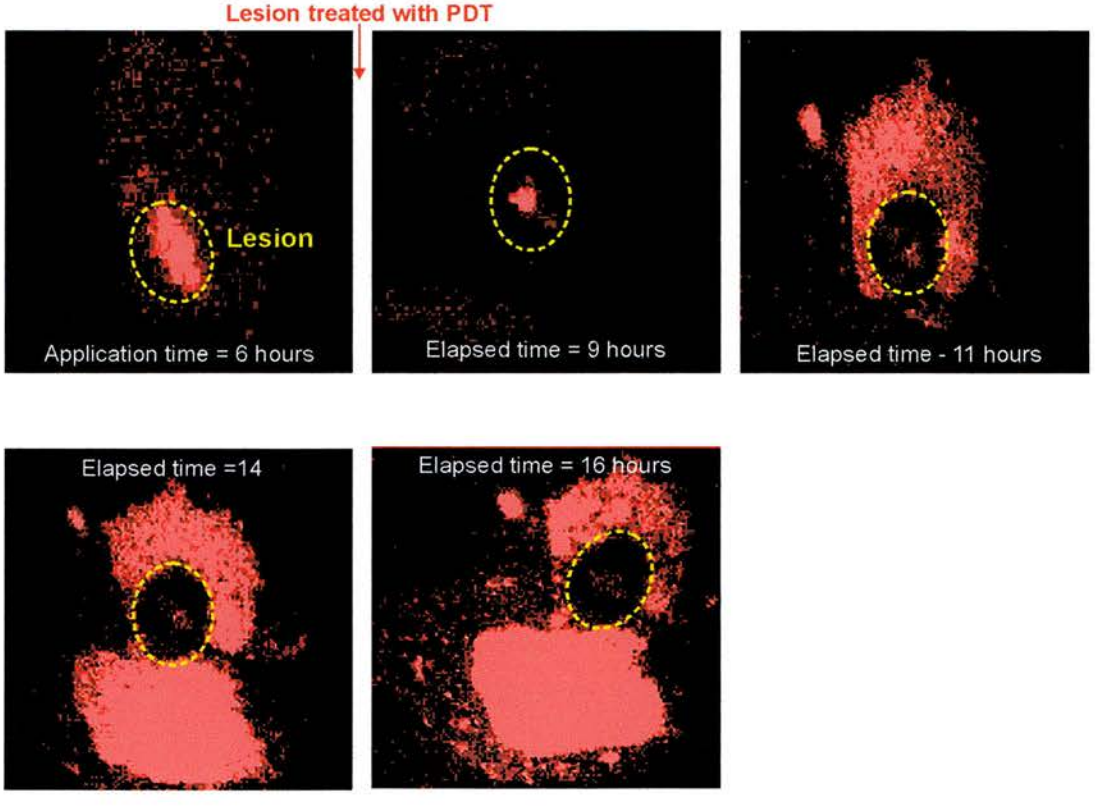

Figure 6.19: Progress of PpIX fluorescence in lesion treated with PDT

As expected the images showed little fluorescence within the tumour after treatment, indicating that the majority of the PpIX concentration was reduced by the photoreaction. The fluorescence present in the images was located

in the surrounding healthy tissue. However, a bright fluorescent spot was located in the centre of the tumour. Without histological clarification, we were unable to determine whether this fluorescent spot was untreated cancerous tissue.

6.4 Summary

A low cost, spectral imaging system has been discussed in this chapter. The results presented here illustrate the potential for the system and the benefits available to the dermatologist.

The system is based on a filtered (BG37) mercury arclamp and a variable frame rate camera, capable of producing fluorescence images of skin tumours. This configuration of the system provides images of the induced PpIX fluorescence, the autofluorescence and the reflected excitation light.

From the results presented here, it is evident that the optimum time for PDT is between an elapsed time of 4 and 8 hours, when the PpIX fluorescence is confined to the cancerous tissue. After an elapsed time of 8 hours or longer, the healthy tissue fluorescence can be used to demarcate the exact tumour border. This is useful to the clinician in deciding a safe margin around the tumour for surgical removal. The healthy tissue fluorescence may also be used for the detection of satellite tumours that may accompany the main tumour site.

The PpIX fluorescence images recorded from the tumour treated by PDT indicate the necessity for fluorescence imaging during treatment, to monitor the residual PpIX concentration, which is based on the fluorescence level. This system would enable the clinician to optimise the duration and fractionation [3] of the treatment light and ensure that all the PpIX was used in the photoreaction.

The imaging of the autofluorescence and reflected excitation light provides further information, which can be used effectively to enhance the contrast between the cancerous and healthy tissues. Either of these channels can also be used to normalise the PpIX fluorescence image to produce a dimensionless constant that is not dependent on the illumination geometry.

The one drawback of this imaging system is that the fluorescence images are not grabbed simultaneously. Thus, if the patient moves between the acquisition of the images, the imaging fields of the three spectral bandwidths are not identical. Consequently, pixel registration is not possible during image processing and hence exact superposition of the images is difficult to achieve. The solution to this problem is discussed in the conclusions chapter that follows.

The potential for this low cost multi-spectral imaging system has been discussed. The system is now being used by the collaborating dermatologists to learn more about fluorescence imaging on the skin. It is therefore reasonable to expect that further refinements of this system can be defined such that it has the potential to become an invaluable diagnostic for cancer detection and monitoring within dermatology.

6.5 References

[1] B. W. Chwirot, S. Chwirot, J. Redzinski, Z. Michniewicz. "Detection of Melanomas Ultraviolet Light-induced Autofluorescence of Human Skin." 1998, *European Journal of Cancer*, **34**, 1730.

[2] K. Svanberg, I. Wang, S. Colleen, I. Idvall, C. Ingvar, R. Rydell, D. Jocham, H. Diddens, S. Brown, G. Gregory, S. Montam, S. Andersson-Engels, S. Svanberg. "Clinical multi colour fluorescence imaging of malignant tumours-initial experience." 1998, *Acta Radiologica*, **39**, 2.

[3] H. Messmann, P. Mlkvy, G. Buonaccorsi, C. L. Davies, A. J MacRoberts and S. G. Bown. "Enhancement of photodynamic therapy with 5-aminolaevulinic acid-induced porphyrin photosensitisation in normal rat colon by threshold and light fractionation studies." 1995, *British Journal of Cancer*, **72**, 589.

CHAPTER SEVEN

GENERAL CONCLUSIONS

This thesis has provided a description of the development of an endoscopically-coupled cancer detection system and a multi-spectral imaging system for use in Dermatology. In this chapter, the development of both optical systems is summarised, including an analysis of potential system improvements that could be implemented in the future.

7.1 Cancer detection

Although there are over a hundred different forms of cancer, the common factor is that the earlier that cancer is detected, the more successful any form of treatment will be. Cancer of the GI tract is a particularly lethal disease because the symptoms are usually only evident after the cancer has become advanced; at which time it may have spread and affected secondary sites. At this stage, any treatment to remove the cancerous tissue has a high mortality and morbidity rate.

Thus, it is vital that patients at high-risk of developing cancer of the GI tract

are screened regularly in an attempt to detect the pre-cancerous cells, before they develop into a malignant tumour. However, these pre-cancerous cells are not evident to the eye and are inherently random in their distribution. For this reason the conventional method of indiscriminately taking biopsies, in the hope of finding any cancerous cells which may be present, is a time consuming and inaccurate process.

In this research, we used a process known as "fluorescence detection" to enable efficient differentiation between the pre-cancerous and healthy tissue within the GI tract. This form of detection involves a photochemical reaction between a tumour-localising, photosensitive drug, and excitation light in a specific spectral band. The resulting emitted fluorescence is used to locate the cancerous tissue.

We subsequently realised that the principles of fluorescence detection could also be applied to the skin. It was felt that the emitted fluorescence originating from cancerous tissue on the skin could be used to clearly demarcate tumour boundaries and optimise the conditions necessary for subsequent photodynamic therapy (PDT).

Throughout this research, the photosensitiser 5-aminolevulinic acid (ALA) was used to induce the contrast between the cancerous and healthy tissue. This photosensitiser is used at Ninewells Hospital because, unlike others, patients are not left photosensitive for long periods after administration. ALA is metabolised out of the body usually within twenty-four hours of administration. Once administered the ALA metabolises at tissue level to produce protoporphyrin IX (PpIX), which can be excited at approximately 400nm to emit a characteristic fluorescence at around 638nm. Due to the requirement for ethical approval for the use of drugs on patients, we had no power to experiment with alternative photosensitisers on patients.

7.2 Collaboration with clinical team

The success of this work has depended heavily on our interactions with the clinicians from the Departments of Surgery and Dermatology from Ninewells Teaching Hospital in Dundee. Initially, in both projects, we spent much time with the clinicians in the operating theatres, endoscopy suites and patient treatment areas, to fully comprehend the design task and the specifications for the equipment.

At each stage of the developmental process, the equipment was evaluated within the clinical environment. In the case of the endoscopically-coupled detection system, trials involved testing the equipment on resected cancerous specimens and later using the equipment in patients. This evaluation process entailed, sometimes twice a week, waiting in the hospital for between 2 and 6 hours. While the clinical evaluation of the detection system was extremely beneficial, it was also inherently time consuming from a researcher viewpoint.

7.3 Endoscopically-coupled cancer detection system

There are a large number of systems, documented in the literature, which have been developed for the early detection of cancerous tissue. However, none of these detection units has achieved widespread use in the clinical environment because, in one way or another, they are inappropriate for use on patients. The major challenge is to develop equipment that effectively detects cancerous tissue within humans, is conducive to the clinical environment and is economically viable to the service provider. In contrast, the detection systems developed in the past have not undergone adequate in-vivo trials, have used expensive pieces of equipment that required

specialist training and involved time-consuming detection techniques.

Currently there are two fluorescence imaging systems commercially available, the Xillix laser induced fluorescence endoscopy gastrointestinal system and the Storz D-Light system. The Xillix system is based on the detection of tissue autofluorescence excited at 437nm, while the Storz system is optimised for detecting ALA induced porphyrin fluorescence.

In the Storz system, the excitation light used is a filtered xenon arc lamp, which I initially tested for use in our detection system. The results discussed in section 3.2.2 illustrate that the filtered mercury lamp induces a significantly higher intensity PpIX fluorescence than the Storz D-Light, which in turn increases the sensitivity of the detection unit. For this reason, Storz have been collaborating with us to construct a more sensitive cancer detection system.

The Xillix system records autofluorescence in a green and a red channel, using two image intensified cameras. The use of two intensified cameras makes the system extremely bulky and intrusive. This system detects autofluorescence only and not fluorescence from an exogenous photosensitiser. The benefit of our system over these two detection units is that it has been specifically designed for use in the oesophagus, unlike the Storz and Xillix systems that were originally designed for use in the bladder[1] and lung[2], respectively. Our detection system it is more sensitive than the Storz system and more conducive to the clinical environment than the Xillix system.

The development of our endoscopically-coupled cancer detection system entailed the construction of two generations of instrumentation. In both systems the photosensitiser was excited by an appropriately filtered 100W mercury arclamp, while the fluorescence was selectively detected by an image intensified CCD camera. Colour images for the purposes of

navigation were acquired using a remote-head colour CCD camera.

After considerable ex-vivo experimentation, it was decided that the first-generation system required modification in three main aspects, to produce a system appropriate for use within patients. The three areas of development were the violet light delivery, the filtering of the mercury lamp and the display of the images. The UV-transmitting optical fibre, used initially for the transmission of the violet light into the body, did not deliver adequate optical power over a wide enough angle of illumination. Therefore, we approached Storz, the endoscope manufacturer, who agreed to custom manufacture, an endoscope with a UV-transmitting illumination fibre bundle fitting our specifications. In comparison to the conventional Storz endoscope, this custom endoscope had an eight-fold improvement in transmission in the violet (~400 nm) region of the spectrum.

In the first generation system, the violet and white light images were acquired consecutively. Because of the muscular movement within the GI tract, the colour and intensified images did not contain identical imaging fields. Hence, the fluorescence data could not be superimposed onto the colour image. In order for the colour and fluorescence images to be grabbed simultaneously, a custom-designed multi-layer dielectric mirror was used to filter the mercury lamp. This filter transmits the mercury spectrum apart from the 600 to 660nm band, which it blocks. This blocked spectral band corresponds to that of PpIX fluorescence and so any detected light at this wavelength arises from tissue fluorescence only.

The third problem with the first-generation detection system was the displaying of the two images. The colour image required reversal, prior to display, due to the presence of the beamsplitter in the optical head. However, the computer was unable to reverse the colour image and carry out real-time image processing algorithms on the intensified image. In the second-generation system, the colour image is displayed on a television

monitor via a Storz image reversal adapter. Consequently, the computer is used to process and display the intensified images in real-time.

The second-generation system is fully conducive for use within the endoscopy suite and operating theatre within the hospital. The equipment is compatible with standard endoscopic techniques and procedures and is easily operated and maintained. The system proved highly effective during initial system evaluation conducted in a sponge model of the GI tract, marked with the fluorescent dye. The clinicians subsequently requested to keep the unit at the hospital to test on patients and to build up a useful database. To assess the performance and accuracy of the detection unit, it continues to be used on patients with diagnosed cancers. The results of these trials have proved so effective that the system will also be used as part of a screening programme for patients at high risk of developing cancer. The fact that the clinicians are operating and using the system independently of ourselves is evidence for its user-compatibility and ease of implementation into a clinical setting.

The results of our work with the first generation endoscopic system have been published [3], while a paper reporting the second generation system has been submitted for publication [4].

7.4 The future for the endoscopically-coupled detection system

The endoscopically-coupled detection system is now at the stage that no further developmental work can be embarked upon until the clinicians have fully evaluated every aspect of the unit. However, there are a number of issues that I believe may add diagnostic value to the system in the future. The optical head, which couples the two cameras to the endoscope, was designed and constructed from Spindler and Hoyer optical components.

Such a construction provided experimental flexibility in the choice of cameras, lenses and filters that were incorporated within the head. Once the system has been fully evaluated, the design of the optical head should be optimised through ray tracing and purpose-built with exact dimensions to accommodate the lenses and filters. These alterations should improve the quality of both the colour and intensified images.

In chapter two, the problems associated with illumination geometry were discussed. If one normalises the fluorescence image against the illumination geometry, a dimensionless ratio could be displayed for each pixel. By using a dimensionless ratio, immunity is provided against variation in distance between fibre bundle and tissue, surface effects and drifts in lamp intensity during an endoscopic procedure. Thus, in our system, the fluorescence image from the intensified camera could be normalised against the blue channel of a digital colour camera. However, in order to achieve such a ratio, there would have to be identical pixel registration between the two images. The normalised fluorescence data could then be superimposed onto the "navigation" image to allow the clinician to identify the exact location of the cancerous tissue.

After observing the spectral results, obtained using the first-generation system, it was obvious that autofluorescence, from endogenous molecules, decreases within cancerous tissue and could thus be used to provide further diagnostic information. While it would be desirable to image this autofluorescence, the green spectral band present in the excitation light would mask the contrast between the cancerous and healthy tissue. Hence, measuring the autofluorescence would not be possible unless the mercury lamp was filtered differently.

The major drawback in this detection system lies in the limiting geometry of collection of the endoscope. As discussed in chapter five, the collection efficiency of the endoscope is approximately 0.5 %, which is the largest loss

in the system. If the diameter of the collection optics were increased, then the sensitivity of the detection unit would improve. Since completing this research, Miles and Professor Cuschieri have approached Storz, who have agreed to manufacture an endoscope, with a larger diameter imaging bundle and collection optics.

It should be noted that while this system was designed for use in the GI tract, there is no reason why it cannot be used for inspection in any part of the anatomy. Once this system has proved effective on patients, Storz may be interested in custom manufacturing endoscopes specific to other parts of the body, in which this detection system may be useful.

7.5 Multi-spectral imaging system for Dermatology

We have developed a low cost multi-spectral imaging system for use by dermatologists. This system is based on a filtered (BG 37) mercury arclamp and a variable frame-rate camera, capable of producing fluorescence images of skin tumours. The configuration of the system facilitates the acquisition of images depicting the induced PpIX fluorescence, the autofluorescence and the reflected excitation light.

Due to the accessibility of the skin and the fact that most skin cancers can be treated effectively, a number of controlled experiments were carried out on patients, which were not possible within the GI tract. This multi-spectral system was used in the clinical environment to determine the wavelength for maximum excitation of PpIX (400nm) and the optimum filtering of the mercury lamp (BG37) to induce the maximum contrast between the cancerous and healthy tissue.

The system was also used, on patients, to determine the behaviour of the PpIX fluorescence over time. From the results presented in chapter six, it is evident that the optimum time for PDT is between an elapsed time of 4 and 8 hours, when the PpIX is confined to the cancerous tissue. After an elapsed time of 8 hours or longer, the healthy tissue fluorescence can be used to demarcate the exact tumour border. This is useful in deciding a safe margin for surgical removal. The healthy tissue fluorescence is also useful for the detection of satellite tumours that may surround the main tumour site.

The results of this work have been published[5].

7.6 The future for the multi-spectral imaging system

In the system reported in chapter six, the main drawback involved the consecutive acquisition of the images in the different spectral bands. Because the images were not grabbed simultaneously, identical pixel registration was sometimes difficult when carrying out image processing. For this reason, an image splitter has subsequently been incorporated into the system, which enables simultaneous grabbing of four identical images in different spectral bands. Figure 7.1 shows the arrangement where an image splitter is attached to the variable-frame-rate, monochrome camera.

The consequence of incorporating the image splitter into the system is that image-processing algorithms, such as the image-ratios discussed in chapter six, can be included in the software because the images have identical pixel registration.

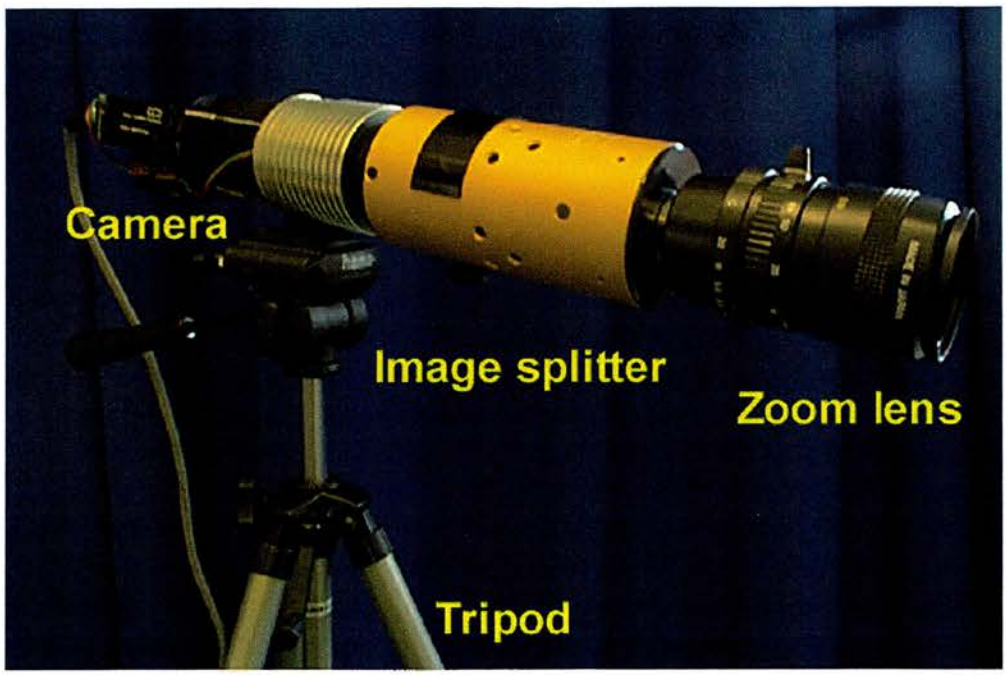

Figure 7.1: Picture of multi-spectral image splitter incorporated into system

Although, this multi-spectral imaging system is being used by the clinicians to monitor a large quantity of patients undergoing PDT, it would be more user-friendly and portable if it was interfaced to a laptop PC. The problem, however, is that the frame-grabber technology for integrating cameras is not yet available for the laptop. However, such frame grabbing technology may become available in the next couple of years.

The future for this imaging system lies in its use, by the dermatologist, for the tailoring of PDT to each patient. Through the monitoring of the normalised PpIX fluorescence, the clinician will be able to decide on the required elapsed time between initial ALA application and treatment, as well as the length of treatment necessary. It will also be used to demarcate the tumour boundary and a margin for the purposes of surgery. Future system evaluation should involve histological confirmations of the fluorescence observations.

One of our intentions for this skin research was for it to form a vehicle in which to optimise the fluorescence detection process on the skin, which is more accessible than the GI tract. Once the various elements of detection, such as filters and image processing algorithms, are optimised, it is hoped that this information will be applied to the endoscopic system.

7.7 Conclusions

This research was initiated in a department with no previous experience or expertise in the field of cancer detection. A very steep learning curve was involved for both myself and my two supervisors in developing equipment suitable for use by clinicians in the clinical setting. This education process not only involved learning about intricacies of the various forms of cancer but also the philosophy of the clinical professionals and of the funding programmes.

Over the past three years, the endoscopic imaging system has received much publicity in both national newspapers and on the regional television news. I also presented the clinical results of both the endoscopic and skin system at the Edinburgh Science Festival this year.

At the end of this three year period, not only are there two working fluorescence imaging systems incorporated within the hospital environment but also a substantial bank of knowledge. This acquired experience now forms the foundation for the continued evolution of these two projects to commercialisation and for the initiation of new medical research.

References

[1] M. Kriegmair, R. Baumgartner, R. Knuchel. "Detection of early bladder cancer by 5-aminolaevulinic acid-induced porphyrin fluorescence." J. Urol., 1996, **155**, 105.

[2] S. Lam, C. MacAulay, J. Hung. " Detection of dysplasia and carcinoma in situ with a lung imaging fluorescence endoscope device." J. Thorac Cardiovasc Surg., 1993, **105**, 1035.

[3] T. McKechnie, A. Jahan, I. Tait, A. Cuschieri, W. Sibbett, M. Padgett. "An Endoscopic System for the early detection of cancers of the GI tract." *Rev. Sci. Instrum.*, 1998, **69**, 2521.

[4] J. Hewett , T. McKechnie, W. Sibbett, I Tait, A Cuscheiri, M. Padgett. "An endoscopic imaging system for fluorescence detection of early stage cancers." *(submitted)*.

[5] T. McKechnie, J. Hewett, W. Sibbett, M. Padgett, C. Clark, J. Ferguson. "Optimisation of 5-aminolaevulinic acid application and light excitation to ensure maximum contrast between cancerous and healthy tissue on the skin." *SPIE*, **3592**, 1999.

Appendix One

Code for the software used in the first-generation endoscopic cancer detection system

This appendix details the computer code that I wrote for the first generation endoscopic cancer detection system. The code was written in the Delphi environment and is based on the Pascal programming language.

The objectives for the code were to interface the intensified and colour camera, the spectrometer, shutter and footswitch to the frame grabber in the computer. The software displayed the colour and intensified images in real-time as well as the spectrometer data. When the footswitch was pressed, the white light was unblocked, the intensified camera shutter closed and the colour image displayed in real-time. On the next compression of the footswitch, the white light was blocked, the shutter opened and the intensified image displayed on the monitor, while displaying the last frame from the colour camera. A gain control was also included on the desktop, which allowed the user to control the pixel intensity of the intensified image.

The code was broken up into five units, the main, spectrometer, monochrome, colour and general. The main unit contains all the code that was linked directly to the form, for example the buttons and scroll bars. One of the most time consuming tasks in this unit was setting up the buffers for the images. Two procedures in this unit (*ImageMouseMove*) displayed the intensity of the image pixels over which the cursor was positioned. Procedures were also included to enable the user to save and load the two images. Buttons were placed on the desktop to allow the user to control the grabbing of the images if the footswitch was not to be used.

In the case of the spectrometer control, code was included to grab and display a single spectrum or to grab continuous spectra and display to the monitor. A separate procedure (*Rchart1MouseMoveInChart*) displayed the wavelength and intensity of the data point over which the cursor was positioned.

The spectrometer unit contains the code for the spectrometer card to grab and display the spectral data. Code was also included which permitted the user to calibrate the spectrometer.

The monochrome unit contains the code for the grabbing and display of the intensified camera images. In this unit the code initiated and configured the video card, allocated the space for the 16bit buffer and grabbed the images.

The colour unit contains the code for the configuration of the colour camera. In this unit, the code for the checking of the status of the footswitch is detailed. Finally, the general unit contains code that displayed the images from the memory to the bitmap.

I am not an experienced computer programmer and hence this code is not necessarily optimally written to achieve the objectives but it certainly worked effectively when used by the clinicians in the clinical environment.

Unit Main;

```
interface

uses
    Windows, Messages, SysUtils, Classes, Graphics, Controls, Forms, Dialogs,
    StdCtrls, ExtCtrls, Menus,ooidrv32, OleCtrls,  graphsv3, RChart,Spectrometer,
    ColourCamera, MonochromeCamera, General;

type
    TForm1 = class(TForm)
    Image1: TImage;
    Image2: TImage;
    ShutterButton: TButton;
    gain: TScrollBar;
    Label3: TLabel;
    gainlabel: TLabel;
    Label6: TLabel;
    Label7: TLabel;
    Label8: TLabel;
    MainMenu1: TMainMenu;
    OpenDialog1: TOpenDialog;
    SaveFileDialog1: TSaveDialog;
    SaveFileDialog2: TSaveDialog;
    File1: TMenuItem;
    SaveColour1: TMenuItem;
    Savegreyscal1: TMenuItem;
    Loadgreyscal1: TMenuItem;
    LoadColour1: TMenuItem;
    OpenDialog2: TOpenDialog;
    Timer2: TTimer;
    Bevel5: TBevel;
    Bevel6: TBevel;
    Label9: TLabel;
    ResetButton: TButton;
    btnSingleScan: TButton;
    btnContinuousScan: TButton;
    btnStopSpectrometer: TButton;
    Bevel9: TBevel;
    Label14: TLabel;
    CheckAutoScale: TCheckBox;
    Timer3: TTimer;
    Label1: TLabel;
    Label4: TLabel;
    Timer4: TTimer;
    Label5: TLabel;
    Bevel1: TBevel;
    Label10: TLabel;
    RChart1: TRChart;
    Label15: TLabel;
    Label19: TLabel;
    Label20: TLabel;
    Label21: TLabel;
    shutterreset: TButton;
    Bevel2: TBevel;
    Bevel3: TBevel;
    Bevel4: TBevel;
    procedure FormCreate(Sender: TObject);
```

```
        procedure FormClose(Sender: TObject; var Action: TCloseAction);
        procedure Image1MouseMove(Sender: TObject; Shift: TShiftState; X,Y: Integer);
        procedure Image2MouseMove(Sender: TObject; Shift: TShiftState; X,Y: Integer);
        procedure gainScroll(Sender: TObject; ScrollCode: TScrollCode;var ScrollPos:
        Integer);
        procedure SaveColour1Click(Sender: TObject);
        procedure Savegreyscal1Click(Sender: TObject);
        procedure Loadgreyscal1Click(Sender: TObject);
        procedure LoadColour1Click(Sender: TObject);
        procedure ShutterButtonClick(Sender: TObject);
        procedure Timer2Timer(Sender: TObject);
        procedure ResetButtonClick(Sender: TObject);
        procedure btnStopSpectrometerClick(Sender: TObject);
        procedure btnSingleScanClick(Sender: TObject);
        procedure btnContinuousScanClick(Sender: TObject);
        procedure Timer3Timer(Sender: TObject);
        procedure Timer4Timer(Sender: TObject);
        procedure RChart1MouseMoveInChart(Sender: TObject; InChart: Boolean;shift:
        TShiftState; rMousePosX, rMousePosY: Double);
        procedure shutterresetClick(Sender: TObject);


private
          { Private declarations }
public
        { Public declarations }
protected
        Procedure DataIsHere(var Message:TMessage);message OOI_DATAREADY;
end;


type
        TArrayOfBytes =array[0..0] of Word;
        PArrayOfBytes =^TArrayOfBytes;


var
        Form1 :TForm1;
        ooip :OOI_PARAM;

        Mono16bitBuffer :THandle;
        SaveMono16bitBuffer :THandle;
        ColourBuffer    :THandle;
        DisplayColourBuffer :THandle;
        Buffer2Mono16   :PArrayOfBytes;
        SaveBuffer2Mono16   :PArrayOfBytes;
        Buffer3Col      :PArrayOfBytes;
        DisplayBuffer3Col      :PArrayOfBytes;
        shutterstate    :Boolean;
        Imagechoice     :Boolean;
        CurrentImage :Integer;

Const
        {size of input Image}
        XArraySize    = 580;              {Intensified}
        YArraySize    = 990;
        XArraySize1   = 580;              {colour}
        YArraySize1   = 990;
        {Spectrometer size}
```

```
        DataArraySize = 700;

implementation
{$R *.DFM}

        procedure FB_CopyVGARect(nX : SmallInt;nY : SmallInt;nWidth : SmallInt;nHeight :
        SmallInt; npDIBBuf : PArrayOfBytes; Pitch : SmallInt;nCopyDir :
        SmallInt);stdcall;external 'FBus32.dll';
        function FB_VideoLive(bLive : SmallInt;nAlign : SmallInt) : SmallInt;stdcall;external
        'FBus32.dll';

        {for shutter, sending voltage high and low}
        function FB_SetIrisLevel (nIrisBits:Short): SmallInt;stdcall;external 'FBus32.dll';


{Create the desktop}
procedure TForm1.FormCreate(Sender: TObject);

begin

        {setup the spectrometer}
        SpecSetup;

        {Setup the colour camera -initiate card}
        ColourSetup;

        {setup the buffer for colour camera}
        {allocate the space for the offscreen buffer to hold the image}
        SetBufColour;
        UpdateTheColourImage;

        {Allocate the space for the second buffer to store 16bit image}
        SetBufMono;
        UpdateTheMonochromeImage;

        {setup code for the control of shutter through the footswitch}
        Setupshutter;

        Imagechoice    :=false;
        Shutterstate   :=true;          {for shutter button}
        Timer2.enabled :=true;          {start grabbing in colour}
        Timer4.Enabled :=true;          {Start footswitch timer}

end;


{close form and free memory}
procedure TForm1.FormClose(Sender: TObject; var Action: TCloseAction);

var
  loop          : Integer;
  i,status      : Integer;

begin

        FreeBuffMono;
        FreeBuffColour;
        FreeSpecMem;                    {free memory from spectrometer}
        Beep;
```

```
        for i := 0 to 3000 do
                status := FB_SetIrisLevel(0);                    {Close shutter}
end;


{displays intensity value of position of cursor on intensified image}
procedure TForm1.Image1MouseMove(Sender: TObject; Shift: TShiftState; X,Y: Integer);

begin
        Label7.Caption:=IntTOStr((Integer(Buffer2Mono16^[X+Y*XArraySize]))*256 div
        32767);
end;


{displays intensity value of position of cursor on intensified image}
procedure TForm1.Image2MouseMove(Sender: TObject; Shift: TShiftState; X,
      Y: Integer);

begin
        Label8.Caption:=IntTOStr(Integer(Buffer3Col^[X+Y*XArraySize1]));
end;


{Displays value of gain on desktop}
procedure TForm1.gainScroll(Sender: TObject; ScrollCode: TScrollCode;var ScrollPos:
Integer);

begin
        gainlabel.Caption:=IntToStr(gain.Position);
end;


{Saves colour image}
procedure TForm1.SaveColour1Click(Sender: TObject);

begin
        SaveFileDialog1.FileName := 'colour.bmp';
        If SaveFileDialog1.Execute then
                begin
                        Image2.Picture.SaveToFile(SaveFileDialog1.FileName);
                        Beep;
                end;
end;


{Saves intensified image}
procedure TForm1.Savegreyscal1Click(Sender: TObject);

var
        FileName : String;
        a,b : Word;

begin
        SaveFileDialog1.FileName := 'grey.bmp';
        if SaveFileDialog1.Execute then
                begin
                        Image1.Picture.SaveToFile(SaveFileDialog1.FileName);
                        Beep;
                end;
```

```
end;

{Load intensified image}
procedure TForm1.Loadgreyscal1Click(Sender: TObject);

begin
        OpenDialog1.FileName := 'grey.bmp';
        if OpenDialog1.Execute then
                begin
                        Image1.Picture.LoadFromFile(OpenDialog1.FileName);
                        Beep;
                end;
end;

{Load colour image}
procedure TForm1.LoadColour1Click(Sender: TObject);

begin
        OpenDialog1.FileName := 'colour.bmp';
        if OpenDialog2.Execute then
                begin
                        Image2.Picture.LoadFromFile(OpenDialog1.FileName);
                        Beep;
                end;
end;

{Grab the intensified image}
Procedure MonoGrab;

var
        return:SmallInt;

begin
                                        {stop grabbing so can transfer image to memory}
        return:=FB_VideoLive(0,0);
                                                {copy rectangle from screen to buffer}
        FB_CopyVGARect(0,0,XArraySize, YArraySize, Buffer2Mono16,-1,2);
        return:=FB_VideoLive(1,2);

        UpdateTheMonochromeImage;                       {Display grabbed image}
end;

{Grab the colour image}
Procedure ColourGrab;

var
        return:SmallInt;

begin
                                        {stop grabbing so can transfer image to memory}
        return:=FB_VideoLive(0,0);
                                                {copy rectangle from screen to buffer}
        FB_CopyVGARect(0,0,XArraySize1,YArraySize1,Buffer3Col,-1,2);
        return:=FB_VideoLive(1,2); {tell video to grab some screens}
```

```
        UpdateTheColourImage;                          {Display grabbed image}
end;


{shutter start button, if not using footswitch}
procedure TForm1.ShutterButtonClick(Sender: TObject);

var
        i,status : Integer;
        return: SmallInt;

begin
        if shutterstate=true then
                begin
                        shutterstate:=false;
                        Form1.Label4.Caption := 'Open' ;
                        MonoSetup;
                        for i := 0 to 100 do
                                status := FB_SetIrisLevel(3000);
                                Imagechoice:= true;
                end
        else
                begin
                        shutterstate:=true;
                        Form1.Label4.Caption := 'Closed';
                        ColourSetup;
                        for i := 0 to 100 do
                                status := FB_SetIrisLevel(0);
                                Imagechoice:= false;
                end
end;


procedure TForm1.Timer2Timer(Sender: TObject);

var
        return:SmallInt;

begin
        if Imagechoice= true then
                MonoGrab
        else
                ColourGrab;
end;


procedure TForm1.Timer4Timer(Sender: TObject);

begin
        Footswitch;
end;


{reset the colour camera grabbing button}
procedure TForm1.ResetButtonClick(Sender: TObject);

var
        return :SmallInt;
        i: Integer;
```

```
begin
        ColourSetup;
end;


{Spectrometer}
procedure TForm1.DataIsHere(var Message:TMessage);

begin
        DataReady;
        OOI_BufferEmpty(HInstance,Message.wParam);
        if ooip.cont=0 then
                begin
                end;
end;


procedure TForm1.btnStopSpectrometerClick(Sender: TObject);

begin
        beep;
        OOI_Stop(HInstance);
        btnSingleScan.enabled:=true;
        btnContinuousScan.enabled:=true;
        btnStopSpectrometer.enabled:=false;
end;


{Grab a single spectrum}
procedure TForm1.btnSingleScanClick(Sender: TObject);

begin
        SingleScan;
end;


{Grab spectral data continuously}
procedure TForm1.btnContinuousScanClick(Sender: TObject);

begin
        ContinuousScan;
end;


{Displays wavelength and intensity data of position of cursor}
procedure TForm1.RChart1MouseMoveInChart(Sender: TObject; InChart: Boolean; shift:
TShiftState; rMousePosX, rMousePosY: Double);

begin
        if (InChart) then
                begin
                        Label15.Caption := floattostrF(Form1.RChart1.MousePosX,
                        ffGeneral, 3, 10);
                        Label19.Caption := floattostrF(Form1.RChart1.MousePosY,
                        ffGeneral, 2, 10);
                end
        else
                begin
```

```
                    Form1.Label15.Caption := 'Nothing';
                    Form1.Label19.Caption := 'Nothing';
                end;
end;


{Resets position of shutter}
procedure TForm1.shutterresetClick(Sender: TObject);

begin
        resetshutter;
end;


end.
```

Unit General;

```
interface

    procedure UpdateTheColourImage;
    procedure UpdateTheMonochromeImage;

implementation
uses
  Main,Windows, Messages, SysUtils, Classes, Graphics, Controls, Forms,
  Dialogs,StdCtrls, ExtCtrls, Menus,ooidrv32, OleCtrls,  graphsv3, RChart,
  MonochromeCamera, ColourCamera;


{display the colour image from the RAM to the bitmap}
procedure UpdateTheColourImage;
var
      return: LongInt;
      a, b :SmallInt;

begin
                                                {reverse orientation of colour image}
      for a := 1 to (XArraySize1 -1) do
            for b := 1 to (YArraySize1 -1) do
                  begin
                        DisplayBuffer3Col^ [ (XArraySize1-a)+b* XArraySize1 ]:=
                                                Buffer3Col^[a+b*XArraySize1];
                  end;
      return :=
      SetBitmapBits(Form1.Image2.Picture.Bitmap.Handle,XArraySize1*YA
            rraySize1,      DisplayBuffer3Col);
      if (return = 0) then
            begin
                  ShowMessage('Cannot set Image2 Bitmap');
                  Form1.Close;
            end;
      Form1.Image2.Repaint;
end;


{display the intensified image from the RAM to the bitmap}
procedure UpdateTheMonochromeImage;
var
      return: LongInt;

begin
      return := SetBitmapBits(Form1.Image1.Picture.Bitmap.Handle,XArraySize*Yar
            raySize, Buffer2Mono16);
      if (return = 0) then
            begin
                  ShowMessage('Cannot set Image1 Bitmap');
                  Form1.Close;
            end;
      Form1.Image1.Repaint;
end;
end.
```

Unit ColourCamera;

```
interface

      Procedure ColourSetup;
      Procedure SetBufColour;
      Procedure FreeBuffColour;
      Procedure Setupshutter;
      Procedure Footswitch;
      Procedure resetshutter;

type
   TarrayOfBytes        = array[0..0] of Word;
    PArrayOfBytes       = ^TArrayOfBytes;

var
  Shutter        :Boolean;
  Oldreturn      :SmallInt;

implementation
uses
   Main,Windows, Messages, SysUtils, Classes, Graphics, Controls, Forms,
   Dialogs,StdCtrls, ExtCtrls, Menus,ooidrv32, OleCtrls, graphsv3, RChart,General,
MonochromeCamera;


   function FB_Init : SmallInt;stdcall;external 'FBus32.dll';
   procedure FB_CopyVGARect(nX : SmallInt;nY : SmallInt;nWidth : SmallInt;nHeight :
SmallInt; npDIBBuf : PArrayOfBytes; Pitch : SmallInt;nCopyDir : SmallInt);stdcall;external
'FBus32.dll';
   function FB_VideoOffscreen(nWidth : SmallInt;nHeight : SmallInt;nDepth :
SmallInt;bScale : Boolean) : SmallInt;stdcall;external 'FBus32.dll';
   function FB_VideoLive(bLive : SmallInt;nAlign : SmallInt) : SmallInt;stdcall;external
'FBus32.dll';
   function FB_GetMiscParm(nIndex : Short;var value : SmallInt) : SmallInt;stdcall;external
'FBus32.dll';
   function FB_SetVideoConfig(nType : SmallInt; nStandard : SmallInt;nSource : SmallInt;
bSyncOnGreen : SmallInt) : SmallInt;stdcall;external 'Fbus32.dll';
   function FB_CheckSwitch (reserved:SmallInt;nTimeOutMS:SmallInt):
SmallInt;stdcall;external 'FBus32.dll';
   function FB_SetIrisLevel (nIrisBits:Short): SmallInt;stdcall;external 'FBus32.dll';

{Setup the colour camera}
Procedure ColourSetup;
var
    return :SmallInt;

begin
        return :=FB_init;                                          {Initiate video card }
        return :=FB_SetVideoConfig (2,1,0,0);                      {configure videocard}
                                                  {set video capture to system memory}
        return :=FB_VideoOffScreen(XArraySize1+1,YArraySize1+1, 16, true);
        return :=FB_VideoLive(1,2);                        {tell video to grab some screens}
end;


{setup the buffer for colour camera}
Procedure SetBufColour;
```

```
begin
                        {allocate the space for the offscreen buffer to hold the image}
        ColourBuffer:= GlobalAlloc(GHND, 2* XArraySize1*YArraySize1);
        if ColourBuffer=0 then
                begin
                        ShowMessage(' GlobalAlloc Failed!');
                end;

                                                        {protect the space just allocated}
        Buffer3Col:= GlobalLock(ColourBuffer);

                                                    {use if display colour via buffer}
                                                {setup a bitmap to display the captured image}
        Form1.Image2.Picture.Bitmap.Handle:= CreateBitmap(XArraySize1,
        YArraySize1,1,16,NIL);

                                                                {setup bitmap params}
        Form1.Image2.Stretch:= false;

                                {allocate the space for the display buffer to hold the image}
        DisplayColourBuffer:= GlobalAlloc(GHND, 2* XArraySize1*YArraySize1);

        if DisplayColourBuffer=0 then
                begin
                        ShowMessage(' GlobalAlloc Failed!');
                end;

                                                        {protect the space just allocated}
        DisplayBuffer3Col:= GlobalLock(DisplayColourBuffer);
end;


{free the memory saved for buffer}
Procedure FreeBuffColour;

begin
        GlobalUnlock(ColourBuffer);
        GlobalFree(ColourBuffer);
        GlobalUnlock(DisplayColourBuffer);
        GlobalFree(DisplayColourBuffer);
end;


{setup the shutter controlled through the footswitch}
Procedure Setupshutter;

begin
        Shutter :=      true;
        Oldreturn :=    -1;
end;


{code to check position of footswitch}
Procedure Footswitch;

var
        return,status :SmallInt;
```

```
        changedstate :Boolean;
        i: integer;

begin
        return:=FB_CheckSwitch(0,0);                                    {check footswitch}

                                {check footswitch has changed position since last test}
        if return=oldreturn
                then
                        changedstate:=false
                else
                        Changedstate:=true;
        oldreturn:= return;

                                    {if footswitch compressed, change shutter position}
        if changedstate then
                begin
                        if return=0 then
                                begin
                                        if Shutter
                                                then
                                                        Shutter:= false
                                                else
                                                        shutter:= true;
                                        Form1.Label1.caption := 'Pedal Down';

                                                {open shutter & grab intensified image}
                                        if shutter=false then
                                                begin
                                                        Form1.Label4.Caption := 'Open' ;

                                                                {grab intensified image}
                                                        MonoSetup;
                                                        for i := 0 to 100 do
                                                                        {Signal to shutter}
                                                        status:=FB_SetIrisLevel(3000);
                                                        Imagechoice:=true;
                                                end
                                        else
                                                    {close shutter & grab colour image}
                                                begin
                                                        Form1.Label4.Caption := 'Closed';

                                                                        {grab colour image}
                                                        ColourSetup;
                                                        for i := 0 to 100 do
                                                                        {Signal to shutter}
                                                        status := FB_SetIrisLevel(0);
                                                        Imagechoice :=false;
                                                end;
                                end
                        else
                                Form1.Label1.caption:='Pedal Up';
                end;
end;

{Button for manual reset of shutter position}
Procedure resetshutter;
```

```
var
        i: integer;
        return,status :SmallInt;
begin
        if  Form1.Label4.Caption = 'Open' then
                begin
                        shutter:=true;
                        Form1.Label4.Caption := 'Closed';
                        ColourSetup;
                        for i := 0 to 100 do
                                status := FB_SetIrisLevel(0);
                        Imagechoice:= false;
                end
        else
                begin
                        shutter:=false;
                        Form1.Label4.Caption := 'Open' ;
                        MonoSetup;
                        for i := 0 to 100 do
                                status := FB_SetIrisLevel(3000);
                        Imagechoice:=true;
                end;
end;


end.
```

Unit Monochrome Camera;

```
interface
        Procedure MonoSetup;
        Procedure SetBufMono;
        Procedure FreeBuffMono;

type
        TArrayOfBytes= array[0..0] of Word;
        PArrayOfBytes = ^TArrayOfBytes;

implementation

Uses
        Main,Windows, Messages, SysUtils, Classes, Graphics, Controls,
        Forms, Dialogs, StdCtrls, ExtCtrls, Menus,ooidrv32, OleCtrls,
        graphsv3, RChart;


{from Elf DMA card}
        function FB_Init : SmallInt;stdcall;external 'FBus32.dll';
        procedure FB_CopyVGARect(nX : SmallInt;nY : SmallInt;nWidth : SmallInt;nHeight
                : SmallInt; npDIBBuf : PArrayOfBytes; Pitch : SmallInt;nCopyDir :
                        SmallInt);stdcall;external 'FBus32.dll';
        function FB_VideoOffscreen(nWidth : SmallInt;nHeight : SmallInt;nDepth :
                        SmallInt;bScale : Boolean) : SmallInt;stdcall;external 'FBus32.dll';
        function FB_VideoLive(bLive : SmallInt;nAlign : SmallInt) : SmallInt;stdcall;external
                'FBus32.dll';
        function FB_SetVideoConfig(nType : SmallInt; nStandard : SmallInt;nSource :
                SmallInt; bSyncOnGreen : SmallInt) : SmallInt;stdcall;external 'Fbus32.dll';


{Setup Intensified Camera}
Procedure MonoSetup;
Var
        return: SmallInt;

begin
        return:= FB_init;                                       {set-up video card}
        return:=FB_SetVideoConfig(0,1,1,0);                     {configure the video card}
                                                {set video capture to system memory}
        return:=FB_VideoOffScreen(XArraySize, YArraySize,16,true);
        return:=FB_VideoLive(1,2);                              {tell video to grab images}
end;


{Allocate the space for the second buffer to store 16bit image}
Procedure SetBufMono;

begin
        Mono16bitBuffer := GlobalAlloc(GHND, 2*XArraySize*YArraySize);
        if Mono16bitBuffer = 0 then
                begin
                        ShowMessage('GlobalAlloc failed!');
                        Halt;
                end;

        Buffer2Mono16:= GlobalLock(Mono16bitBuffer);            {protect the space}
```

```
        Form1.Image1.Stretch  := False;                          {setup picture params}
                                                                 {Setup a bitmap}
        Form1.Image1.Picture.Bitmap.Handle :=
                CreateBitmap(XArraySize,YArraySize, 1, 16, NIL);


                                                                 {To save the intensified images}
        SaveMono16bitBuffer := GlobalAlloc(GHND, XArraySize*YArraySize);
        if SaveMono16bitBuffer = 0 then
                begin
                        ShowMessage('GlobalAlloc failed!');
                        Halt;
                end;

        SaveBuffer2Mono16:= GlobalLock(SaveMono16bitBuffer);
end;


{Free memory space reserved for images }
Procedure FreeBuffMono;

begin
        GlobalUnlock(Mono16bitBuffer);
        GlobalFree(Mono16bitBuffer);
end;



end.
```

Unit Spectrometer;

```
interface

type
        DataArray= array[0..2047]of single;
        Procedure SpecSetup;
        Procedure FreeSpecMem;
        Procedure DataReady;
        Procedure SingleScan;
        Procedure ContinuousScan;
        procedure GetMaxIndexValue(var MaxWavelength : integer; var MaxWavelength1 :
        integer;
        var MaxIndex2: integer;var MaxIndex3: integer;
         integer);
var
        Master:^DataArray;
        Slave1:^DataArray;
        Slave2:^DataArray;
        Slave3:^DataArray;
        Registered : Boolean;


implementation
uses
        Main,Windows, Messages, SysUtils, Classes, Graphics, Controls, Forms,
        Dialogs,StdCtrls, ExtCtrls, Menus,ooidrv32, OleCtrls,  graphsv3, RChart;

var
        ooip:OOI_PARAM;


{Setup Spectrometer}
Procedure SpecSetup;
begin
        New(Master);
        Registered:=false;
        New(Slave1);
        New(Slave2);
        New(Slave3);
end;


{Free spectrometer memory}
Procedure FreeSpecMem;
begin
        Dispose(Master);
        Dispose(Slave1);
        Dispose(Slave2);
        Dispose(Slave3);
        If Registered then
                begin
                        OOI_UnRegister(HInstance);
                end;
end;


procedure DataReady;
```

```
const
        {Z= 333.3238;                          {Variables for calibrating spectrometer}
        C1= 0.650007;
        C2=-0.0002;} {old values of spectrometer}

        {Z= 334.9207; {new values changed on 26/11/97}
        { C1=0.621;
        C2=-0.00013; }

        Z= 334.6317; {new values changed on 26/11/97}
        C1=0.5839;
        C2=-0.000057;

var
        i:integer;

begin

        Form1.RChart1.ClearGraf;
        Form1.RChart1.MoveTo(Z+(C1*298)+(C2*298*298), Master^[298]);
        for i := 300 to DataArraySize-1 do
        Form1.RChart1.DrawTo(Z+(C1*i)+(C2*i*i), Master^[i]);
        if (Form1.CheckAutoScale.Checked) then
                Form1.RChart1.AutoRange(3)
        else
                Form1.RChart1.ShowGraf;



        {Code for calibrating the spectrometer, making wavelength into pixel values}
        {Form1.RChart1.ClearGraf;
        Form1.RChart1.MoveTo((2), Master^[2]);
        for i := 3 to DataArraySize-1 do
                Form1.RChart1.DrawTo((i), Master^[i]);
        if (Form1.CheckAutoScale.Checked) then
                Form1.RChart1.AutoRange(3)
        else
                Form1.RChart1.ShowGraf; }
end;


procedure SingleScan;
var
        tempflt:single;
        tempstr:string;
begin
        ooip.ssize:=sizeof(OOI_PARAM);
        ooip.dev:=0;
        ooip.cmd:=CMD_NONE;
        ooip.msg:=0;
        ooip.res:=0;
        ooip.fdc:=0;
        ooip.dsf:=100;
        ooip.boxcar:=1;
        ooip.average:=30;
        ooip.chan_ena[0]:=1;
        ooip.chan_ena[1]:=0;
        ooip.chan_ena[2]:=0;
        ooip.chan_ena[3]:=0;
```

```
        ooip.changed:=1;
        ooip.ovrr_ok:=1;
        ooip.cont:=0;
        ooip.flash_cont:=0;
        ooip.scan_dark:=0;
        ooip.correct_dark:=0;
        ooip.extrig:=0;
        ooip.hWnd:=Form1.handle;
        ooip.host:=HInstance;
        ooip.chdat[0]:=Master;
        ooip.chdat[1]:=Slave1;
        ooip.chdat[2]:=Slave2;
        ooip.chdat[3]:=Slave3;
        if Registered=false then
                begin
                        OOI_Register(addr(ooip));
                end;

        Form1.btnSingleScan.enabled:=true;
        Form1.btnContinuousScan.enabled:=true;
        Form1.btnStopSpectrometer.enabled:=false;
        OOI_ParamSet(addr(ooip));
        OOI_SingleScan(HInstance);

end;

procedure ContinuousScan;

begin
        ooip.ssize:=sizeof(OOI_PARAM);
        ooip.dev:=0;
        ooip.cmd:=CMD_NONE;
        ooip.msg:=0;
        ooip.res:=0;
        ooip.fdc:=0;
        ooip.dsf:=100;
        ooip.boxcar:=1;
        ooip.average:=30;
        ooip.chan_ena[0]:=1;
        ooip.chan_ena[1]:=0;
        ooip.chan_ena[2]:=0;
        ooip.chan_ena[3]:=0;
        ooip.changed:=1;
        ooip.ovrr_ok:=1;
        ooip.cont:=1;
        ooip.flash_cont:=0;
        ooip.scan_dark:=0;
        ooip.correct_dark:=0;
        ooip.extrig:=0;
        ooip.hWnd:=Form1.handle;
        ooip.host:=HInstance;
        ooip.chdat[0]:=Master;
        ooip.chdat[1]:=Slave1;
        ooip.chdat[2]:=Slave2;
        ooip.chdat[3]:=Slave3;
        if Registered=false then
                begin
                        OOI_Register(addr(ooip));
                end;
```

```
        Form1.btnSingleScan.enabled:=false;
        Form1.btnContinuousScan.enabled:=false;
        Form1.btnStopSpectrometer.enabled:=true;
        OOI_ParamSet(addr(ooip));
        OOI_ContinuousScan(HInstance);
        Beep;
end;
```

{Find maximum value on graph}

```
procedure GetMaxIndexValue(var MaxWavelength : integer; var MaxWavelength1 : integer;
var MaxIndex2: integer;var MaxIndex3: integer; var MaxIndex4: integer;ArrayIn:
DataArray;ArraySize : integer);

const
        { Z= 333.3238;
        C1= 0.650007;
        C2=-0.0002; }  {old values}

        Z= 334.9207; {new values changed on 26/11/97}
        C1=0.621;
        C2=-0.00013;


var
        i : integer;
        MaxIndex:integer;
        MaxIndex1:integer;
        tempMax : double;
        tempMax1 :double;
        tempMax2 :double;
        tempMax3 :double;
        tempMax4 :double;

begin
        tempMax := ArrayIn[0];
        MaxIndex := 0;
        tempMax1 :=ArrayIn[0];
        MaxIndex1 := 0;
        tempMax2 :=ArrayIn[0];
        MaxIndex2 := 0;
        tempMax3 :=ArrayIn[0];
        MaxIndex3 := 0;
        tempMax4 :=ArrayIn[0];
        MaxIndex4 := 0;
        for i := 0 to ArraySize do
                begin
                        If ArrayIn[i] > tempMax then
                                begin
                                        tempMax:= ArrayIn[i];
                                        MaxIndex := i;
                                        MaxWavelength:=  Round(
                                        Z+(C1*MaxIndex)+(C2*MaxIndex*MaxIndex));
                                end;
                end;

        for i := 0 to ArraySize do
                if ((i <> MaxIndex) and (abs(i-MaxIndex) > 40)) then
```

```
                    if ArrayIn[i] > tempMax1 then
                        begin
                            tempMax1 := ArrayIn[i];
                            MaxIndex1 := i;
                            MaxWavelength1:= Round( Z+(C1*MaxIndex1
                            )+(C2*MaxIndex1*MaxIndex1));

                        end;
    for i := 0 to ArraySize do
    if ((i <> MaxIndex) and (i <> MaxIndex1) and
    (abs(i-MaxIndex)>45) and (abs(i-MaxIndex1)>45)) then
    if ArrayIn[i] > tempMax2 then
        begin
            tempMax2 := ArrayIn[i];
            MaxIndex2 := Round( Z+(C1*i)+(C2*i*i));
        end;

    for i := 0 to ArraySize do
        if ((i <> MaxIndex) and (i <> MaxIndex1)and (i <> MaxIndex2) and(abs(i-
        MaxIndex)>25) and (abs(i-MaxIndex1)>25)) and
        (abs(i-MaxIndex2)>25)then
        if ArrayIn[i] > tempMax3 then
            begin
                tempMax3 := ArrayIn[i];
                MaxIndex3 := Round( Z+(C1*i)+(C2*i*i));
            end;

    for i := 0 to ArraySize do
    if ((i <> MaxIndex) and (i <> MaxIndex1)and (i <> MaxIndex2)and (i <> MaxIndex3)
    and (abs(i-MaxIndex)>25) and (abs(I-MaxIndex1)>25)) and (abs(i-MaxIndex2)>25)
    and (abs(i-MaxIndex3)>25) then
        if ArrayIn[i] > tempMax4 then
        begin
            tempMax4 := ArrayIn[i];
            MaxIndex4 :=  Round( Z+(C1*i)+(C2*i*i));
        end;
end;

end.
```

Appendix Two

Code for the software used in the dermatology cancer detection system

This appendix details the computer code that I wrote for the dermatology cancer detection unit. Like the endoscopic software, the code is written in the Delphi environment. In this system, only one monochrome-integrating camera (Cohu) was used with a different frame grabber (Kane card) to that used in the endoscopic arrangement. The software was written to display four images from the monochrome camera on the form. While one image was set to display the frames from the monochrome camera, in real-time, the remaining three bitmaps displayed the respective last captured frames.

The software is split between three units, control, spec and mono. The control unit contains the code that is directly linked to the form, for example the buttons and bitmaps. In the control unit, the spectrometer is configured, the monochrome camera initiated and the buffers allocated. The form contained three scroll bars to control the integration time of the camera, the

gain and the pixel offset. The values of each of these parameters were displayed independently for each image. Relevant buttons controlled the update of each of the four images, which displayed consecutively.

The code in the unit named spec contains identical code to that of appendix one (unit spectrometer), for the control of the spectrometer. The mono unit contains the code for the initialisation of the monochrome integrating camera as well as the allocation of the greyscale palette.

I learnt to write the computer code for this research with the kind assistance of my two colleagues Paul Lesso and Darren Steers.

Unit Control;

```
interface

uses
    Windows, Messages, SysUtils, Classes, Graphics, Controls, Forms, Dialogs,
    RChart, ExtCtrls, StdCtrls,Spec, mono,ooidrv32;

type
    TForm1 = class(TForm)
    Image1: TImage;
    Image2: TImage;
    Image3: TImage;
    RChart1: TRChart;
    Image4: TImage;
    BtnGrabRedImage: TButton;
    Bevel1: TBevel;
    Bevel2: TBevel;
    Bevel3: TBevel;
    Bevel4: TBevel;
    Bevel5: TBevel;
    BtnGrabGreenImage: TButton;
    BtnGrabRandomImage: TButton;
    Integration: TScrollBar;
    intlabel: TLabel;
    Gain: TScrollBar;
    Offset: TScrollBar;
    Label1: TLabel;
    label2: TLabel;
    label3: TLabel;
    Gainlabel: TLabel;
    offsetlabel: TLabel;
    timer1: TTimer;
    Bevel6: TBevel;
    RedImageIntegration: TLabel;
    RedImageGain: TLabel;
    RedImageOffset: TLabel;
    BlueImageIntegration: TLabel;
    BlueImageGain: TLabel;
    BlueImageOffset: TLabel;
    GreenImageIntegration: TLabel;
    GreenImageGain: TLabel;
    GreenImageOffset: TLabel;
    RandomImageIntegration: TLabel;
    RandomImageGain: TLabel;
    RandomImageOffset: TLabel;
    BtnStopSpectrometer: TButton;
    BtnSingleScan: TButton;
    BtnContinuousScan: TButton;
    Label4: TLabel;
    CursorWavelength: TLabel;
    CursorIntensity: TLabel;
    CheckAutoScale: TCheckBox;
    Bevel7: TBevel;
    Label5: TLabel;
    Bevel8: TBevel;
    Bevel9: TBevel;
    FirstImage: TLabel;
```

```
    FirstImageY: TLabel;
    FirstImageX: TLabel;
    Label6: TLabel;
    Label7: TLabel;
    Label8: TLabel;
    Label9: TLabel;
    Edit1: TEdit;
    Edit2: TEdit;
    procedure FormCreate(Sender: TObject);
    procedure FormClose(Sender: TObject; var Action: TCloseAction);
    procedure Timer1Timer(Sender: TObject);
    procedure IntegrationScroll(Sender: TObject; ScrollCode: TScrollCode;
    var ScrollPos: Integer);
    procedure GainScroll(Sender: TObject; ScrollCode: TScrollCode;
    var ScrollPos: Integer);
    procedure OffsetScroll(Sender: TObject; ScrollCode: TScrollCode;
    var ScrollPos: Integer);
    procedure BtnGrabRedImageClick(Sender: TObject);
    procedure BtnGrabBlueImageClick(Sender: TObject);
    procedure BtnGrabGreenImageClick(Sender: TObject);
    procedure BtnGrabRandomImageClick(Sender: TObject);
    procedure BtnStopSpectrometerClick(Sender: TObject);
    procedure BtnSingleScanClick(Sender: TObject);
    procedure BtnContinuousScanClick(Sender: TObject);
    procedure RChart1MouseMoveInChart(Sender: TObject; InChart: Boolean;
    Shift: TShiftState; rMousePosX, rMousePosY: Double);
    procedure Image1MouseMove(Sender: TObject; Shift: TShiftState; X,
    Y: Integer);
    procedure Edit1Change(Sender: TObject);
    private
    { Private declarations }
    public
    { Public declarations }
    protected
    procedure DataIsHere (var Message:TMessage);message OOI_DATAREADY;
    end;

type
    TArrayOfBytes= array[0..0] of Byte;
    PArrayOfBytes = ^TArrayOfBytes;
    DataArray=array[0..2047]of single;

const
    {Size of input Image}
    ArraySize=512;          {Cohu camera}
    NumberOfImages =4;
    {Spectrometer size}
    DataArraySize =1100;

var
    Form1: TForm1;
    ooip:OOI_PARAM;

    {These are for test buffer}
    hBuffer : array[0..NumberOfImages] of THandle;
    Buffer1Mono:  array[0..NumberOfImages] of PArrayOfBytes;
    CurrentImage:Integer;
```

```
implementation

{$R *.DFM}

{These are functions from DLL}
procedure setup_buffers;external 'grab';
procedure free_buffers;external 'grab';


{Create desktop}
procedure TForm1.FormCreate(Sender: TObject);

begin

        {setup the spectrometer}
        SpecSetup;

        {Setup Cohu Camera}
        MonoSetup;

        {Set-up DLL globals}
        setup_buffers;

        {Ensure camera is in low-res mode}
        WritePort11;

        {Allocate the space for the second buffer to store 8bit image}
        SetBufMono;
        for CurrentImage:=0 to 4 do
                UpdateTheMonochromeImage;
                GreyScale_Palette;
                timer1.enabled:= False;
end;


{Free memory space reserved for images}
procedure TForm1.FormClose(Sender: TObject; var Action: TCloseAction);
begin
FreeBuffMono;
        free_buffers;

        {free memory from spectrometer}
        FreeSpecMem;
        Beep;
end;


{Timer procedure}
procedure TForm1.Timer1Timer(Sender: TObject);
begin

        GrabImage(CurrentImage);
        ShowImage(CurrentImage);
        if CurrentImage=1 then
        begin

                RedImageIntegration.Caption:= IntToStr(Integration.Position);
                RedImageGain.Caption:= IntToStr(Gain.Position);
                RedImageOffset.Caption:= IntToStr(Offset.Position);
```

```
        end
        else
        if CurrentImage=2 then
        begin
                BlueImageIntegration.Caption:= IntToStr(Integration.Position);
                BlueImageGain.Caption:= IntToStr(Gain.Position);
                BlueImageOffset.Caption:= IntToStr(Offset.Position);
        end
        else
        if CurrentImage=3 then
        begin
                GreenImageIntegration.Caption:= IntToStr(Integration.Position);
                GreenImageGain.Caption:= IntToStr(Gain.Position);
                GreenImageOffset.Caption:= IntToStr(Offset.Position);
        end
        else
        if CurrentImage=4 then
        begin
                RandomImageIntegration.Caption:= IntToStr(Integration.Position);
                RandomImageGain.Caption:= IntToStr(Gain.Position);
                RandomImageOffset.Caption:= IntToStr(Offset.Position);
        end;
end;
```

{Integration scroll bar}

```
procedure TForm1.IntegrationScroll(Sender: TObject; ScrollCode: TScrollCode; var
ScrollPos: Integer);
begin

        intlabel.Caption:=IntToStr(Integration.Position);
 end;
```

{Gain scrollbar}

```
procedure TForm1.GainScroll(Sender: TObject; ScrollCode: TScrollCode; var ScrollPos:
Integer);
begin
        Gainlabel.Caption:=IntToStr(Gain.Position);
end;
```

{Offset scrollbar}

```
procedure TForm1.OffsetScroll(Sender: TObject; ScrollCode: TScrollCode;var ScrollPos:
Integer);
begin
        offsetlabel.Caption:=IntToStr(Offset.Position);
end;
```

{Grab red image}

```
procedure TForm1.BtnGrabRedImageClick(Sender: TObject);
begin
CurrentImage:=1;

        if timer1.enabled=false then
        begin
```

```
                timer1.enabled:=True;
                BtnGrabRedImage.Caption:='Grabbing';
                BtnGrabBlueImage.Caption:='Grab Blue Image';
                BtnGrabGreenImage.Caption:='Grab Green Image';
                BtnGrabRandomImage.Caption:='Grab Random Image';
        end
        else
        begin
                timer1.enabled:= False;
                BtnGrabRedImage.Caption := 'Grab Red Image';
        end;
end;

{Grab blue image}
procedure TForm1.BtnGrabBlueImageClick(Sender: TObject);
begin
        CurrentImage:=2;
        if timer1.enabled=false then
        begin
                timer1.enabled:=True;
                BtnGrabBlueImage.Caption:='Grabbing';
                BtnGrabRedImage.Caption:='Grab Red Image';
                BtnGrabGreenImage.Caption:='Grab Green Image';
                BtnGrabRandomImage.Caption:='Grab Random Image';
        end
        else
        begin
                timer1.enabled:= False;
                BtnGrabBlueImage.Caption := 'Grab Blue Image';
        end;
end;

{Grab green image}
procedure TForm1.BtnGrabGreenImageClick(Sender: TObject);
begin
        CurrentImage:=3;
        if timer1.enabled=false then
        begin
                timer1.enabled:=True;
                BtnGrabGreenImage.Caption:='Grabbing';
                BtnGrabBlueImage.Caption:='Grab Blue Image';
                BtnGrabRedImage.Caption:='Grab Red Image';
                BtnGrabRandomImage.Caption:='Grab Random Image';
        end
        else
        begin
                timer1.enabled:= False;
                BtnGrabGreenImage.Caption := 'Grab Green Image';
        end;
end;

{Grab random image}
procedure TForm1.BtnGrabRandomImageClick(Sender: TObject);
begin
```

```
        CurrentImage:=4;

        if timer1.enabled=false then
        begin
                timer1.enabled:=True;
                BtnGrabRandomImage.Caption:='Grabbing';
                BtnGrabBlueImage.Caption:='Grab Blue Image';
                BtnGrabGreenImage.Caption:='Grab Green Image';
                BtnGrabRedImage.Caption:='Grab Red Image';
        end
        else
        begin
                timer1.enabled:= False;
                BtnGrabRandomImage.Caption := 'Grab Random Image';
        end;
end;
```

{Spectrometer}

```
procedure TForm1.DataIsHere(var Message:TMessage);
begin

        DataReady;
        OOI_BufferEmpty(HInstance,Message.wParam);
        if ooip.cont=0 then
        begin

                BtnSingleScan.enabled:=true;
                BtnContinuousScan.enabled:=true;
                BtnStopSpectrometer.enabled:=false;
        end;
end;
```

{Stop sepectromeetr grabbing}

```
procedure TForm1.BtnStopSpectrometerClick(Sender: TObject);
begin

        beep;
        OOI_Stop(HInstance);
        BtnSingleScan.enabled:=true;
        BtnContinuousScan.enabled:=true;
        BtnStopSpectrometer.enabled:=false;
end;
```

{Grab single spectrum}

```
procedure TForm1.BtnSingleScanClick(Sender: TObject);
begin

        SingleScan;
end;
```

{Grab continuous spectra}

```
procedure TForm1.BtnContinuousScanClick(Sender: TObject);
begin

        ContinuousScan;
```

```
end;


{Spectrometer cursor value}
procedure TForm1.RChart1MouseMoveInChart(Sender: TObject; InChart: Boolean;Shift:
TShiftState; rMousePosX, rMousePosY: Double);
begin
        if (InChart) then
        begin
        CursorWavelength.Caption := floattostrF(Form1.RChart1.MousePosX, ffGeneral, 3,
        10);
        CursorIntensity.Caption := floattostrF(Form1.RChart1.MousePosY, ffGeneral, 2,
        10);
        end
        else
        begin
                Form1.CursorWavelength.Caption := 'Nothing';
                Form1.CursorIntensity.Caption := 'Nothing';
        end;
end;


{Cursor value in image}
procedure TForm1.Image1MouseMove(Sender: TObject; Shift: TShiftState; X,Y: Integer);
begin
        FirstImage.Caption:=IntTOStr((Integer(Buffer1Mono[1]^[X+Y*ArraySize])){*256 div
        32767});
        FirstImageX.Caption:=IntToStr(X);
        FirstImageY.Caption:=IntToStr(Y);

end;


procedure TForm1.Edit1Change(Sender: TObject);
Var
        X,Y:Integer ;

begin
        Y:=StrToInt(Edit1.text);
        X:=StrToInt(Edit2.text);
        Label6.Caption:=IntTOStr(Integer(Buffer1Mono[1]^[X+Y*ArraySize]));
end;

end.
```

Unit mono;

```
interface
        Procedure MonoSetup;
        Procedure SetBufMono;
        Procedure FreeBuffMono;
        Procedure PrepareMono;
        Procedure WritePort11;
        Procedure WritePort13;
        procedure UpdateTheMonochromeImage;
        Procedure GrabImage(image:Integer);
        Procedure GreyScale_Palette;
        Procedure ShowImage(pict:Integer);

implementation

Uses
Control,Windows, Messages, SysUtils, Classes, Graphics, Controls, Forms, Dialogs,
StdCtrls, ExtCtrls, Menus{,ooidrv32}, OleCtrls,    graphsv3, RChart;

        {From the Kane DLL}
        procedure ram_on;external 'Wcx95';
        procedure reset_cx;external 'Wcx95';
        function grab : LongInt;external 'Wcx95';
        function init_library : PChar ; external 'wcx95';
        function grab_triggered( delay : WORD; TimeOut : Word) : Word;external 'Wcx95';
        procedure clear_field_counter;external 'Wcx95';
        function read_field_counter_high : Integer;external 'Wcx95';
        function read_field_counter_low : Integer;external 'Wcx95';
        procedure write_port(portid : WORD; value : Byte);stdcall;external
        'Wcx95.dll';

        {These are functions from my DLL}
        function get_handle : THandle;external 'grab';
        procedure setup_buffers;external 'grab';
        procedure grab2;external 'grab';
        procedure card_gain(gain : Integer);cdecl;external 'grab';


{Setup monochrome camera}
Procedure MonoSetup;
Var
        rtnString : string;
begin
        rtnString := StrPas(init_library);
        if not(rtnString = '') then
        ShowMessage(rtnString);
end;


{Setup the buffer for monochrome camera}
Procedure SetBufMono;
var
        i:integer;
begin
                                {Allocate the space for the first buffer to store 8bit image}
        for i:=0 to NumberOfImages do
```

```
        begin
                hBuffer[i]:= GlobalAlloc(GHND, ArraySize*ArraySize);
                if hBuffer[i] = 0 then
                begin
                        ShowMessage('GlobalAlloc failed!');
                        Halt;
                end;

                {protect the space}
                Buffer1Mono[i]:= GlobalLock(hBuffer[i]);
        end;

        {setup picture params}
        Form1.Image1.Stretch  := False;

        { Setup a bitmap}
        Form1.Image1.Picture.Bitmap.Handle := CreateBitmap(ArraySize,ArraySize, 1, 8,
        NIL);
        Form1.Image2.Stretch  := False;

        {Setup a bitmap}
        Form1.Image2.Picture.Bitmap.Handle := CreateBitmap(ArraySize,ArraySize, 1, 8,
        NIL);

        Form1.Image3.Stretch  := False;

        {Setup a bitmap}
        Form1.Image3.Picture.Bitmap.Handle := CreateBitmap(ArraySize,ArraySize, 1, 8,
        NIL);

        Form1.Image4.Stretch  := False;
        {Setup a bitmap}
        Form1.Image4.Picture.Bitmap.Handle := CreateBitmap(ArraySize,ArraySize, 1, 8,
        NIL);

end;


{Setup the greyscale palette}
Procedure GreyScale_Palette ;
var
        i : integer;
        rp: Word;
        HPold: HPalette;
        rtnString: string;
        pGreyScalePalette : PLogPalette;
        hGreyScalePalette : HPalette;
        palLength: Integer;
        palsize: LongInt;

begin

        {create the greyscale palette with 256 levels}
        palLength := 256;
                try
                        palSize:= 2*SizeOf(Word) + palLength*SizeOf(TPaletteEntry);
                        GetMem(pGreyScalePalette, palSize);
                        with pGreyScalePalette^ do
                                begin
```

```
                                        palVersion := $0300;
                                        palNumEntries := palLength;
                                        for i := 0 to palLength-1 do
                                                begin
                                                        palPalEntry[i].peRed := Byte(i);
                                                        palPalEntry[i].peGreen := Byte(i);
                                                        palPalEntry[i].peBlue := Byte(i);
                                                        palPalEntry[i].peFlags := $0;
                                                end;
                                end;

        hGreyScalePalette := CreatePalette(pGreyScalePalette^);

        with Form1.Image1.Canvas do
                begin
                        HPold := SelectPalette(Handle, hGreyScalePalette, True);
                        rp := RealizePalette(Handle);
                end
        except
                ShowMessage('Cannot allocate Greyscale!!');

        end;
end;


{Free memory}
Procedure FreeBuffMono;
var
  hGreyScalePalette:HPalette;
  pGreyScalePalette:PLogPalette;
  palsize:LongInt;
  loop:Integer;

begin

{Free memory space reserved for images}
   for loop :=0 to NumberOfImages do
      begin
         GlobalUnlock(hBuffer[loop]);
         GlobalFree(hBuffer[loop]);
      end;

end;


{Prepare monochrome camera for grabbing}
Procedure PrepareMono;
begin
   write_port($26E, 13);
   clear_field_counter;
   write_port($26E, 12);
   clear_field_counter;
end;


{Grab image}
Procedure WritePort11;
begin
        write_port($26E, 11);
```

```
end;

{Stop grabbing image}
Procedure WritePort13;
begin
        write_port($26E, 13);
end;

{display the image from the RAM to the bitmap}
procedure UpdateTheMonochromeImage;
var
  return: LongInt;
  i:integer;

begin

        if CurrentImage =1 then
                begin
                        return :=
                        SetBitmapBits(Form1.Image1.Picture.Bitmap.Handle,ArraySize*Arr
                        aySize, Buffer1Mono[0]);
                        Form1.Image1.Repaint;
                end
        else
                if CurrentImage =2 then
                        begin
                                return :=
                                SetBitmapBits(Form1.Image2.Picture.Bitmap.Handle,Array
                                Size*ArraySize, Buffer1Mono[0]);
                                Form1.Image2.Repaint;
                        end
                else
                        if CurrentImage =3 then
                                begin
                                        return :=
                                        SetBitmapBits(Form1.Image3.Picture.Bitmap.Handl
                                        e,ArraySize*ArraySize, Buffer1Mono[0]);
                                        Form1.Image3.Repaint;
                                end
                        else
                                if CurrentImage =4 then
                                        begin
                                                return :=
                                                SetBitmapBits(Form1.Image4.Picture.Bitm
                                                ap.Handle,ArraySize*ArraySize,
                                                Buffer1Mono[0]);
                                                Form1.Image4.Repaint;
                                        end;

        if (return = 0) then
                begin
                        ShowMessage('Cannot set Image Bitmap');
                        Form1.Close;
                end;

end;
```

```
Procedure GrabImage(image:Integer);
var
  a,b : Word;
  i : Integer;
  temp : Byte;

begin
   PrepareMono;
   for i := 0 to (Form1.Integration.Position)*100000 do
      begin
      end;

   WritePort13;
   grab2;

   hBuffer[CurrentImage] := get_handle;
   Buffer1Mono[CurrentImage] := GlobalLock(hBuffer[CurrentImage]);

end;


procedure ShowImage (pict:Integer);
var
  return:LongInt;
  a,b:Word;
  temp:LongInt;

begin

   for a:= 0 to (ArraySize-1) do
      for b :=0 to (ArraySize-1) do
         begin
               temp := Trunc((Buffer1Mono[CurrentImage]^[a+b*ArraySize]-
               Form1.Offset.Position) * (Form1.Gain.Position)/10);
               if (temp < 10 ) Then
                     Buffer1Mono[0]^[a+b*ArraySize] := 10
               else
                     if (temp >245) then
                           Buffer1Mono[0]^[a+b*ArraySize] := 245
                     else
                           Buffer1Mono[0]^[a+b*ArraySize] := temp;
         end;

         UpdateTheMonochromeImage;


end;
end.
```

Unit Spec;

```
interface

type
        DataArray= array[0..2047]of single;
        Procedure SpecSetup;
        Procedure FreeSpecMem;
        procedure DataReady;
        procedure SingleScan;
        procedure ContinuousScan;
        procedure GetMaxIndexValue(var MaxWavelength : integer; var MaxWavelength1 :
        integer, var MaxIndex2: integer;var MaxIndex3: integer; var MaxIndex4:
        integer;ArrayIn: DataArray;ArraySize : integer);
var
        Master:^DataArray;
        Slave1:^DataArray;
        Slave2:^DataArray;
        Slave3:^DataArray;
        Registered : Boolean;

implementation

uses
        Control,Windows, Messages, SysUtils, Classes, Graphics, Controls, Forms,
        Dialogs,StdCtrls, ExtCtrls, Menus,ooidrv32, OleCtrls,  graphsv3, RChart;



{Setup spectrometer}
Procedure SpecSetup;
begin
        New(Master);
        Registered:=false;
        New(Slave1);
        New(Slave2);
        New(Slave3);
end;


{Free memory}
Procedure FreeSpecMem;
begin
        Dispose(Master);
        Dispose(Slave1);
        Dispose(Slave2);
        Dispose(Slave3);
        If Registered then
                begin
                        OOI_UnRegister(HInstance);
                end;
end;


procedure DataReady;
const
        {Z= 333.3238;                                   {Calibrating spectrometer}
        C1= 0.650007;
```

```
        C2=-0.0002;} {old values of spectrometer}

        {Z= 334.9207; {new values changed on 26/11/97}
        { C1=0.621;
        C2=-0.00013; }

        {Z= 334.6317; {new values changed on 26/11/97}
        {C1=0.5839;
        C2=-0.000057;}

        Z= 334.5149; {new values changed on 30/6/98}
                C1=0.58096;
    C2=-0.000051;

var
        i:integer;

begin

        {Used to start higher up the wavlenghth scale}
        {Form1.RChart1.ClearGraf;
        Form1.RChart1.MoveTo(Z+(C1*298)+(C2*298*298), Master^[298]);
        for i := 300 to DataArraySize-1 do
                Form1.RChart1.DrawTo(Z+(C1*i)+(C2*i*i), Master^[i]);
                if (Form1.CheckAutoScale.Checked) then
                        Form1.RChart1.AutoRange(3)
                else
                        Form1.RChart1.ShowGraf; }

        Form1.RChart1.ClearGraf;
        Form1.RChart1.MoveTo(Z+(C1*2)+(C2*2*2), Master^[2]);
        for i := 2 to DataArraySize-1 do
        Form1.RChart1.DrawTo(Z+(C1*i)+(C2*i*i), Master^[i]);
        if (Form1.CheckAutoScale.Checked) then
                Form1.RChart1.AutoRange(3)
        else
                Form1.RChart1.ShowGraf;


        {Code for calibrating the spectrometer, making wavelength into pixel values}
        {Form1.RChart1.ClearGraf;
        Form1.RChart1.MoveTo((2), Master^[2]);
        for i := 3 to DataArraySize-1 do
                Form1.RChart1.DrawTo((i), Master^[i]);
                if (Form1.CheckAutoScale.Checked) then
                        Form1.RChart1.AutoRange(3)
                else
                        Form1.RChart1.ShowGraf; }
end;


{Scan Spectrometer once}
procedure SingleScan;
var
        tempflt:single;
        tempstr:string;
begin
        ooip.ssize:=sizeof(OOI_PARAM);
        ooip.dev:=0;
```

```
        ooip.cmd:=CMD_NONE;
        ooip.msg:=0;
        ooip.res:=0;
        ooip.fdc:=0;
        ooip.dsf:=100;
        ooip.boxcar:=1;
        ooip.average:=30;
        ooip.chan_ena[0]:=1;
        ooip.chan_ena[1]:=0;
        ooip.chan_ena[2]:=0;
        ooip.chan_ena[3]:=0;
        ooip.changed:=1;
        ooip.ovrr_ok:=1;
        ooip.cont:=0;
        ooip.flash_cont:=0;
        ooip.scan_dark:=0;
        ooip.correct_dark:=0;
        ooip.extrig:=0;
        ooip.hWnd:=Form1.handle;
        ooip.host:=HInstance;
        ooip.chdat[0]:=Master;
        ooip.chdat[1]:=Slave1;
        ooip.chdat[2]:=Slave2;
        ooip.chdat[3]:=Slave3;
        if Registered=false then
        begin
                OOI_Register(addr(ooip));
        end;

        Form1.BtnSingleScan.enabled:=true;
        Form1.BtnContinuousScan.enabled:=true;
        Form1.BtnStopSpectrometer.enabled:=false;
        OOI_ParamSet(addr(ooip));
        OOI_SingleScan(HInstance);

end;


{Scan Spectrometer continuously}
procedure ContinuousScan;

begin
    ooip.ssize:=sizeof(OOI_PARAM);
    ooip.dev:=0;
    ooip.cmd:=CMD_NONE;
    ooip.msg:=0;
    ooip.res:=0;
    ooip.fdc:=0;
    ooip.dsf:=100;
    ooip.boxcar:=1;
    ooip.average:=30;
    ooip.chan_ena[0]:=1;
    ooip.chan_ena[1]:=0;
    ooip.chan_ena[2]:=0;
    ooip.chan_ena[3]:=0;
    ooip.changed:=1;
    ooip.ovrr_ok:=1;
    ooip.cont:=1;
    ooip.flash_cont:=0;
```

```
    ooip.scan_dark:=0;
    ooip.correct_dark:=0;
    ooip.extrig:=0;
    ooip.hWnd:=Form1.handle;
    ooip.host:=HInstance;
    ooip.chdat[0]:=Master;
    ooip.chdat[1]:=Slave1;
    ooip.chdat[2]:=Slave2;
    ooip.chdat[3]:=Slave3;
    if Registered=false then
    begin
       OOI_Register(addr(ooip));
    end;

    Form1.BtnSingleScan.enabled:=false;
    Form1.BtnContinuousScan.enabled:=false;
    Form1.BtnStopSpectrometer.enabled:=true;
    OOI_ParamSet(addr(ooip));
    OOI_ContinuousScan(HInstance);
    //label2.Caption:= FloatToStr(Master^[500]);
    Beep;
end;
```

{Obtain maximum intensity}

```
procedure GetMaxIndexValue(var MaxWavelength : integer; var MaxWavelength1 : integer;
                                   var MaxIndex2: integer;var MaxIndex3: integer; var
                                   MaxIndex4: integer;ArrayIn: DataArray;ArraySize : integer);
const

        { Z= 333.3238;
        C1= 0.650007;
        C2=-0.0002;  }  {old values}

        {Z= 334.9207; {new values changed on 26/11/97}
        {C1=0.621;
        C2=-0.00013; }

        Z= 334.5149; {new values changed on 30/6/98}
        C1=0.58096;
        C2=-0.000051;

var
  i : integer;
  MaxIndex:integer;
  MaxIndex1:integer;
  tempMax : double;
  tempMax1 :double;
  tempMax2 :double;
  tempMax3 :double;
  tempMax4 :double;

begin
        tempMax := ArrayIn[0];
        MaxIndex := 0;
     tempMax1 :=ArrayIn[0];
     MaxIndex1 := 0;
     tempMax2 :=ArrayIn[0];
     MaxIndex2 := 0;
```

```
tempMax3 :=ArrayIn[0];
MaxIndex3 := 0;
tempMax4 :=ArrayIn[0];
MaxIndex4 := 0;
for i := 0 to ArraySize do
   begin
         If ArrayIn[i] > tempMax then
               begin
                     tempMax:= ArrayIn[i];
                     MaxIndex := i;
                     MaxWavelength:=  Round(
                     Z+(C1*MaxIndex)+(C2*MaxIndex*MaxIndex));
               end;
   end;

   for i := 0 to ArraySize do
   if ((i <> MaxIndex) and (abs(i-MaxIndex) > 40)) then
         if ArrayIn[i] > tempMax1 then
               begin
                     tempMax1 := ArrayIn[i];
                     MaxIndex1 := i;
                     MaxWavelength1:= Round( Z+(C1*MaxIndex1
                     )+(C2*MaxIndex1*MaxIndex1));

               end;
   for i := 0 to ArraySize do
         if ((i <> MaxIndex) and (i <> MaxIndex1) and
               (abs(i-MaxIndex)>45) and (abs(i-MaxIndex1)>45)) then
         if ArrayIn[i] > tempMax2 then
               begin
                     tempMax2 := ArrayIn[i];
                     MaxIndex2 := Round( Z+(C1*i)+(C2*i*i));
               end;

   for i := 0 to ArraySize do
         if ((i <> MaxIndex) and (i <> MaxIndex1)and (i <> MaxIndex2) and
               (abs(i-MaxIndex)>25) and (abs(i-MaxIndex1)>25)) and (abs(i-
               MaxIndex2)>25)then
                     if ArrayIn[i] > tempMax3 then
                           begin
                                 tempMax3 := ArrayIn[i];
                                 MaxIndex3 := Round( Z+(C1*i)+(C2*i*i));
                           end;

   for i := 0 to ArraySize do
         if ((i <> MaxIndex) and (i <> MaxIndex1)and (i <> MaxIndex2)and (i <>
         MaxIndex3) and (abs(i-MaxIndex)>25) and (abs(i-MaxIndex1)>25)) and
         (abs(i-MaxIndex2)>25) and (abs(i-MaxIndex3)>25) then
               if ArrayIn[i] > tempMax4 then
                     begin
                           tempMax4 := ArrayIn[i];
                           MaxIndex4 :=  Round( Z+(C1*i)+(C2*i*i));
                     end;
end;
end.
```